Polar Ethylene Copolymer Films for Solar Applications – Optical Properties and Aging Behavior

Dissertation

Gernot Oreški

submitted to

University of Leoben

Leoben, Austria

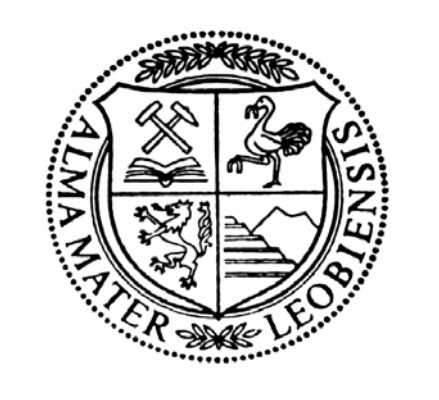

October 2008

Academic Advisor:

O. Univ.-Prof. Dr. Reinhold W. Lang

University of Leoben, Leoben, Austria

Supervisor:

Ao. Univ.-Prof. Dr. Gernot M. Wallner

University of Leoben, Leoben, Austria

Referees:

O. Univ.-Prof. Dr. Reinhold W. Lang
University of Leoben, Leoben, Austria

Prof. Dr. Volker Wittwer
Fraunhofer Institute for Solar Energy Systems ISE, Freiburg, Germany

I declare in lieu of oath, that I wrote this dissertation and performed the associated research myself, using only the support indicated in the acknowledgements and literature cited.

Leoben, October 2008 *Dipl.-Ing. Gernot Oreski*

ACKNOWLEDGEMENTS

The studies underlying this Dissertation have been performed at the Institute of Materials Science and Testing of Plastics (IWPK) at the University of Leoben (Leoben, A) and at the Polymer Competence Center Leoben GmbH (Leoben, A).

I would like to thank Prof. Reinhold W. Lang, Head of the IWPK and former director of the PCCL, for the permanent interest in the field of polymeric solar materials and for reviewing my Dissertation. I also thank Dr. Volker Wittwer (Fraunhofer Institute for Solar Energy Systems) for his interest and the attendance to serve as secondary reviewer.

My best thanks go to my supervisor Dr. Gernot Wallner, for the many discussions and ideas that contributed considerably to the scientific quality of this work. Moreover, in the many hours thinking about and discussing the best way to present the results in our joint papers, I learned from him the fundamental principles of scientific writing.

Furthermore I want to express my gratitude to the following colleagues, who performed their Bachelor and Diploma Theses on thermal properties and aging behavior of etyhelene copolymer films (Daniel Angerbauer, Roland Eder, Regina Krasser-Lamik) under the supervision of Dr. Wallner and myself. I am also grateful to my colleague DI Daniel Tscharnuter, who helped me to implement the mathematical models presented in Papers 1 and 3.

Special thanks are due to Dr. Alf Wegenberger (Institute of Plastics Processing, University of Leoben) for the extrusion of the polymer films and Dr. Giesbert Rieß (Institute of Chemistry of Polymeric Materials, University of Leoben) for his help in FTIR spectroscopy.

I would like to thank all the staff of the IWPK and the PCCL for their constant willingness to help me to resolve all the difficulties, large and small, that I have encountered during my work in the last years.

This research work was performed at the Polymer Competence Center Leoben (PCCL) within research projects I-S.9 and II-S.5 in cooperation with the Institute of

Materials Science and Testing of Plastics at the University of Leoben. The PCCL is founded by the Austrian Government and the State Governments of Styria and Upper Austria within the K_{plus} program of the Austrian Ministry of Traffic, Innovation and Technology.

Leoben, October 2008

Abstract

Ethylene copolymers based on acrylic acids and acrylates are an interesting alternative to ethylene(vinyl acetate) (EVA) for photovoltaic (PV) encapsulation and for greenhouse films. These materials provide similar or better mechanical and optical properties and a slightly better aging behavior. Up to now polar ethylene copolymers have not been investigated systematically for solar applications. Hence, the main objectives of the dissertation are to provide a fundamental understanding of the optical properties of transparent ethylene copolymer films in the wavelength range relevant for solar applications (ultraviolet (UV) to the infrared range (IR)) and to provide a comprehensive description of the degradation behavior of ethylene copolymer films under solar engineering relevant conditions.

To obtain the optical properties, a systematic spectroscopical characterization of 26 polar ethylene copolymer films was carried out in the solar and infrared range. To determine the absorption and the scattering coefficients in the solar range, two models with 4 and 5 radiation fluxes, respectively, were implemented and used. Integral infrared optical properties were calculated, on the one hand, based on published theories and formulas assuming a constant index of refraction from the visible range as input parameter. On the other hand, advanced methods were implemented and applied to determine the spectral infrared optical properties of high absorbing, thick polymer films in all regions of the spectral range (transparent, semi-transparent and non-transparent regions).

To characterize the aging behavior, polar ethylene copolymer films were weathered artificially. On the one hand, analytical test methods such as thermoanalysis, FTIR- and UV/VIS/NIR spectroscopy were applied to check physical and chemical changes. On the other hand, a comprehensive mechanical characterization was done. The significance of analytical and mechanical methods to describe the aging behavior was checked on stabilized multi-layer EVA films. The ultimate mechanical properties were correlated to weathering induced morphological and chemical changes. Unstabilized films were used to investigate

the intrinsic weathering behavior of ethylene copolymer materials with comonomer contents around 10%.

The investigated ethylene copolymer films were highly transparent in the solar range of radiation, with hemispheric transmittance values above 91% and hemispheric reflectance values of about 8%. No differences in optical properties due to comonomer type and comonomer content could be observed. Both models revealed a significant forward scattering behavior of the films. Due to the strong forward scattering behavior of all investigated films the diffuse reflectance is nearly exclusively confined to the surface. In general, the 4-flux model described the optical properties better than the 5-flux model. Similar absorption coefficient values ranging from 0.4 to 0.6 cm^{-1} were obtained for all investigated films. While ethylene(acrylic acid/butylacrylate) terpolymer showed the lowest scattering coefficient (10.9 cm^{-1} (5-flux) and 6.8 cm^{-1} (4-flux)), the highest scattering coefficient (26.2 cm^{-1} (5-flux) and 35.2 cm^{-1} (4-flux)) was found for ethylene(butylacrylate) copolymer. For polar ethylene copolymer films scattering was identified as the dominating extinction mechanism; absorptions had only negligible impact on the solar optical properties.

A linear correlation between the concentration of the highly effective carbon–oxygen group within the macromolecular structure and the infrared optical thickness was found for 50 µm thick films. This correlation is in good agreementwith a previously established correlation for better infrared radiation absorbing polymeric materials consisting of carbon, hydrogen and oxygen atoms. Complex index of refraction data (n, k) were generated. Regarding the real part n, a good agreement was obtained for both methods, the transmittance/reflectance procedure (T/R method) used for transparent and semitransparent regions, and the Single Substractive Kramers-Kronig (SSKK) algorithm applied for non-transparent regions. The highest values for the extinction coefficient k were determined for the CH_2 stretching vibration. For the investigated films n and k values ranging from 1.3 to 1.6 and from 10^{-4} to 0.25 were determined, respectively. The k values were dependent on comonomer content and film thickness.

Using IR spectroscopy, hydroxyl, vinylidene and acid groups were identified as main degradation products of commercially available EVA films with different

thickness and multi-layer structure. By IR and UV/VIS/NIR-spectroscopy the consumption of stabilizers was detected. Post crystallization was detected by DSC measurements. The analytical results of the weathered films were correlated to ultimate mechanical properties determined for unnotched and notched specimens. The results suggested that degradation of the investigated polymer films is strongly confined to the surface. In contrast to the 30 µm thick film, the aging processes on the surface of the 200 µm thick films were not reflected by mechanical properties. Nevertheless, tensile tests appeared to be the most versatile method for describing aging phenomena. Both chemical aging and physical aging as well as local (initial) and global aging effects were reflected by mechanical properties. Unstabilized ethylene copolymer films based on acrylic acids and acrylates exhibited a highly ductile behavior and high flexibility. Similar degradation behavior could be observed for all investigated films. Due to formation of chromophoric degradation products, yellowing could be observed and hemispheric transmittance values dropped slightly from values above 91% to values between 88.5 and 90.5%. The unstabilized films showed significant embrittlement due to weathering. After 750h of weathering both strain-at-break and stress-at-break values of all ethylene copolymer films dropped significantly below 50% of the initial values.

Kurzfassung

Ethylen-Copolymere auf Basis von Acrylsäuren und Acrylaten sind eine vielversprechende Alternative für Ethylen/Vinyl/Acetat-Copolymer (EVA) in der Einkapselung von Solarzellen und als Gewächshausfolien. Diese Materialien weisen ähnliche mechanische und optische Eigenschaften wie EVA auf, zusätzlich ein leicht besseres Alterungsverhalten. Bis jetzt wurde noch keine systematische Studie in Bezug auf Ethylen-Copolymere und ihre Eignung für Solarenergieanwendungen gemacht. Das Hauptziel dieser Dissertation ist daher, ein grundlegendes Verständnis für die optischen Eigenschaften von transparenten Ethylen-Copolymer-Folien im relevanten Wellenlängenbereich für Sonnenenergieanwendungen (von Ultraviolett (UV) bis Infrarot (IR)) zu schaffen und eine umfassende Beschreibung des Alterungsverhaltens der Folien unter anwendungsrelevanten Bedingungen zu liefern.

An insgesamt 26 Folien wurde eine systematische spektroskopische Untersuchung im solaren und infraroten Wellenlängenbereich durchgeführt. Für die Bestimmung des solaren Absorptions- und Streukoeffizienten wurden zwei Modelle mit 4 bzw. 5 Strahlenflüssen implementiert und angewendet. Unter der Annahme eines konstanten Brechungsindex aus dem sichtbaren Wellenlängenbereich wurden einerseits die integralen infrarot-optischen Eigenschaften anhand bereits publizierter Methoden berechnet. Andererseits wurden erweiterte Methoden implementiert und angewendet, um die spektralen infrarot-optischen Eigenschaften von stark absorbierenden, dicken Folien über alle Regionen des Spektralbereichs (transparent, semi-transparent, opak) zu ermitteln.

Zur Beschreibung des Alterungsverhaltens wurden die Folien zuerst künstlich bewittert und dann charakterisiert. Um Änderungen in der chemischen Struktur und der Morphologie nachzuweisen, wurden analytische Methoden wie Thermoanalyse, IR und UV/VIS Spektroskopie verwendet. Zusätzlich wurde eine umfassende mechanische Charakterisierung durchgeführt. Die Aussagekraft der einzelnen analytischen und mechanischen Methoden zur Beschreibung des Alterungsverhaltens wurde anhand stabilisierter Mehrschichtfolien aus EVA

überprüft. Die mechanischen Kennwerte wurden mit den alterungsbedingten Änderungen in chemischer Struktur und Morphologie korreliert. Um die intrinsische Bewitterungsstabilität zu ermitteln, wurden unstabilisierte Ethylen-Copolymer-Folien mit einem Comonomergehalt von ca. 10% untersucht.

Die untersuchten Ethylen-Copolymer-Folien sind hochtransparent im solaren Bereich, mit hemisphärischen Transmissionswerten größer 91% und hemisphärischen Reflexionswerten um 8%. Es wurden keine Unterschiede in den optischen Eigenschaften aufgrund der unterschiedlichen Comonomertypen und -anteile gefunden. Beide Modelle ergaben ein deutliches Vorwärtsstreuverhalten der untersuchten Folien. Aufgrund des ausgeprägten Vorwärtsstreuverhaltens kann die diffuse Reflexion nahezu ausschließlich auf die Oberflächentopographie der Folien zurückgeführt werden. Im Allgemeinen nähert das 4-Fluss-Modell die optischen Eigenschaften deutlich besser an als das 5-Fluss-Modell. Beide Modelle errechneten ähnliche Absorptionskoeffizienten, die für alle Materialien zwischen 0,4 und 0,6 cm^{-1} liegen. Während das Ethylen/Acrylsäure/Butylacrylat-Terpolymer den niedrigsten Streukoeffizient (10,9 cm^{-1} (5-Fluss) and 6,8 cm^{-1} (4-Fluss)) zeigte, wies das Ethylen/Butylacrylat-Copolymer die höchsten Werte von 26,2 cm^{-1} (5-Fluss) bzw. 35,2 cm^{-1} (4-Fluss) auf. Streuung wurde als dominanter Extinktionsmechanismus von Ethylen-Copolymer-Folien identifiziert, Absorptionen sind im solaren Wellenlängenbereich vernachlässigbar.

Zwischen der infrarot-optischen Dicke von 50 µm dicken Folien und der Konzentration der Carbonyl bzw. Carboxyl Gruppen in der Polymerkette wurde ein linearer Zusammenhang gefunden. Dieser Zusammenhang fügt sich ausgezeichnet in eine früher erstellte Korrelation für stark IR-absorbierende Polymere, deren Ketten aus Kohlenstoff, Sauerstoff und Wasserstoffatomen bestehen. Zusätzlich wurde der komplexe Brechungsindex (n, k) mittels der Transmission/Reflexion-Methode (T/R) für den transparenten und semi-transparenten Bereich und mittels eines erweiterten Kramers-Kronig Algorithmus für den opaken Bereich berechnet. Für den Realteil n ergab sich eine gute Übereinstimmung beider Methoden. Die höchsten Werte für den Extinktionskoeffizienten k wurden für die CH_2-Streckschwingung gefunden. Für die untersuchten Folie ergaben sich für n-Werte zwischen 1,3 und 1,6 und für k-Werte

zwischen 10^{-4} und 0,25. Außerdem waren die Werte für k abhängig vom Comonomergehalt und der Foliendicke.

Die Hauptabbauprodukte von kommerziellen EVA Gewächshausfolien - Hydroxyl-, Vinyliden- und Säuregruppen - wurden mittels IR-Spektroskopie identifiziert. Der Verbrauch von Stabilisierungsmitteln während der Auslagerung wurde mittels IR und UV/VIS-Spektroskopie detektiert. Mit DSC-Messungen wurde Nachkristallisation nachgewiesen. Die Ergebnisse der analytischen Methoden wurden mit mechanischen Eigenschaften aus Versuchen an ungekerbten und gekerbten Proben korreliert. Die Resultate weisen auf eine stark auf die Oberfläche begrenzte Alterung hin. Im Unterschied zu den 30 µm dicken Folien, beeinflusst die oberflächennahe Alterung die mechanischen Eigenschaften der 200 µm dicken Folie nicht. Dennoch sind Zugversuche an ungekerbten und gekerbten Probekörpern die vielseitigste Methode zur Beschreibung des Alterungsverhaltens, da sowohl chemische und physikalische Alterung als auch lokale und globale Alterungseffekte berücksichtigt werden.

Unstabilisierte Ethylen-Copolymer-Filme basierend auf Acrylsäuren und Acrylaten zeigten ein duktiles mechanisches Verhalten und hohe Flexibilität. Alle untersuchten Werkstoffe zeigten ein ähnliches Alterungsverhalten. Aufgrund der Bildung von farbgebenden Abbauprodukten konnte eine Vergilbung samt der Abnahme der hemisphärischen Transmissionswerte von über 91% auf Werte zwischen 88,5 und 90,5% beobachtet werden. Alle Folien zeigten eine starke Versprödung aufgrund der künstlichen Bewitterung. Bereits nach 750 h im Xenontester ergaben sich für alle untersuchten Ethylen-Copolymer-Folien um deutlich mehr als 50% reduzierte Werte für Bruchdehnung und Bruchspannung.

Table of Content

1 Introduction and Scope

Currently, polymer films are used in many solar energy related applications (Wallner et al, 2002; Oreski and Wallner, 2005). These include encapsulation of photovoltaic modules and transparent covers for greenhouse and solar thermal applications.

The advantages of using polymers are their excellent optical properties, tailor made properties, flexible processability low weight and low cost. Commodity and engineering polymers such as poly(methyl methacrylate) (PMMA), polycarbonate (PC) or ethylene/tetrafluoroethylene copolymer (ETFE), polyethylene (PE) and ethylene(vinylacetate) copolymer (EVA) are used as transparent cover materials (Papadakis et al., 2000). Regarding transparent insulation systems with black absorbers, PMMA, PC and in particular cellulose acetate (CA) have been identified (Wallner et al, 2002). For encapsulation of photovoltaic modules various polymer films are used depending on the module and cell types. Using glass/glass technology, solar cells are embedded mainly in poly(vinyl butyral) (PVB) and to some extend in ionomer (ionized ethylene(methacrylic acid) copolymer). Regarding glass/plastic technology, state of the art are EVA as solar cell encapsulant (Czanderna and Pern, 1996) and multi layer films consisting of PET and poly(vinyl fluoride) (PVF) as backsheet materials. Furthermore, thermoplastic polyurethane and liquid silicon rubber are used as encapsulant and other fluoropolymers like ETFE or poly(vinylidene fluoride) (PVDF) as backsheet materials (Oreski and Wallner, 2005).

Ethylene copolymer films based on vinylacetates and acrylic acids are already used for different solar applications. The dominant encapsulation material for PV-modules is EVA. Certain requirements have to be met by the encapsulant. The material has to provide structural support and physical isolation of the solar cells and to maintain electrical isolation (Czanderna and Pern, 1996). To deal with different thermal expansions of the materials used in a module (glass, solar cell, interconnects) and to avoid over-stressing and cracking, the material has to be a low modulus, elastomeric material. Furthermore, a maximum optical coupling

between the solar cell and the incident solar irradiation in a prescribed spectral region with an initial transmission of at least 90% and a loss of smaller than 5% after 20 years of module lifetime has to be achieved and maintained (Czanderna and Pern, 1996). The total reflection loss of a module should be minimized by optimal matching of refractive indices of the materials inside the module (Krauter und Hanitsch, 1996). Further requirements are low cost, good processability, low water absorption and permeability, high resistance to UV degradation and thermal oxidation, good adhesion and chemical inertness. The encapsulation material has to guarantee a lifetime of 20 to 30 years with a total loss in module performance of 20% over a 20 year period (Czanderna and Pern, 1996). For PV applications the vinyl acetate content of EVA is 33% by weight. Furthermore the films are equipped with several stabilizers (UV absorber, light stabilizers, antioxidants) and slow or fast curing agents for chemical cross-linking during the lamination process (Czanderna and Pern, 1996). Besides the time and energy consuming module lamination process, the major drawback of EVA is the formation of acetic acid during oxidation. Acetic acid can lead to corrosion of the metal parts in a PV module and to loss in adhesion and subsequent delamination (Czanderna and Pern, 1996; Klemchuk et al., 1997; Kempe et al., 2007). Furthermore the formed acetic acid accelerates the oxidation process of EVA (Sultan and Sörvik, 1991; Kempe et al., 2007). Films made of ionized ethylene(methacrylic acid) copolymers (ionomers) are relatively new on the market (Roekens and Beyer, 2007), providing similar properties to EVA with the advantage of a physical cross linking process. In addition, no acetic acid is formed during weathering (McNeill and Barbour, 1987; McNeill and Alston, 1998).

Greenhouse films should provide good resistance against environmental influences (e.g. solar radiation, temperature, wind and snow loads, hail, agrochemicals) and certain mechanical properties. In addition, the optical properties are of prime importance. The photosynthetically active radiation (PAR) should reach the crop, while radiation outside the PAR is not always desirable, e.g. near infrared radiation during the warm season. Diffuse radiation caused by scattering at the covering films, which leads to an isotropic radiation distribution and only weak shadowing effects, is desirable in several applications (Papadakis et al., 2002). Also the transmission of UV light can be of importance. For example,

UV absorbing films can prevent crop diseases caused by several fungi. On the other hand, UV radiation may be needed for plant growth or pollination (Kittas and Baille, 1998; Papadakis et al., 2002). Another basic requirement for greenhouse films is high absorbance of heat radiation (2.5-60 µm). The infrared optical properties are relevant for the calculation of radiative heat transfer in greenhouse structures, as thermal radiation transfer is the most important heat loss mechanism in polymer covered greenhouses (Papadakis et al., 2000). The performance and service life of transparent polymer films depend on the original properties of the material and its changes due to exposure to climate. Furthermore, factors which are particular to greenhouses have certain effects on aging of polymer films. For example, structure of the greenhouse and the microclimate inside is of importance as well as the use of agrochemicals. The durability of polymer films used for greenhouse applications varies from a minimum of one year to a maximum of two or three years. At the end of its useful life all this plastic is classified as waste. In order to avoid a huge amount of plastic waste, an enhanced lifetime is desirable (Dilara and Briassoulis, 2000). Nearly all greenhouse films on the market today are co-extruded films, which consist of several PE and EVA layers. Additional EVA layers with 4-10 m% vinylacetate comonomer increase the flexibility, the mechanical strength, the resistance to UV radiation and the IR absorbance of the film (Dilara and Briassoulis, 2000). To enhance the lifetime of greenhouse films, UV-absorbers, quenchers and hindered amine light stabilizers are added.

In addition to EVA various polar ethylene copolymer films have been developed and introduced into the market. Instead of vinyl acetate acrylate side groups such as methylacrylate (MA), ethylacrylate (EA) and butylacrylate (BA) and acidic side groups such as acrylic acid (AA) and methacrylic acid (MAA) are copolymerized with ethylene (E). These polymers are already used for cable and wire applications (McNeill and Mohammed, 1995), where the introduction of polar carbonyl side groups improves the adhesion properties compared to non-polar ethylene homopolymers. The mechanical and optical properties are comparable to EVA. Degradation studies on EVA, EBA, EEA and EMA showed that acrylate side groups of EBA, EEA and EMA revealed higher thermal stability than the VA side

group of EVA (Sultan and Sörvik, 1991; Jäger et al., 2002). And compared to EVA, no corrosive acetic acid was formed during thermal aging.

For solar applications the optical properties in the solar and infrared range are of prime importance (Vargas et al., 1998). Also long-term stability under different service conditions has to be provided. So far, no systematic investigation to describe the optical properties in the solar and infrared range of wavelength has been done for polar ethylene copolymer films. Furthermore, no investigations of the aging behavior under application relevant weathering conditions were found for polar ethylene copolymer films.

Therefore two main objectives can be defined. One primary objective of this Dissertation is to provide a good understanding of the optical properties of transparent ethylene copolymer films from the ultraviolet (UV) to the infrared range (IR) of light. Second, a detailed characterization and description of the degradation behavior of ethylene copolymer films after accelerated aging should be done.

The scientific approach of the thesis includes the application of spectroscopic methods to measure the optical properties. Furthermore, mathematical models for the determination of the relevant optical properties (complex index of refraction, absorption coefficient, scattering coefficient) from spectroscopic measurements in the solar and infrared wavelength range are developed and implemented. The results are interpreted according to polymer physical relations and structure-property correlations are elaborated. As to the weathering behavior, ethylene copolymer films are weathered artificially and are exposed to UV radiation, heat and humidity. The aging and degradation behavior is characterized by thermoanalysis, tensile tests and FTIR- and UV/VIS/NIR spectroscopy, and the obtained properties are correlated to weathering induced morphological and chemical changes.

According to the scientific approach the work is separated into two main chapters:

1 Optical properties of polar ethylene copolymers

1.1 Solar optical properties

1.2 Infrared optical properties

2 Aging and degradation behavior of polar ethylene copolymer films

Both chapters contain an introduction into the specific problem and the publications. The introduction should present the special topic, the methodology and the important findings of each publication.

This dissertation consists of 5 publications, in all of which the author of this Dissertation is listed as first author. Two of the papers (Papers 2 and 3) have already been published in reviewed journals. The other three papers (Papers 1, 4 and 5) are already submitted and currently under review. In the meantime, one of these papers (Paper 5) has been accepted with minor revisions.

2 Optical Properties of Polar Ethylene Copolymers

A complete knowledge of interaction of polymers with radiation ranging from ultraviolet (UV) to infrared (IR) is of prime importance for all solar applications, as the optical properties of materials define energy gain and loss. In the following, the optical properties of ethylene copolymer films are described in detail. According to the main radiative energy fluxes in solar systems, the focus is first given to solar optical properties and second to infrared optical properties.

2.1 Solar Optical Properties

Usually, light is scattered when the material contains particles or domains in the same order of the wavelength of the incoming light. In several studies (Bheda and Spruiell, 1986; White et al., 1986; Wallner et al., 2002; Wallner et al., 2005), light scattering has been identified as the dominant extinction mechanism for transparent polymer films. Absorbance was shown to be negligible for polymer films in the solar range of wavelength. For transparent polymer films, significant absorptions can be seen above 1000nm due to mid-IR overtones of carbon hydrogen single bond vibrations and below 300nm due to the carbonyl group of the comonomer groups. In contrast, scattering occurs over the whole range of wavelength.

Several models to describe the scattering behavior (Vargas and Niklasson, 1997) have been derived from the radiative transfer theory (Chandrasekhar, 1960), leading to models using 2-fluxes (Kubelka and Munk, 1931), 3-fluxes (Manara et al., 2005) or 5-fluxes (Burger, 2005). With more fluxes used the scattering behavior is described more accurately, as the direct and diffuse parts of transmittance and/or reflectance are considered. A 4-flux model by Maheu et al. (1984) has been used to calculate the scattering coefficient of polymer films for transparent insulation applications (Teichert et al., 2002; Wallner et al., 2002; Wallner et al., 2005).

In general there are few quantitative data on solar optical properties of transparent polymer films available in literature. Often, solely the transmittance and reflectance

data were measured and discussed, but without performing a systematic investigation of absorption and scattering behavior (Krauter and Hanitsch, 1996; Kittas and Baille, 1998; Papadakis et al., 2000). Pollet et al. (2005) investigated the diffuse transmittance of transparent cover material and measured the bidirectional transmittance distribution function, which gives a meaning of the forward diffusion pattern of transmitted radiation. However, no optical coefficients were calculated. Furthermore, mainly integral values were calculated (Wallner et al., 2002; Wallner et al., 2005). Regarding materials, mostly the classical transparent cover materials such as PMMA, PC, PET, PE and EVA are dealt with (Wallner et al., 2002; Wallner et. al, 2005; Papadakis et al., 2000; Pern, 1996). For polar ethylene copolymer films no spectral optical coefficients are described in literature.

Hence, the main objective of this part of the work is to determine the solar optical properties of polar ethylene copolymers and to calculate spectral scattering and absorption coefficients using direct and diffuse transmittance and reflectance spectra.

For the systematic investigation of the optical properties UV/VIS/NIR spectroscopy was used. Two different n-flux models with 4 and 5 radiation fluxes, respectively, are implemented for transparent polymer films and their results are compared. In this study, spectral data are used for modeling the scattering and absorption coefficients and compared to results derived from integral weighted data.

In Paper 1 it is revealed, that the investigated ethylene copolymer films are highly transparent in the solar range of radiation. No differences in optical properties due to comonomer type and comonomer content could be observed. Significant absorptions were found above 1000nm due to mid-IR overtones of carbon-hydrogen single bond vibrations and below 300nm due to the carbonyl group of the comonomer groups. The applied 4- and 5-flux models revealed a significant forward scattering behavior of the films. In general, the 4-flux model described the optical properties far better than the 5-flux model. Due to the strong forward scattering behavior of all investigated films the diffuse reflectance is nearly exclusively confined to the surface topography. Interestingly, both models show smaller deviations for low scattering films.

Paper 1: Determination of Solar Optical Properties of Transparent Polymer Films using UV/VIS Spectroscopy

Oreski, G., Tscharnuter, D., Wallner, G.M.

submitted to Solar Energy Materials and Solar Cells (October 2008)

Determination of Solar Optical Properties of Transparent Polymer Films using UV/VIS Spectroscopy*

Oreski G. [1], Wallner G.M. [2]

[1]Polymer Competence Center Leoben GmbH, Roseggerstraße 12, A-8700 Leoben, A

[2]Institute of Materials Science and Testing of Plastics, University of Leoben, Franz Josef Straße 18, A-8700 Leoben, A

Corresponding Author, email: oreski@pccl.at, fax: +43 3842 429 626

Abstract

In this paper, 4- and 5-flux models were implemented and used for the determination of absorption and scattering coefficients of transparent polymer films by UV/VIS/NIR spectroscopy. The models were applied for a systematic characterization of polar ethylene copolymer films in the solar radiation range. The investigated ethylene copolymer films were highly transparent in the solar range of radiation, with hemispheric transmittance values above 91% and hemispheric reflectance values of about 8%. Both models revealed a significant forward scattering behavior of the films. The 4-flux model fitted hemispheric and diffuse transmittance far better than the 5-flux model. Hemispheric reflectance values were overestimated by both models. Similar absorption coefficient values ranging from 0.4 to 0.6 cm^{-1} were obtained for all investigated films. While ethylene(acrylic acid/butylacrylate) terpolymer showed the lowest scattering coefficient (10.9 cm^{-1} (5-flux) and 6.8 cm^{-1} (4-flux)), the highest scattering coefficient (26.2 cm^{-1} (5-flux) and 35.2 cm^{-1} (4-flux)) was found for ethylene(butylacrylate) copolymer.

* Paper submitted to Solar Energy Materials and Solar Cells (October 2008).

1. Introduction

Due to their excellent optical properties (high transparency) as well as further polymer specific advantages (material properties can be tailored within a wide range, very flexible processibility, low cost), polymeric films posses an outstanding potential for many solar applications. Polymeric materials are already used for many different solar energy related components. Concerning solar thermal systems plastics play a decisive role as transparent cover and/or convection suppressing material. For photovoltaic (PV) applications transparent plastics are used as encapsulation materials (Czanderna and Pern, 1996).

An exact knowledge of the scattering and absorption behavior is important for applications related to solar energy and energy efficiency (Vargas et al., 1998). Usually, light is scattered or absorbed, when the material contains particles or domains in the same order of the wavelength of the incoming light. In several studies (Wallner et al., 2002; Wallner et al., 2005; Teichert et al., 2002), light scattering has been identified as the dominant extinction mechanism. Absorbance was often negligible in the solar range of wavelength.

Several models to describe the scattering behavior have been derived from the radiative transfer theory (Chandrasekhar, 1960). Whereas 2-flux models are often used as a simple approximation (Kubelka and Munk, 1931), a model of at least four radiation fluxes is necessary to describe the scattering behavior accurately, as the direct and diffuse parts of transmittance and/or reflectance are considered (Vargas and Niklasson, 1997). A 4-flux model by Maheu et al. (1984) has been used in recent studies (Wallner et al., 2002; Wallner et al., 2005; Teichert et al., 2002) to calculate the scattering coefficient of polymer films for transparent insulation applications. In another study, the scattering coefficient determined by a 3-flux model was used to calculate the pore size distribution of alumina and magnesia ceramics (Manara et al., 2005a). In case of highly anisotropic scattering, a 5-flux model showed to be more appropriate (Burger, 1998). So far, the 3- and 5-flux models have been used on ceramics and loose powders only (Kuhn et al., 1993; Burger, 1998; Manara et al., 2005a; Manara et al., 2005b).

The main objective of this paper is to determine the solar optical properties such as scattering and absorption coefficient using direct and diffuse transmittance and reflectance spectra. Tthe 5-flux model is implemented for transparent polymer films and compared to the results of the well proven 4-flux model. In recent studies (Wallner et al., 2002; Wallner et al., 2005), the input data for the 4-flux model have already been weighted by AM1.5 global solar irradiance source function. In this study, spectral data are used to model spectral scattering and absorption coefficients.

2. Experimental

Polar ethylene copolymer film types with comonomer contents between 1.7 and 18 m% and three different comonomer types (acids, acrylates and acetates) were investigated. As to the acid comonomers acrylic acid (AA) and methacrylic acid (MAA) were chosen. Regarding the acrylate comonomers, butylacrylate (BA), ethylacrylate (EA) and methylacrylate (MA) are currently in use for ethylene (E) copolymer materials. Furthermore, widely used ethylene(vinylacetate) copolymers (EVA) as well as a terpolymer material with two different comonomers (acrylic acid and butylacrylate (AA/BA) were investigated. Further details as to these materials such as comonomer content and film thickness are listed in Table 1. The material resins were supplied by Arkema (Colombes, F) (EBA), Basell (Hoofddorp, NL) (EAA/BA), Dow (Midland, USA) (EAA) and DuPont (Wilmington, USA) (EMAA, EEA, EMA, EVA). Except for processing aids the materials did not contain any stabilizers and additives. Films with thicknesses ranging from 70 to 125 µm were cast at the Institute of Polymer Processing, University of Leoben, using a Rosendahl RO400 single screw extruder (Rosendahl Maschinen GmbH, Pischelsdorf, A) with a chill roll unit of SML Maschinengesellschaft mbH (Lenzing, A). The UV/VIS/NIR measurements were carried out using a Lambda 950 UV/VIS/NIR spectrometer (Perkin Elmer Analytical Sciences, Überlingen, D) with integrating sphere. Hemispherical and diffuse transmittance and reflectance spectra were recorded from 250 to 2500 nm in 5 nm steps.

Table 1: Investigated ethlylene copolymer films.

material	comonomer	content, m%	film thickness, µm
EAA	acrylic acid	9.7	125
EMAA	methacrylic acid	8.7	90
EMA	methylacrylate	9	100
EEA	ethylacrylate	12	115
EBA	butylacrylate	7	125
EAA-BA	acrylic acid; butylacrylate	AA4; BA7	125
EVA	vinylacetate	18	125

3. Mathematical modelling

3.1 The 5-flux model

The governing equation for the propagation of light in an isotropically scattering and absorbing medium which is illuminated by a directional beam is the equation of radiative transfer (ERT) (Chandrasekhar, 1960).

$$\mu \frac{dI(\tau,\mu)}{d\tau} = I(\tau,\mu) - \frac{\omega_0}{2}\int_{-1}^{+1} p(\mu,\mu')I(\tau,\mu')d\mu' - \frac{\omega_0}{4\pi}S(\tau) \qquad (1)$$

In this equation, $\tau = (s+a)d$ is the optical depth and $\omega_0 = \frac{s}{s+a}$ is the single scattering albedo, with ***s***, ***a*** and ***d*** as scattering coefficient, absorption coefficient and film thickness, respectively. $p(\mu, \mu_0)$ is the scattering phase function, which gives the probability of scattering from direction μ_0 to μ. The intensity $I(t, \mu)$ describes the diffuse radiation field at an optical depth τ in the direction $\mu = \cos\theta$, where θ is the angle to the outward normal. Azimuthal symmetry is assumed. $S(\tau)$ is the intensity of the directional beam including internal reflections (Manara et al., 2005b) at depth τ. This integro-differential equation can be approximately solved by the discrete ordinate method (Chandrasekhar, 1960). The integral is

approximated by a quadrature rule that employs a set of $2n$ discrete directions μ_i with corresponding weights a_i such that

$$\int_{-1}^{+1} p(\mu_i,\mu')I(\tau,\mu')d\mu' \approx \sum_{j=-n}^{n} a_j \underbrace{p(\mu_i,\mu_j)}_{:=p_{ij}} \underbrace{I_j(\tau,\mu_j)}_{:=I_j} \tag{2}$$

where it is understood that $\mu_{-i} = -\mu_i$ and $a_{-i} = a_i$. With this approximation, the ERT turns into a set of coupled linear differential equations. Chandrasekhar used the Gauss quadrature, where $\mu_i \neq 0$. Kaganer (Kaganer, 1969) suggested that a quadrature which employs $\mu_0 = 0$ should be used. Since the derivative in equation (1) is multiplied with μ, it vanishes in the equation for $i = 0$. Thus, by including $\mu_0=0$ only an algebraic equation is added to the system which can be easily solved for I_0. Substitution of the solution into the remaining equations results in equations similar to those obtained by Gauss quadrature. The latter have been solved by Chandrasekhar (1960). The solution is obtained in a straight forward manner. First, the solution of the homogeneous system is determined. Second, a particular solution of the inhomogeneous system is sought.

The full solution is given by linear combination of both solutions. The coefficients of the linear combination are determined by the boundary conditions. By making an exponential ansatz for each I_i, Chandrasekhar derived a solution to the problem stated above. The solution will be formulated in matrix equations. After eliminating I_0, the equations read

$$\frac{dI_i}{d\tau} - \frac{1}{\mu_i} I_i + \frac{1}{\mu_i} \sum_{j=-n}^{n} \tilde{a}_j (\chi_i p_{0j} + pi_j) I_j = -\frac{1}{\mu_i} \frac{\omega_0^2}{4\pi} (\chi_i p_{01} + p_{i1}) S(\tau) \tag{3}$$

where

$$\chi_i = \frac{\omega_0 a_0 p_{i0}}{2} \frac{1}{1-\omega_0 a_0 p_0/2}$$

These equations can be written in matrix from by defining the vectors of intensities

$$(\mathbf{I})_i = I_i \tag{4}$$

$$(\mathbf{F})_i = -\frac{1}{\mu_i}\frac{\omega_0}{4\pi}(\chi_i p_{01} + p_{i1}) \tag{5}$$

and the matrix for scattering

$$(\mathrm{S})_{ij} = \frac{1}{\mu_i}\frac{\omega_0}{2}(\chi_i p_{01} + p_{i1})a_j - \frac{1}{\mu_i}\delta_{ij} \tag{6}$$

δ_{ij} is the Kronecker delta, which is 1 for $i = j$ and 0 for $i \neq j$. With these definitions equation (3) is written as

$$\frac{d\mathbf{I}}{\mathrm{d}\tau} + \mathrm{S}\mathbf{I} = \mathbf{F}\mathrm{S}(\tau) \tag{7}$$

Letting

$$\mathbf{I} = \mathbf{g}e^{-\lambda\tau}$$

turns the homogeneous equation into the eigenvalue equation

$$\mathrm{S}\mathbf{g} = -\lambda\mathbf{g} \tag{8}$$

An analytical solution of this problem exists for *n = 1*. For higher approximations numerical methods are required to compute the eigenvectors ***g*** and eigenvalues λ.

To find a particular solution of the inhomogeneous system the source term *S (τ)* has to be examined. The intensity of the directional beam at an optical depth τ is given by the sum of the intensities of the primary beam and each of its reflections on the sample boundary. Upon reflection, the intensity is diminished by a factor R_s and the optical path increases. R_s is the reflectance of the specimen and is calculated using the Fresnel equations (Hecht, 2002). Thus the intensity of the *n*-th reflection is given by

$$(1-R_s)R_s^{2n+1}e^{-2(n+1)\tau_0+\tau}$$

(9)

for even *n* and

$$(1-R_s)R_s^{2(n+1)}e^{-2(n+1)\tau_0-\tau}$$

(10)

for odd *n*, (s. Fig. 1). Carrying out the summation to $n = \infty$ and adding the primary beam's intensity $(1-R_s)e^{-\tau}$ yields

$$S(\tau)=(1-R_s)\frac{R_s e^{\tau}+e^{2\tau_0}e^{-\tau}}{e^{2\tau_0}-R_s^2}$$

(11)

Therefore a solution of the form is sought

$$\mathbf{I}=\mathbf{u}e^{\tau}+\mathbf{v}e^{-\tau}\,\mathsf{I}$$

and

$$\mathbf{u}=(1+S)^{-1}(1-R_s)\frac{R_s}{e^{2\tau_0}-R_s^2}\mathbf{F}e^{\tau}$$

(12)

$$\mathbf{v}=(1-S)^{-1}(1-R_s)\frac{e^{2\tau_0}}{e^{2\tau_0}-R_s^2}\mathbf{F}e^{-\tau}$$

(13)

is obtained.

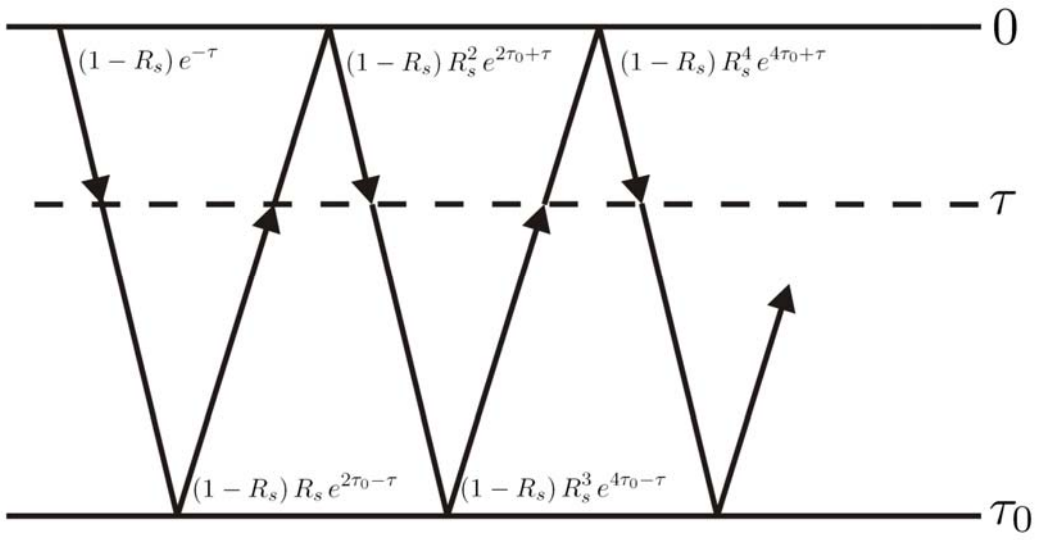

Fig. 1: Multiple internal reflections with decreasing intensities. The reflected beams are drawn at a non-perpendicular angle for illustration purposes only.

In case the albedo equals $\left(\sum_{j=1}^{1}\tilde{a}_j\big/\left(1-\mu_j^2\right)\right)^{-1}$, the inverse matrix of *1*±*S* does not exist and thus a solution using this ansatz is not possible. There is no discussion of this singular value of the albedo available in the literature. But unless the specimen's albedo happens to be near that value it is not necessary to consider this problem.

The general solution is given by a linear combination of the solutions to the homogeneous equation and the particular solution

$$\mathbf{I}=\sum_{j=-n}^{n}L_j\mathbf{g}_j e^{-\lambda_j\tau}+\mathbf{u}e^{\tau}+\mathbf{v}e^{-\tau} \tag{14}$$

The coefficients L_j are determined by the boundary conditions. Boundary conditions that consider reflections on the boundaries (Manara et al. 2005b) were chosen. From the complete solution, the hemispherical reflectance and transmittance can be calculated as functions of the albedo ω_0 and the optical depth τ_0.

According to the quadrature formula used by Kaganer (1969), the directions are given by the roots of the Jacobi polynomial $P_n^{(0,1)}(2\mu-1)$ and the weights by $1/a_i = \mu_i^2(1-\mu_i)\left(P_n^{(0,1)\prime}(2\mu_i-1)\right)^2$, $a_0 = 2-\sum_j a_j$.

The scattering phase function models various types of scattering behavior. A number of choices of phase functions exists which are suitable for different scattering mechanisms. The phase function employed in this work is the Henyey-Greenstein phase function (Burger, 1998)

$$p(\cos\gamma) = \frac{1-g_2}{\left(1+g^2-2g\cos\gamma\right)^{3/2}} \tag{15}$$

where γ is the scattering angle and the parameter g defines the anisotropy of the scattering and is therefore called anisotropy factor. For computational speed a Legendre polynomial expansion (Chandrasekhar, 1960) is useful.

$$p(\mu,\mu') \approx \sum_{k=0}^{2n-1}(2n-1)g^n P_n(\mu)P_n(\mu') \tag{16}$$

3.2 The 4-flux model

Another discretization of equation (1) using four intensity components has been investigated by Maheu et al. (1984). Their 4-flux model includes a collimated beam and diffuse radiation in both the positive and negative direction. The equations read

$$\frac{dI_c}{dz} = (a+s)I_c \tag{17}$$

$$\frac{dJ_c}{dz} = -(a+s)J_c \tag{18}$$

for the collimated beams in forward *(I)* and backward *(J)* direction and

$$\frac{dI_d}{dz} = \varepsilon a I_d + \varepsilon(1-\zeta)s(I_d - J_d) - (1-\zeta)sJ_c - \zeta s I_c \tag{19}$$

$$\frac{dJ_d}{dz} = -\varepsilon a I_d + \varepsilon(1-\zeta)s(J_d - I_d) + (1-\zeta)sI_c + \zeta s J_c \tag{20}$$

where ***z*** is the geometrical depth, and ***a*** and ***s*** are the absorption and scattering coefficients, respectively. The forward scattering ratio ζ is the ratio of forward scattered energy and total scattered energy. ε is called average crossing parameter and accounts for the average path length εdz a diffuse beam has to travel to cross a depth ***dz***. The solution of this specific model is given in detail in reference (Maheu et al., 1984).

3.3 The inverse problem

From either of the two models the transmitted and reflected intensities are expressed as functions of the scattering and absorption parameters. A nonlinear optimization algorithm provided by MATLAB is used to determine the albedo and the optical depth from the measured hemispheric transmittance $T_{h,m}$ and reflectance $R_{h,m}$ and the diffuse transmittance and reflectance $T_{d,m}$ and $R_{d,m}$ by matching the measured values to the model solutions.

In case of the 5-flux model, the anisotropy factor ***g*** was determined empirically. As transparent films do not absorb light between 400 and 800nm, the albedo ω has to be 1 by definition. Therefore, g was chosen to fit this side condition best and was set constant over the whole spectral range.

In case of the 4-flux model, the error function, that is the sum of the square of the difference between experimental and theoretical values, was minimized and the variables ***s, a*** and forward scattering ratio ζ were optimized numerically.

$$\begin{aligned} E(\omega_0, \tau_0, \zeta) = &\left(R_h(\omega_0, \tau_0, \zeta) - R_{h,m}\right)^2 + \left(T_h(\omega_0, \tau_0, \zeta) - T_{h,m}\right)^2 \\ &+ \left(Rd(\omega_0, \tau_0, \zeta) - R_{d,m}\right)^2 + \left(T_d(\omega_0, \tau_0, \zeta) - T_{d,m}\right)^2 \end{aligned} \tag{20}$$

4. Results and discussion

In the following the solar optical film properties are described and discussed. Figure 2 depicts representative hemispheric and diffuse transmittance and reflectance spectra of 125 µm thick EAA-BA and EBA films.

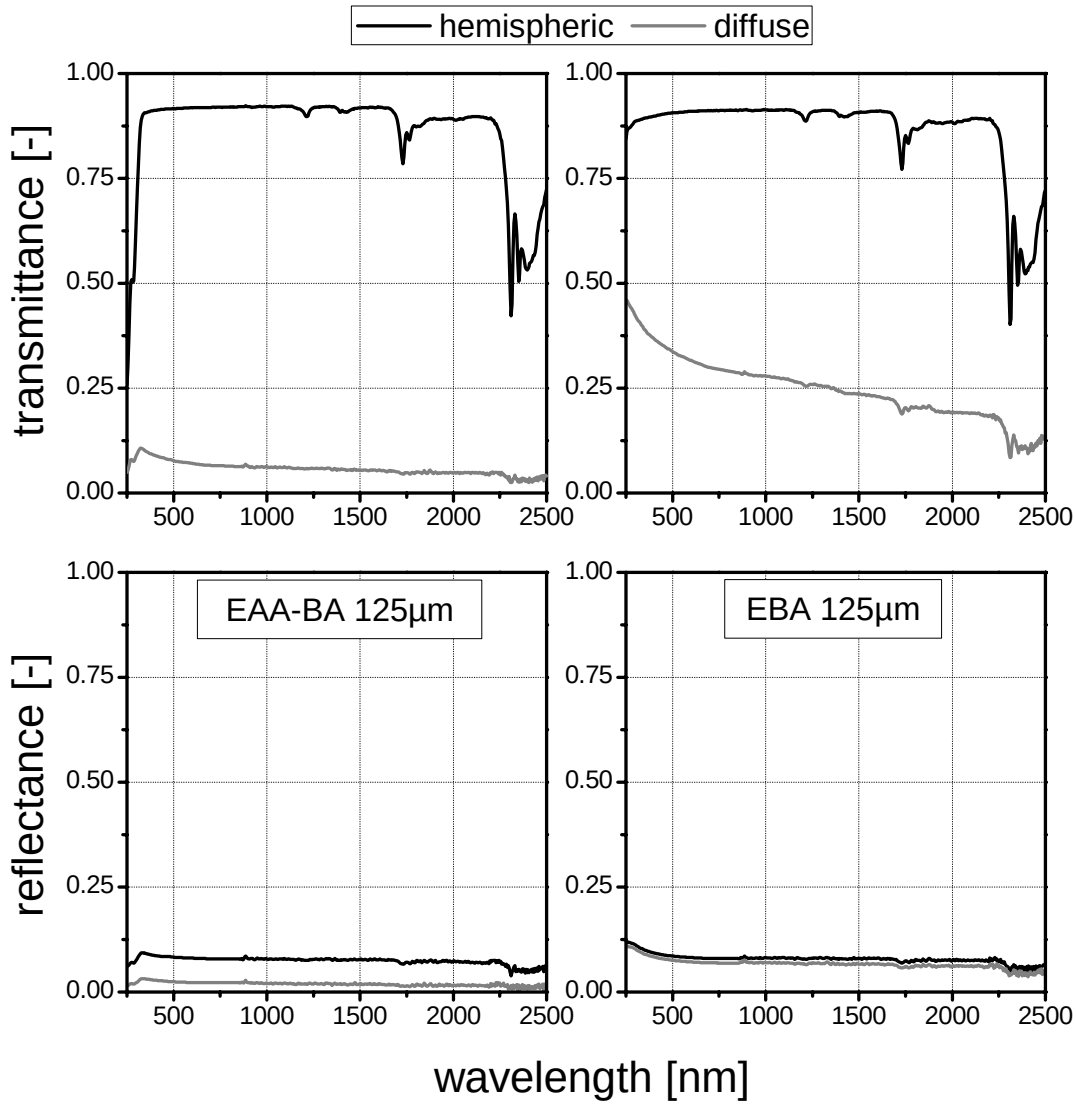

Fig. 2: Hemispheric and diffuse transmittance (top) and reflectance (bottom) spectra of 125 µm thick EAA-BA (left) and EBA (right) films.

In general, all investigated materials show only few interactions with the solar radiation, and thus the hemispheric transmittance and reflectance spectra are similar. For better comparability all spectra were weighted by AM1.5 global solar irradiance source function. The integral values are displayed in Table 2.

Table 2: Measured and calculated optical properties (T_h, T_d, R_h, R_d, ζ, g) of the investigated films. All values are weighted by a AM1.5 global solar irradiance source function, except for the g value of the 5-flux model, which was determined empirically.

			T_h	T_d	R_h	R_d
EAA-BA	measured		0,912	0,068	0,080	0,022
125 µm	4-flux	ζ = 0,92	0,908	0,069	0,086	0,012
	5-flux	g = 0,56	0,909	0,019	0,082	0,019
EBA	measured		0,903	0,298	0,082	0,072
125 µm	4-flux	ζ = 0,95	0,892	0,300	0,103	0,042
	5-flux	g = 0,65	0,843	0,042	0,151	0,043
EEA	measured		0,910	0,086	0,081	0,055
115 µm	4-flux	ζ = 0,82	0,897	0,088	0,099	0,026
	5-flux	g = 0,58	0,897	0,023	0,093	0,023
EMA	measured		0,914	0,138	0,082	0,053
100 µm	4-flux	ζ = 0,91	0,900	0,140	0,096	0,026
	5-flux	g = 0,60	0,888	0,026	0,104	0,026
EAA	measured		0,914	0,104	0,081	0,041
125 µm	4-flux	ζ = 0,90	0,902	0,105	0,092	0,020
	5-flux	g = 0,59	0,899	0,023	0,094	0,023
EMAA	measured		0,913	0,208	0,082	0,061
90 µm	4-flux	ζ = 0,93	0,898	0,210	0,098	0,033
	5-flux	g = 0,62	0,869	0,033	0,122	0,033
EVA	measured		0,917	0,084	0,079	0,045
125 µm	4-flux	ζ = 0,86	0,903	0,086	0,092	0,021
	5-flux	g = 0,58	0,903	0,021	0,088	0,021

The investigated ethylene copolymer films are highly transparent in the solar range of radiation with hemispheric transmittance values above 91% and hemispheric reflectance values of about 8%. The diffuse transmittance and reflectance values range from 8 to 38% and 2.5 to 7%, respectively. Significant absorptions can be seen above 1000 nm due to mid-IR overtones of carbon hydrogen single bond vibrations and below 300 nm due to the carbonyl group of the comonomer groups.

As EAA-BA and EBA films showed the lowest and highest scattering behavior of the investigated polyethylene copolymer films, in the following the results of the n-flux models are displayed and discussed for these representative films. Both models reveal a significant forward scattering behavior of the films, as anisotropy factor values of 5-flux model are bigger than 0 and the forward scattering ratios of 4-flux model are bigger than 0.5, which correspond to the values for isotropic scattering. For the 5-flux model, anisotropy factor values between 0.56 for EAA-BA and 0.65 for EBA were determined (Table 2). Interestingly, a linear correlation between *g* and integral diffuse transmittance and reflectance values was found.

Figure 3 depicts the forward scattering ratio ζ, calculated by the 4-flux model. All films showed an increase in ζ from the IR to the UV region. EAA-BA, EBA, EMA, EMAA and EAA exhibited only a slight increase, with values between 0.8 and 0.9 in the IR region, and values well above 0.9 at 250 nm

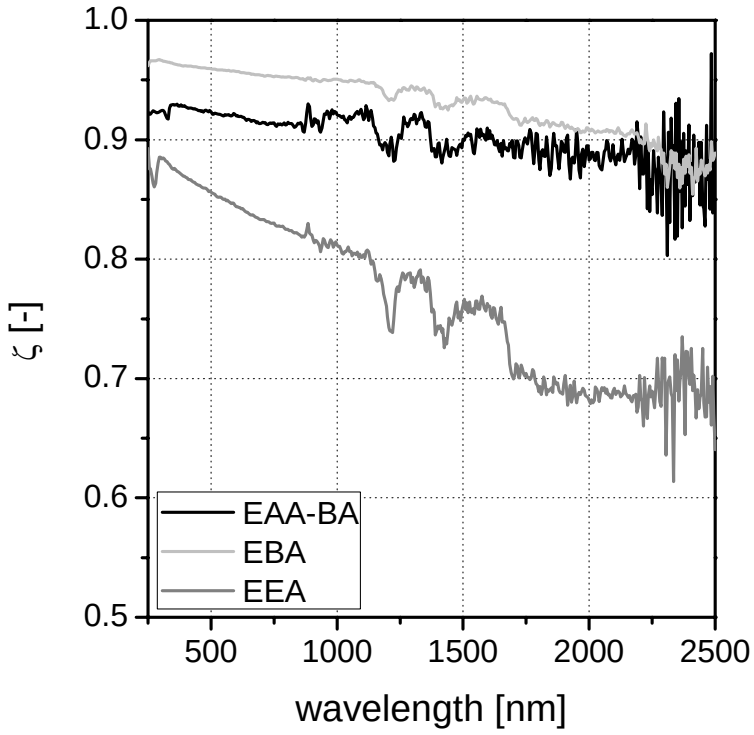

Fig. 3: Forward scattering ratio ζ of EAA-BA, EBA and EEA films, determined by 4-flux model.

For EEA and EVA ζ values around 0.7 were calculated at 2500 nm, which increased significantly up to 0.9 in the UV region. EBA exhibited the highest ζ values over the whole wavelength range, EEA the lowest. In contrast to the 5-flux model no correlation between diffuse transmittance and reflectance values and forward scattering ratio was found.

Figures. 4 and 5 depict the calculated and measured hemispheric and diffuse transmittance and reflectance spectra of EAA-BA and EBA. For EAA-BA, both models provide an excellent approximation for hemispheric transmittance spectra.

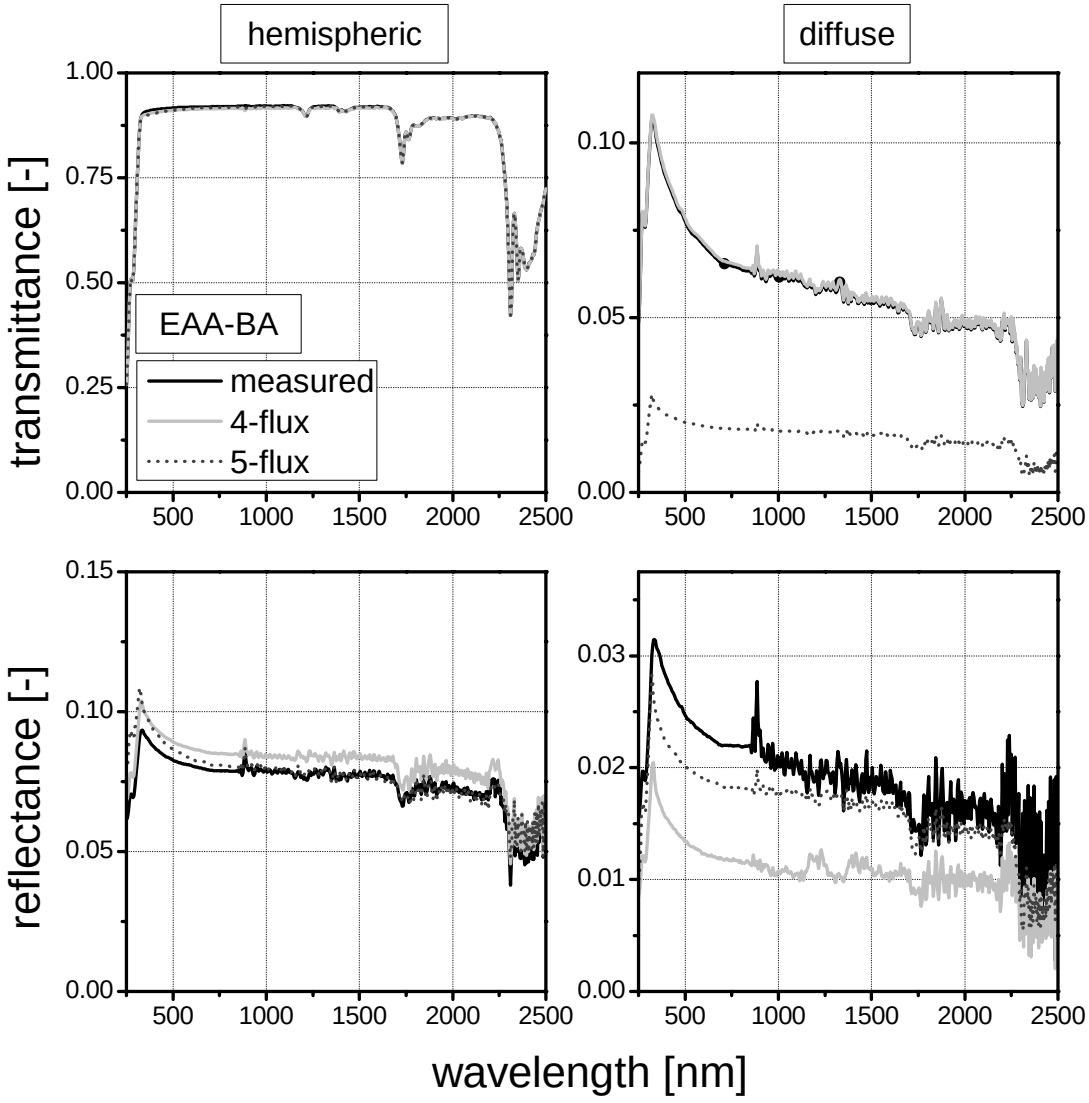

Fig. 4: Comparison of measured and calculated hemispheric (left) and diffuse (right) transmittance (top) and reflectance (bottom) spectra of 125 µm thick EAA-BA.

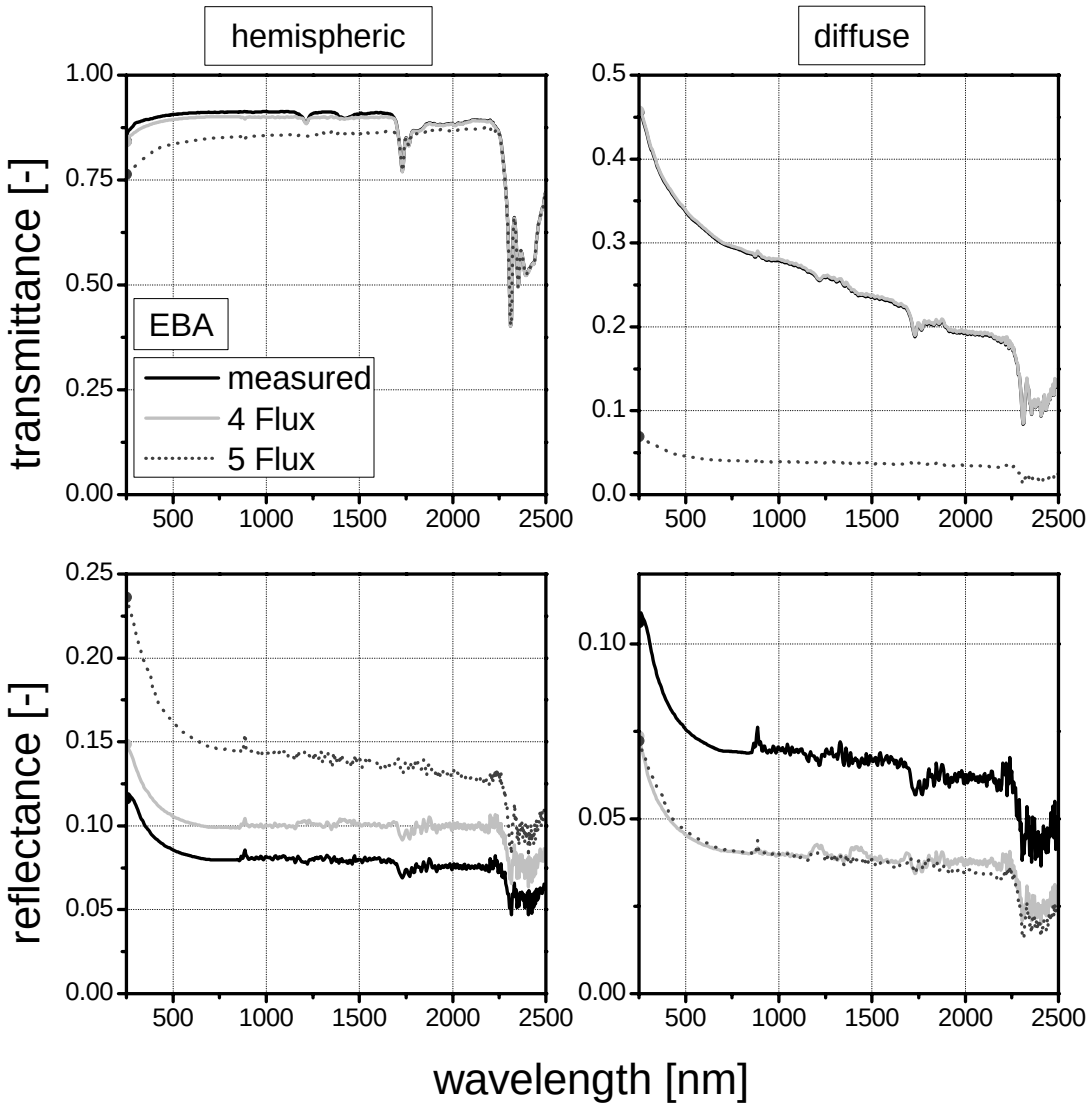

Fig. 5: Comparison of measured and calculated hemispheric (left) and diffuse (right) transmittance (top) and reflectance (bottom) spectra of 125 µm thick EBA.

Hemispheric reflectance spectra show also good agreement with modeled data. The 5-flux model exhibited good agreement from 2500 to about 800 nm. But in the visible region slightly higher reflectance values were obtained by the 5-flux model. 4-flux model overestimated hemispherical reflectance a bit, showing values of 0.086 compared to a measured reflectance value of 0.08. Regarding diffuse transmittance, the 4-flux model exhibited a far better approximation than the 5-flux model, indicating excellent agreement with the measured data. In contrast, the 5-flux model revealed significant lower values. Diffuse reflectance values were

underestimated by both models, gaining values of 0.019 (5-flux) and 0.012 (4-flux) compared to 0.022 (measured).

The highly scattering EBA film revealed a more complex behavior of the applied n-flux models. Whereas the 4-flux model (T_h=0.903) approximated the measured hemispheric transmittance spectra quite well, showing a slightly lower value of 0.892, the 5-flux model (T_h=0.843) underestimated the measured data significantly. As a consequence, the 5-flux model overestimated the hemispheric reflectance spectra in the same amount, showing a value of 0.151 compared to the measured value of 0.082. But also the 4-flux model calculated slightly higher reflectance values (0.103).

As revealed for the weakly scattering EAA-BA film, the 4-flux model exhibited a far better approximation of diffuse transmittance spectra than the 5-flux model, showing excellent agreement with the measured spectra. The 5-flux model underestimated the measured spectra significantly. Both models obtained similar diffuse reflectance values of 0.043 (5-flux) and 0.042 (4-flux), which are nevertheless significantly lower than the measured value of 0.072.

By comparing the modeled and calculated spectra of all investigated films it is assured that the 4-flux model fits hemispheric and diffuse transmittance far better than the 5-flux model. The values, weighted by AM1.5, are collected in Table 2. The deviation of the values determined by the 4-flux model relative to its measured values ranges from 0.5 to 1.5% and 0.5 to 2.5 for hemispheric and diffuse transmittance values, respectively. The 5-flux model fits the hemispheric transmittance of low scattering films (EAA-BA, EEA, EAA, EVA) well, with deviations smaller than 1.5%. But for the high scattering films (EBA, EMAA, EMA), which have a hazy appearance, deviations around 5% are found. Diffuse transmittance spectra are strongly underestimated by the 5-flux model with more than 75% smaller calculated values.

Hemispheric reflectance values are overestimated by both models. In case of low scattering films both models obtained 10 to 20% higher values. For high scattering films, significant higher hemispheric reflectance values were obtained by the 5-flux model. This corresponds well with the lower hemispheric transmittance values of both models. In absolute numbers, for both models the decrease of hemispheric

transmittance values is more or less the same as the increase in hemispheric reflectance values. It is assumed that these systematic deviations are derived from simplification of the boundary conditions of both models. Diffuse reflectance values are strongly underestimated by both models, showing about 50% lower values than measured. Due to the strong forward scattering behavior of all investigated films the diffuse reflectance is nearly exclusively confined to the surface topography (Wallner et al., 2002; Wallner et al., 2005). As both models do not contain parameters describing surface topography, this may be a possible explanation for the significantly lower values. Hence, the surface topography has to be investigated for better understanding. Due to these findings, the 4-flux model seems to describe the optical properties better than the 5-flux model. The hemispheric and diffuse transmittance spectra are fitted well and the fit of the hemispheric reflectance is acceptable. Interestingly, both models show smaller deviations for low scattering films.

Figures 6 and 7 show the spectral absorption and scattering coefficients, obtained by 4- and 5-flux models. For better comparison absorption and scattering coefficients were weighted with AM 1.5. As expected, absorption coefficients are very low for transparent polymer films. From 300 to about 1500 nm a value lower than 10^{-4} cm^{-1} was found. Below 300 nm and above 1500 nm the absorption coefficient corresponds well with the absorption peaks in hemispheric transmittance spectra due to carbonyl groups and carbon hydrogen single bonds, respectively. Values bigger than 50 cm^{-1} are reached by the highest peak around 2315 nm. Both models showed little differences in absorption coefficients and delivered similar values for all investigated films, ranging from 0.4 to 0.6 cm^{-1}. The sensitivity of the modeling was checked by the small absorption peak at 1230 nm. For low scattering films (EAA-BA, EEA, EAA, EVA), the absorption peak was better reproduced by the 4-flux model. For medium and high scattering films (EMA, EBA, EMAA) this peak is badly reproduced by both models.

Figure 7 shows the spectral scattering coefficient of low scattering EAA-BA and high scattering EBA film. Again, both models showed different behavior for low and high scattering films. In case of low scattering films, the 5-flux model delivers significantly higher values over the whole wavelength range. EAA-BA revealed the

lowest scattering coefficient with values of 10.9 cm^{-1} (5-flux) and 6.8 cm^{-1} (4-flux). EEA, EAA and EVA showed values around 13 cm^{-1} (5-flux) and 10 cm^{-1} (4-flux). For high scattering films the values obtained by the 4-flux model are higher or equal to values obtained by the 5-flux model.

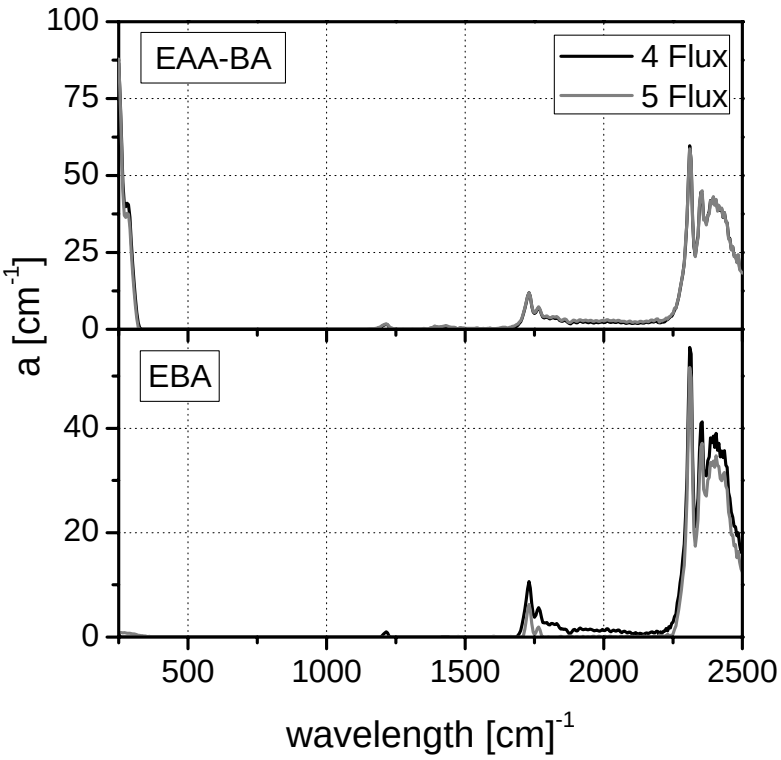

Fig. 6: Absorption coefficient *a* as a function of wavelength for EAA-BA (top) and EBA (bottom).

The highest scattering coefficient of 35.2 cm^{-1} (4-flux) was found for EBA. Furthermore, for EBA the 4-flux model delivered higher values than the 5-flux model nearly over the whole range of wavelength. Only for wavelengths bigger than 2200 nm the 5-flux model gained higher values. For EMAA the changeover is shifted to around 1300 nm. Interestingly, using the 5-flux model a higher scattering coefficient was found for EMAA (27.2 cm^{-1}) than for EBA (26.2 cm^{-1}), although the diffuse transmittance and reflectance values are significantly higher for EBA. By comparison, the 4-flux model delivered a higher value for EBA. Apart from the fact, that the 5-flux model poorly approximates the diffuse transmittance spectra, in previous studies using the 4-flux model a significant dependence of the scattering coefficient on the film thickness was found (Wallner et al., 2005). With increasing

film thickness a decreasing scattering coefficient was obtained. The difference in film thickness presumably caused the higher scattering coefficient value of EMAA. For EMA both models calculated the same value of about 19 cm^{-1} and the changeover can be found at 750 nm. Below 750 nm the 4-flux model delivered higher values, above 750 nm the 5-flux model were found to be higher.

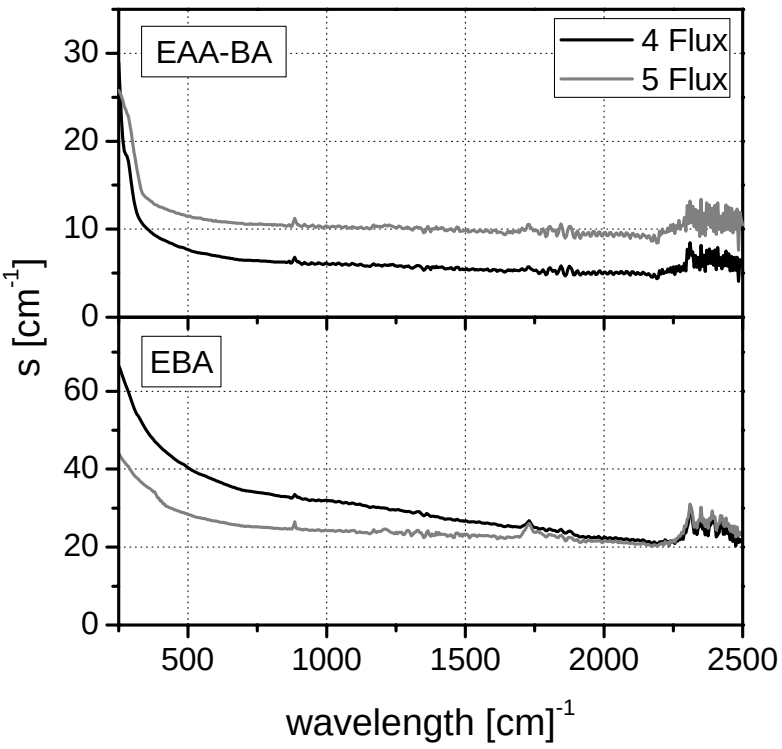

Fig. 7: Scattering coefficient ***s*** as a function of wavelength for EAA-BA (top) and EBA (bottom).

In previous studies, weighted data were used as input data for the 4-flux model (Wallner et al., 2002; Wallner et al., 2005). Regarding the forward scattering ratio ζ and the scattering coefficient ***s*** no difference between results gained from integral and spectral input data could be observed. But for the absorption coefficient, a significant difference was detected. With spectral input data, the low mid IR absorptions are considered and lead to absorption coefficient values between 0.4 and 0.6 cm^{-1}. Using integral input data, the absorption coefficient values converge towards 10^{-8} cm^{-1}, which is the predefined lower limit in the numerical calculation.

5. Summary and Conclusion

The investigated ethylene copolymer films are highly transparent in the solar range of radiation, with hemispheric transmittance values above 91% and hemispheric reflectance values of about 8%. The diffuse transmittance and reflectance values range from 8 to 38% and 2.5 to 7%, respectively. Significant absorptions can be seen above 1000 nm due to mid-IR overtones of carbon hydrogen single bond vibrations and below 300 nm due to the carbonyl group of the comonomer groups. No differences in optical properties due to comonomer type and comonomer content could be observed.

Both models reveal a significant forward scattering behavior of the films, as anisotropy factor values of 5-flux model are bigger than 0 and the forward scattering ratios of 4-flux model are bigger than 0.5, which correspond to the values for isotropic scattering.

4-flux model fits hemispheric and diffuse transmittance far better than the 5-flux model. Hemispheric reflectance values are overestimated by both models. Diffuse reflectance values are strongly underestimated by both models, showing about 50% lower values than measured. Due to the strong forward scattering behavior of all investigated films the diffuse reflectance is nearly exclusively confined to the surface. In general, the 4-flux model described the optical properties better than the 5-flux model. Interestingly, both models show smaller deviations for low scattering films.

With regards to the absorption coefficients, with both models similar integral values were found for all investigated films, (ranging from 0.4 to 0.6 cm^{-1}). As to the scattering coefficient, both models showed different behavior for low and high scattering films. In case of low scattering films, 5-flux model deliver significant higher values over the whole wavelength range. In case of high scattering films the values obtained by 4-flux model are higher or equal to values obtained by 5-flux model. EAA-BA showed the lowest scattering coefficient with values of 10.9 cm^{-1} (5-flux) and 6.8 cm^{-1} (4-flux), the highest scattering coefficient of 26.2 cm^{-1} (5-flux) and 35.2 cm^{-1} (4-flux) was found for EBA. Summarized, for the polar ethylene copolymer films scattering was identified as the dominating extinction mechanism; absorptions had only negligible impact on the solar optical properties.

6. References

Burger, T. (1998). „Radiative Transfer in Disperse Media - New Procedures in Spectroscopic Infrared Analysis", Dissertation, Universität Würzburg, D.

Chandrasekhar, S. (1960). "Radiative Transfer", Dover Publications Inc, Mineola.

Czanderna, A.W., Pern, F.J. (1996). Sol. Energ. Mat. Sol. C. **43**, 101.

Hecht, E. (2002). "Optics". Addison-Wesley Longman, München, D.

Kaganer, M. G. (1969). Opt. Spectrosc. **26**, 240.

Kubelka, P., Munk, F. (1931). Z. techn. Phys. **12** , 593.

Kuhn, J., Korder, S., Arduini-Schuster, M.C., Caps, R., Fricke, J. (1993). Rev. Sci. Instrum. **64**, 2523.

Maheu, B., Letoulouzan, J.N., Gouesbet, G. (1984). Appl. Optics **23**, 3353.

Manara, J., Caps, R., Fricke, J. (2005a). Int. J. Thermophys. **26**, 531.

Manara, J., Reidinger, M., Korder, S., Arduini-Schuster, M., Fricke, J. (2005b) In Proc. "Seventeenth European Conference on Thermophysical Properties" (ECTP2005), Bratislava, SK.

Teichert, C., Haas, A., Wallner, G.M., Lang, R.W. (2002). Macromol. Symp. **181**, 457.

Vargas, W.E., Niklasson, G.A. (1997). J. Opt. Soc. Am. A **14**, 2243.

Vargas, W.E., Lushiku, E.M., Niklasson, G.A., Nilsson, T.M.J. (1998). Sol. Energ. Mat. Sol. C. **52**, 343.

Wallner, G.M., Platzer, W., Lang, R.W. (2005). Sol. Energy **79**, 583.

Wallner, G.M., Lang, R.W., Platzer, W., Teichert, C. (2002). Macromol. Symp. **181**, 399.

2.2 Infrared Ooptical Properties

The transparency of plastics to the infrared range of wavelength is ranging from highly transparent to almost completely opaque depending on the molecular structure of the polymer. For transparent films, scattering in the IR is almost negligible. In contrast, silica glass is almost completely opaque to the IR spectrum (Goetzberger and Wittwer, 1993). The interaction of infrared radiation with polymers is well described in the literature (Günzler and Heise, 1996). Molecules have specific frequencies at which they rotate or vibrate corresponding to discrete energy levels. In order for a vibrational mode in a molecule to be IR active, it must be associated with changes in the permanent dipole. Simple diatomic molecules have only one bond, which may stretch. More complex molecules with different atom types lead to more absorption bands and more complex spectra, showing characteristic wave numbers for each molecular group.

Often, solely the infrared transmittance spectra of polymer films are measured and discussed (Papadakis et al., 2000), without doing a systematic investigation of absorption behavior or calculating optical constants. In previous studies, the integral infrared optical properties of application relevant transparent insulation materials (PC, PMMA, PET, CA) were investigated (Wallner et al., 2005). For polymers consisting of C,O and H atoms, the carbon-oxygen single bond was identified as a highly effective IR absorbing group for polymers, and a good correlation between the concentration of the functional carbon-oxygen group and the infrared optical thickness as well as absorbance was found. Except for EVA, for polar ethylene copolymer films no data on infrared optical properties could be found in the literature. And while for low IR absorbing materials often simple methods assuming a constant real part of the refractive index are used and integral values were obtained (Platzer et al., 1988; Wallner et al., 2005), for high IR absorbing materials comprehensive methods allowing for the spectral determination of both, the real and imaginary part of the refractive index (n, k), are a prerequisite (Mehling, 1998; Wallner et al., 2005).

Hence, the main objective of this section of the Dissertation is to determine the relevant infrared optical properties of polar ethylene copolymer films and to obtain

an understanding of the physical relationships between the material structure and the infrared optical properties of polar ethylene copolymers. Therefore, a systematic investigation of the optical properties was done using IR spectroscopy.

Integral infrared optical properties are calculated based on published theories and formulas assuming a constant index of refraction from the visible range as input parameter (Rubin, 1982; Platzer 1988; Wallner et al., 2005). The influence of comonomer type and comonomer content on infrared optical properties is discussed and the correlation derived for average and excellent IR absorbing polymeric materials (PC, PMMA, PET, CA) is extended to polar ethylene copolymers. Furthermore, advanced methods to determine the spectral infrared optical properties of high absorbing, thick polymer films in all regions of the spectral range (transparent, semi-transparent and non-transparent regions) are implemented and applied.

In Paper 2 of this Dissertation, a good correlation between the concentration of the functional carbon-hydroxyl and the carbon-oxygen group and the infrared optical thickness as well as the hemispherical emittance was found for 50 µm thick ethylene copolymer films. The carbon-hydroxyl group of the acidic copolymers appeared to be slightly more effective than the carbon-oxygen single bond of the acetate and acrylate copolymers. The correlation fitted well in a previously established correlation for better infrared radiation absorbing polymeric materials consisting of carbon, hydrogen and oxygen atoms.

In Paper 3, spectral complex index of refraction data were generated for various ethylene copolymer films. Regarding n, a good agreement was obtained for both methods applied. The highest k values were determined for the CH_2 stretching vibration. The k values were dependent on comonomer content and film thickness. The combination of both methods allowed for an accurate determination of n and k in the entire IR region relevant for solar applications.

Paper 2: Structure-Infrared Optical Property-Correlations of Polar Ethylene Copolymer Films for Solar Applications

Oreski, G., Wallner, G.M.

Solar Energy Materials and Solar Cells 90 (2006) 1208.

Available online at www.sciencedirect.com
SCIENCE DIRECT®
Solar Energy Materials & Solar Cells
ELSEVIER
Solar Energy Materials & Solar Cells 90 (2006) 1208–1219
www.elsevier.com/locate/solmat

Structure–infrared optical property-correlations of polar ethylene copolymer films for solar applications

G. Oreski*, G.M. Wallner

Polymer Competence Center Leoben GmbH, Parkstr. 11, Institute of Materials Science and Testing of Plastics, University of Leoben, Franz-Josef-Str. 18, A-8700 Leoben, Austria

Received 11 May 2005; accepted 11 July 2005
Available online 22 August 2005

Abstract

In this paper, an understanding of the physical relationships between the material structure and the infrared optical properties of polar ethylene homo and copolymers for solar applications is described. The infrared optical properties are relevant for the heat transport of transparent insulation structures based on these materials. To establish structure–property-correlations molecular structure parameters such as comonomer content and the concentration of carbon–oxygen single bond and carbon–hydroxyl groups, respectively, were determined. For 50 μm thick films a good correlation between the concentration of the functional carbon–hydroxyl and the carbon–oxygen group and the infrared optical thickness as well as the hemispherical emittance was found. The carbon–hydroxyl group appears to be slightly more effective than the carbon–oxygen single bond.

Keywords: Polyethylene copolymer; Infrared optical properties; Transparent insulation; Polymer film

1. Introduction

Polymeric materials are already used for many different solar energy-related components. Concerning solar thermal systems plastics play a decisive role as

*Corresponding author. Fax: +43 3842 429 626.
E-mail address: oreski@pccl.at (G. Oreski).

0927-0248/$ - see front matter © 2005 Elsevier B.V. All rights reserved.
doi:10.1016/j.solmat.2005.07.005

transparent cover and/or convection suppressing material. For solar electrical applications plastics are mainly used as encapsulation materials. Especially for solar thermal systems the infrared (IR) optical properties of plastics are of prime importance. Contrary to silica glass, which is almost completely opaque to the IR spectrum, the transparency of plastics to the IR spectrum ranges from highly transparent to almost completely opaque depending on the molecular structure of the polymer.

While for solar thermal systems with a black absorber an infrared radiation absorbing cover material is favourable, for solar thermal systems with a selective absorber a non-absorbing cover material is advantageous. Furthermore, infrared transparent materials are of great importance for radiative cooling technology.

Regarding the application of polymeric materials as transparent cover and/or convection suppressing device polycarbonate (PC) is often used. As shown in previous research work, PC is a material with average infrared transparency [1 3]. For transparent insulation (TI) systems with black absorbers polymeric materials such as poly methyl methacrylate (PMMA), poly ethylene terephthalate (PET) and in particular cellulose acetate (CA) with better to excellent infrared absorption have been identified [1]. CA is already in use for polymer film-based rectangular honeycomb structures (www.wacotech.de). Polyolefines such as polyethylene or polypropylene are well known as highly infrared transparent polymeric materials. However, despite the poor infrared absorption properties polyetyhlene homopolymers and copolymers are widely used as greenhouse covering materials [4]. Polyolefines are among the cheapest polymeric materials. To improve the infrared absorption of polyolefines polar copolymers of ethylene and vinylacetate (EVA) have been developed. Currently further polar copolymers-based on acrylates and acrylic acids, which are supposed to have a better long-term stability under aging conditions, are under development and being brought into the market [5].

In a previous study [1,2] the carbon oxygen single bond was identified as highly effective IR absorbing group for polymers with service temperatures of up to 100 °C. A good correlation between the concentration of the functional carbon oxygen group and the infrared optical thickness as well as emittance or absorbance was found for PC, PMMA, PET and CA films with a thickness of 50 μm. The overall objective of this paper is to establish structure infrared optical property-correlations for polar ethylene copolymer films, which are already in use for solar energy applications, e.g. EVA, and which are currently under development. A specific objective is to extend the correlation derived for average and excellent IR absorbing polymeric materials such as PC, PMMA, PET and CA to rather weakly IR absorbing polymeric materials such as polar ethylene copolymers.

2. Methodology

To attend the above objectives, systematic polymer physical and radiation physical investigations at plastics films were made. First, a market survey was carried out on commercially available transparent ethylene copolymer materials. In total,

more than 30 different types of polar ethylene copolymer grades were selected for the investigations. The materials were extruded to films. They were characterized spectroscopically in the relevant infrared range for a blackbody temperature of 20 °C, which is an average temperature of a transparent insulation wall absorber or a greenhouse. Integral infrared optical properties were calculated based on published theories and formulas assuming a constant index of refraction from the visible range as input parameter [6,7]. To establish structure property-correlations molecular structure parameters such as comonomer content and the concentration of carbon oxygen single bond and carbon hydroxyl group were determined.

3. Experimental

3.1. Polymer film types

Polar ethylene copolymer film types with comonomer contents between 1.7 and 30 m% and three different comonomer types (acids, acrylates and acetates) were investigated (Table 1). As the acids comonomers acrylic acid (AA) and methacrylic acid (MAA) were chosen. Regarding acrylate comonomers butylacrylate (BA), ethylacrylate (EA) and methylacrylate (MA) are currently in use for ethylene (E) copolymer materials. Furthermore, widely used ethylene vinylacetate copolymers (EVA) as well as a terpolymer material with two different comonomers (acrylic acid and butylacrylate (AA/BA) were investigated.

The material resins were supplied by Arkema (EBA, EVA), Basell (EAA/BA), BP (EMAA), Dow (EAA, EEA), DuPont (EMAA, EBA, EEA, EMA, EVA), Exxon (EAA, EVA), Leuna (EVA), Polimeri Europa (EVA) and Repsol YPF (EVA). Except for the Polimeri Europa materials which were supplied as films, films with various thicknesses ranging from 90 to 150 μm were cast on a Rosendahl RO400

Table 1
Investigated polar ethylene (E) copolymers (material type, comonomer unit and comonomer content)

Material type	Comonomer	Content (m%)
Acids		
EAA	Acrylic acid	6, 6.5, 9.7
EMAA	Methacrylic acid	1.7, 8.7
Acrylates		
EBA	Butylacrylate	6, 7, 8, 17
EEA	Ethylacrylate	12, 15
EMA	Methylacrylate	9, 9.5, 30
acetates		
EVA	Vinylacetate	5, 7, 9, 12, 14, 15, 17, 18, 24
acid/acrylate		
EAA/BA	Acrylic acid	AA 4
	Butylacrylate	BA 7

single screw extruder (Pischelsdorf, Austria) with a chill roll unit of SML Maschinengesellschaft mbH (Lenzing, Austria).

3.2. Determination of infrared optical film properties

Over the medium IR range from 370 to 4000 cm^{-1} (2.5 27 μm) the direct-beam transmittance spectra at normal incidence, the normal normal transmittance values, τ_{nn}, were obtained with a Perkin Elmer Spectrum One spectrometer (Perkin Elmer; Überlingen, Germany). Thus, the Planck radiation of a blackbody at 20 °C was covered to approximately 86%. According to Ref. [6] scattering of the material was neglected, because observed surface or bulk defects were much smaller than infrared wavelengths. To model the heat transport of transparent insulation structures or greenhouse covers, input parameters such as the integral hemispherical absorbance or equivalent emittance, α_h or ε_h, which is a function of the integral infrared absorption coefficient, κ_{IR}, are required [8,9]. The procedure for determining the integral emittance coefficient starting from the spectral, i.e., wavenumber, ν-dependent transmittance data is shown in Fig. 1.

The directional spectral emittance, $\varepsilon_\phi(\nu)$, was calculated for both transverse electric and transverse magnetic polarization using the spectral normal normal transmittance, the film thickness and the constant index of refraction as input parameters according to Ref. [6]. For polar ethylene copolymers refractive indexes ranging from 1.47 to 1.52 are given in the literature (http://www.texloc.com/closet/cl_refractiveindex.html). For the calculations an average refractive index of 1.50 was used. The hemispherical spectral emittance, $\varepsilon_h(T)$for unpolarized radiation was found by ideally directional averaging with 5° steps and averaging over both polarization directions. Finally, the total hemispherical temperature-dependent

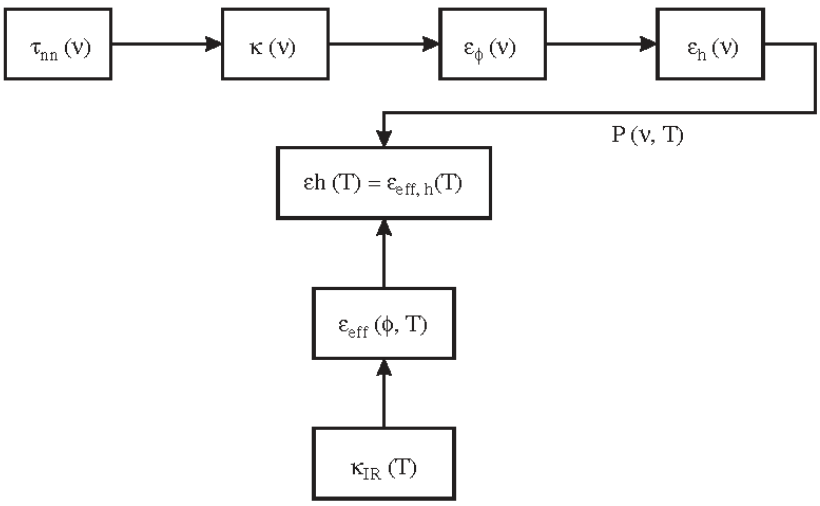

Fig. 1. Calculation procedure for the total infrared absorption coefficient, $\kappa_{IR}(T)$, from the wavenumber-dependent normal–normal transmittance data, τ_{nn}.

emittance, $\varepsilon_h(T)$, was determined by averaging the spectral values, weighted by a blackbody emissive power, $P(\nu,T)$, at each wavenumber. The temperature was set at 20 °C. The effective temperature-dependent absorption coefficient, $\kappa_{IR}(T)$, was found by an inverse fit. Although κ_{IR} in general is temperature dependent, in this paper the absorption coefficient for 20 °C is described and discussed, as this temperature is of special relevance for transparent insulation wall and greenhouse applications.

4. Results and discussion

For transparent insulation wall and greenhouse applications it is crucial to absorb the infrared radiation as well as possible in order to keep the heat radiation low. Thus, high-IR absorption is required in the range between 200 and 1500 cm^{-1}, in which a blackbody at 20 °C emits most. In Figs. 2 4 normal-normal transmittance spectra over the medium IR range are shown for selected acid, acrylate and acetate ethylene copolymers with thicknesses of 90 μm (EMAA), 125 μm (EBA) and 150 μm (EVA). Significant absorptions in the investigated polar polyethylene copolymers can be attributed to CH_2 groups (at about 1470 and 720 cm^{-1}), to C O single bonds (between 1300 and 1000 cm^{-1}) and to hydroxyl (O H) groups in acid copolymers (at about 950 cm^{-1}). Below 1000 cm^{-1} mainly molecular vibrations of the polymer chain contribute to the absorption. However, the molecular vibrations are rather weak for the investigated polymers. Close to the maximum of the emissive power function of a blackbody at 20 °C, the narrow absorption peak at 720 cm^{-1} of the CH_2 group can be found for all investigated polymers. CH_2 groups are rather weak dipoles with low

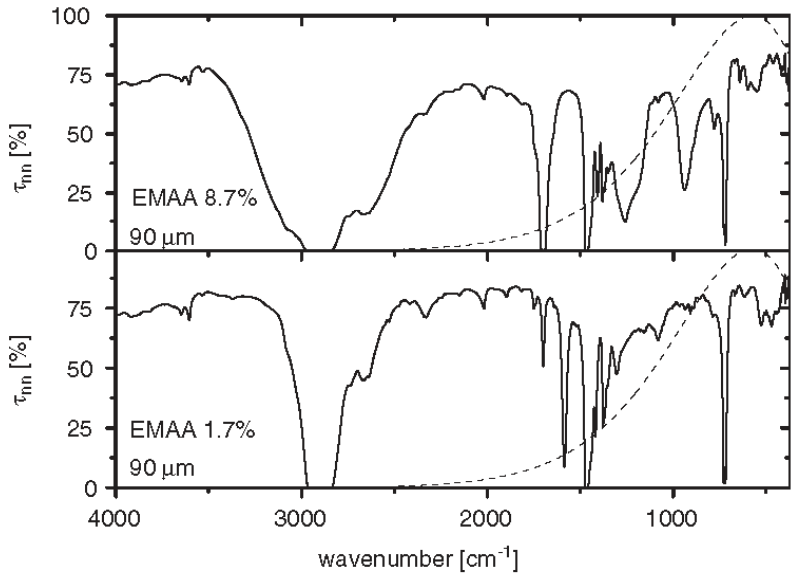

Fig. 2. Normal–normal transmittance (τ_{nn}) spectra for 90 μm thick ethylene methacrylic acid copolymer films with 8.7 (top) and 1.7 m% (bottom) comonomer content and emissive power function for a blackbody at 20 °C.

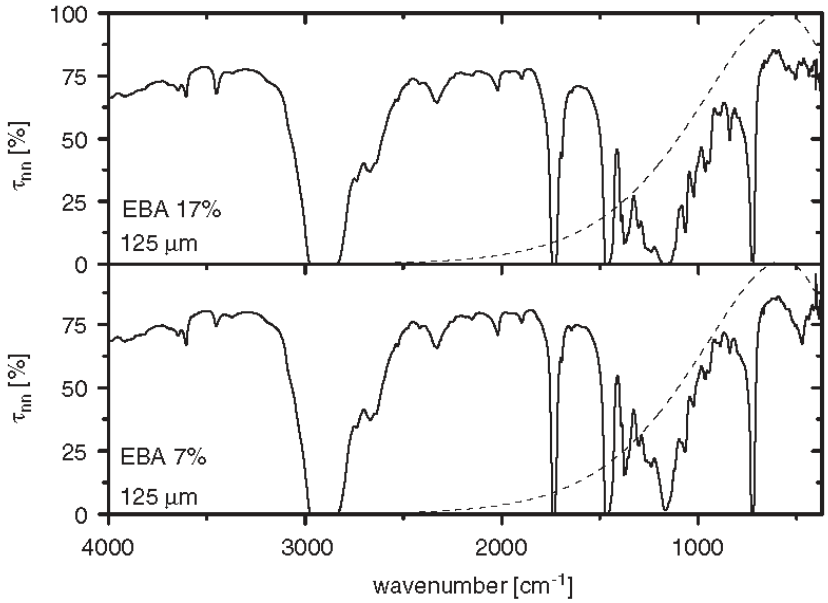

Fig. 3. Normal–normal transmittance (τ_{nn}) spectra for 125 µm thick ethylene butylacrylate copolymer films with 17 (top) and 7 m% (bottom) comonomer content and emissive power function for a blackbody at 20 °C.

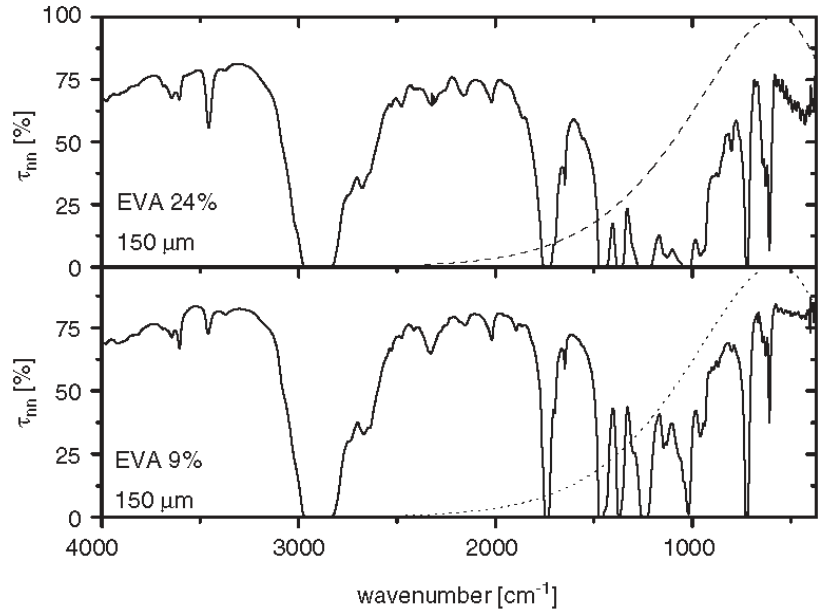

Fig. 4. Normal–normal transmittance (τ_{nn}) spectra for 150 µm thick ethylene vinylacetate copolymer films with 24 (top) and 9 m% (bottom) comonomer content and emissive power function for a blackbody at 20 °C.

absorbance in the relevant IR wavelength range. In contrast, C O and O H single bonds are stronger dipoles with an higher specific absorbance in the relevant range. However, in polar ethylene copolymers CH_2 groups are dominating. As shown in Fig. 2, for a 90 μm thick ethylene methacrylic acid copolymer film with a comonomer content of about 9 m% no total absorptions appear in the range below 1400 cm^{-1}.

For film thicknesses above 100 μm and comonomer contents above 10 m% total absorptions with broad peaks can be found due to C O functional group vibrations (Figs. 3 and 4). In the infrared wavelength range scattering of the material was neglected and the integral infrared absorption coefficient for the description of the total hemispherical infrared emittance was calculated assuming a constant index of refraction from the visible range. The validity of this assumption was checked for stronger infrared radiation absorbing polymeric materials by comparison of hemispherical emittance spectra, which were calculated from both the experimental normal normal transmittance spectra and complex refractive index data over the infrared spectral region, which are published for some polymer materials in a previous work [2]. Regarding the indexes of refraction there are few values given in the literature for the investigated polymers (http://www.texloc.com/closet/cl_refractiveindex.html). These are ranging from 1.47 to 1.52. For the calculations of all polymers an average value of 1.50 was used. Doing a sensitivity analysis for 100 μm thick polar polyethylene copolymer films considering an uncertainty in the index of refraction value of ± 0.03 results in errors of the integral infrared absorption coefficient (κ_{IR}) smaller than $\pm 1.6\%$.

In Fig. 5 the infrared optical thickness data, $\kappa_{IR}d$, are plotted for the investigated polymer films as a function of thickness. The values for the infrared optical thickness of the investigated polymers range from 0.2 to 1.0. The $\kappa_{IR}d$ values increase with increasing film thickness. In contrast to highly absorbing materials discussed in Refs. [1,2] the increase of the infrared optical thickness as a function of film thickness levels off only slightly for polar ethylene copolymers at higher film thicknesses. As shown in Ref. [7] for polystyrene and in Refs. [2,10] for various polymer films including polymers with C, H and O atoms, which are also in the primary chemical structure of the investigated polar ethylene copolymers, it is adequate to calculate the infrared optical thickness for various film thicknesses based on measured spectral data for one reference thickness. For transparent insulation structures for wall applications with black absorbers in many cases polymer films with a thickness of 50 μm are appropriate. Thus, in this work based on spectral data of about 100 μm thick films, infrared optical thickness and hemispherical emittance values for 50 μm thick films were calculated. In general, a good agreement was found between experimental and theoretical curves. Only for EVA with 24 m% comonomer content the absorption coefficients were underestimated up to 3.5% by the theoretical approach based on experimental data of a 130 μm thick film (Fig. 5).

Furthermore, to establish structure property-correlations the concentrations of functional groups within the macromolecular structure of the polymers were determined by the use of the equation $c100 = a\rho/M$, where a is the number of bonds or groups per polymer repeat unit, ρ is the bulk density of the polymer, and M is the molecular weight of the polymer repeat unit [11].

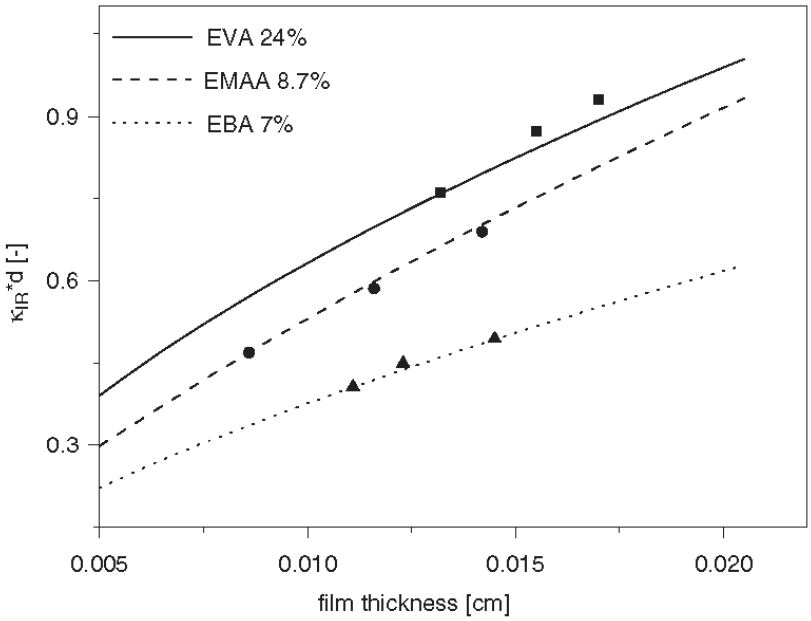

Fig. 5. Infrared optical thickness, $\kappa_{IR}d$, of selected polymer films as a function of film thickness, d (dots: measured values; curves are determined based on the spectral data of the thinnest film).

Figs. 6 and 7 show the correlation between $\kappa_{IR}d$ and the concentration of carbon hydroxyl groups (c_{C-O-H}) and ether-groups (carbon oxygen carbon) (c_{C-O-C}) for the investigated polar ethylene copolymers, respectively. The lowest infrared optical thickness values were obtained for the ethylene methacrylic acid copolymer (EMAA) with a comonomer content of 1.7 m%. Ethylene methylacrylate copolymer (EMA) with 30 m% comonomer content and ethylene vinylacetate copolymer (EVA) with 24 m% comonomer content yielded the highest values. For the investigated ethylene copolymers with a film thickness of 50 μm the density of the C O H and C O C groups determines the infrared optical thickness. A linear relationship between the concentration of the C O H or C O C groups and the infrared optical thickness and the total hemispherical emittance was found.

A detailed, material-specific analysis reveals differences in the $\kappa_{IR}d$ vs. c_{C-O-H} and $\kappa_{IR}d$ vs. c_{C-O-C} correlations (Fig. 8). For a certain concentration of the C O H or C O C functional group, the acid copolymers EAA and EMAA exhibit better infrared absorption properties than the acrylate (EBA, EMA) and acetate (EVA) copolymers. Furthermore the tendency can be perceived that acrylate comonomers with bigger side groups (methyl vs. butyl) exhibit a slightly better infrared absorption efficiency.

This can be attributed to material-dependent differences in the IR spectra, especially in the region between 1300 and 900 cm^{-1}. The acidic copolymers show a peak at about 950 cm^{-1} caused by the carboxylic group of the polymer. This intense peak is located very next to the emittance maximum of a black body at 20 °C. For the acrylic and acetic copolymers following ranking as to infrared optical thickness

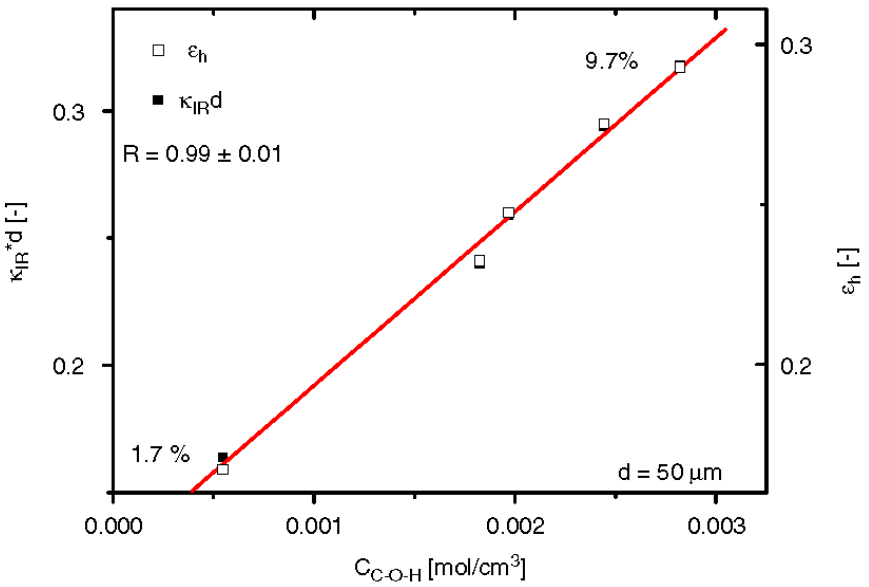

Fig. 6. Correlation between infrared optical thickness, $\kappa_{IR}d$, or hemispherical emittance, ε_h, and concentration of carbon–hydroxyl groups (c_{C-O-H}) of ethylene acrylic acid copolymers (EAA and EMAA) with comonomer contents ranging from 1.7 to 9.7 m%.

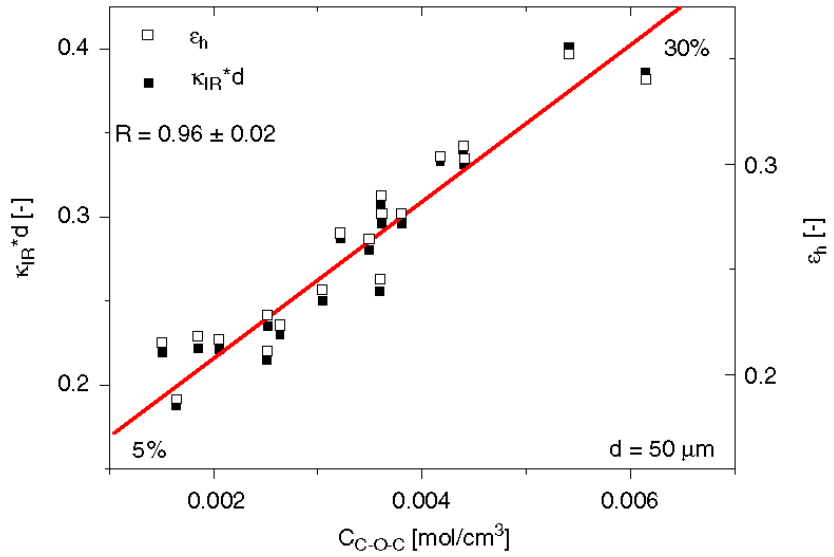

Fig. 7. Correlation between infrared optical thickness, $\kappa_{IR}d$, or hemispherical emittance, ε_h, and concentration of carbon–oxygen–carbon (ether) groups of ethylene acrylate or acetate copolymers (EBA, EEA, EMA and EVA) with comonomer contents ranging from 5 to 30 m%.

was obtained: EVA > EBA > EMA. For EEA and EMAA no linear fit was done due to few material variations. The ranking can be explained by the different chemical composition of the copolymers. EVA shows an intense peak at 1020 cm^{-1},

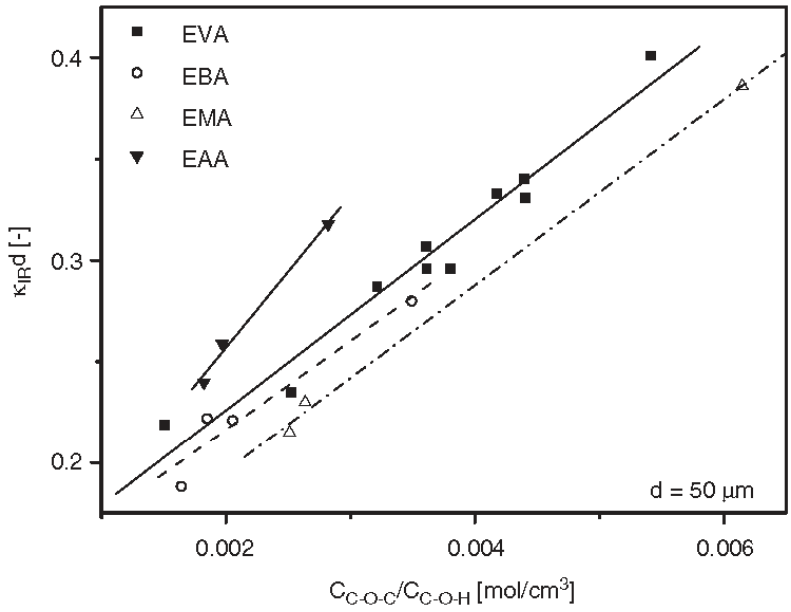

Fig. 8. Correlation between infrared optical thickness, $\kappa_{IR}d$ and concentration of carbon–oxygen–carbon and carbon–hydroxyl groups, respectively, of EAA, EBA, EMA and EVA copolymers.

which is less pronounced for EBA and EMA. The maximum absorption for EBA (1175 cm^{-1}) and EMA (1160 cm^{-1}) is nearly at the same wavenumber, but EBA shows more medium absorption peaks between the maximum and 900 cm^{-1}. Therefore EBA shows higher $\kappa_{IR}d$ values at same C O C concentrations than EMA, but lower values than EVA.

In Fig. 9 the correlated data for the investigated polar ethylene copolymers are plotted together with results of a previous work [1,2,10], where polymeric materials with high-infrared absorption was aimed at. A linear correlation between the infrared optical thickness and the concentration of C O C groups was found for polymeric films with a thickness of 50 µm for both, excellent infrared absorbing polymers such as cellulose triacetate (CTA) and weakly infrared absorbing polymers such as ethylene copolymers with low-polar comonomer content. It should be emphasized that the linear correlation works for polymers with aliphatic (all included polymers) and aromatic (PC and PET) groups within the molecular structure.

Considering a small-celled transparent insulation structure with a material content of 3 v%, a film thickness of 50 µm, a structure thickness of 10 cm and two highly emitting surfaces ($\varepsilon = 0.9$) with 20 °C inside and 0 °C outside, a polar ethylene copolymer material with an infrared optical thickness of 0.30 yields a heat conductance (Λ) value of about 1.25 W/(m^{2}K), while a PC material ($\kappa_{IR}d = 0.69$) and a CA material ($\kappa_{IR}d = 1.25$) give Λ-values of 0.91 and 0.75 W/(m^{2}K), respectively. This calculation based on a model developed by Platzer [8] and validated for a variety of polymeric materials in Refs. [10,12] shows, that with an

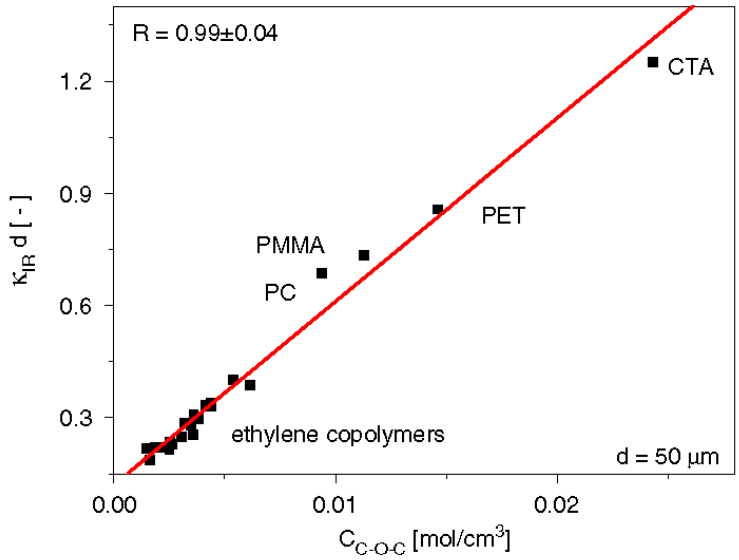

Fig. 9. Correlation between infrared optical thickness, $\kappa_{IR}d$ and concentration of carbon–oxygen single bonds within the macromolecular structure of various polymers for a film thickness of 50 µm.

ethylene copolymer material with an infrared optical thickness about four times lower than for CA about 66% higher heat conductance values are yielded.

5. Summary and conclusions

The infrared optical thickness values of various polar ethylene homo and copolymers with comonomer contents between 5 and 30 m% and film thicknesses between 50 and 200 µm are ranging from 0.2 to 1.0. A linear correlation between the concentration of the highly effective carbon oxygen group within the macromolecular structure and the infrared optical thickness was found for 50 µm thick films. This correlation fits well in a previously established correlation for better infrared radiation absorbing polymeric materials consisting of carbon, hydrogen and oxygen atoms.

Acknowledgements

This research work was performed at the Polymer Competence Center Leoben (PCCL) within research project S.9 in cooperation with the Institute of Materials Science and Testing of Plastics at the University of Leoben. The PCCL is founded by the Austrian Government and the State Governments of Styria and Upper Austria within the Kplus program of the Austrian Ministry of Traffic, Innovation and Technology. The authors wish to express their acknowledgements to Arkema, Basell,

DOW, DuPont, Leuna, Polimeri Europa and Repsol YPF for providing the materials.

References

[1] G.M. Wallner, R.W. Lang, W. Platzer, C.H. Teichert, Optical properties of polymer films for transparent insulation, Macromol. Symposia 181 (2002) 399–410.
[2] G.M. Wallner, W. Platzer, R.W. Lang, Structure–property correlations of polymeric films for transparent insulation wall applications. Part 2: Infrared optical properties, Solar Energy, 2005, in press
[3] P.T. Tsilingiris, Comparative evaluation of the infrared transmission of polymer films, Energy Conversion Manage 44 (2003) 2839–2856.
[4] G. Papadakis, D. Briassoulis, G. Scarascia Mugnozza, G. Vox, P. Feuilloley, J.A. Stoffers, Radiometric and thermal properties of and testing methods for, greenhouse covering materials, J. Agric. Eng Res. 77 (2000) 7–38.
[5] K.M. Jäger, R.C. Dammert, B.Å. Sultan, Thermal degradation studies of different polar polyethylene copolymers, J. Appl. Poly. Sci. 84 (2001) 1465–1473.
[6] M. Rubin, Infrared properties of polyethylene terephthalate films, Solar Energy Mater 6 (1982) 375–380.
[7] W.J. Platzer, Solare Transmission und Wärmetransportmechanismen bei transparenten Wärmdämmaterialien, Ph.D. Thesis, Albert Ludwigs Universität, Freiburg, Germany, 1988.
[8] W.J. Platzer, Calculation procedure for collectors with a honeycomb cover of rectangular cross section, Solar Energy 48 (1992) 381–393.
[9] J.E.Y. Hum, K.G.T. Hollands, J.L. Wright, Analytical model for the thermal conductance of double-compound honeycomb transparent insulation with validation, Solar Energy 76 (2004) 85–91.
[10] G. Wallner, Kunststoffe für die transparente Wärmedämmung–Polymerphysikalische Einflüsse und Modellierung, Ph.D. Thesis, Montanuniversität Leoben, Leoben, Austria, 2000.
[11] C.A. Sergides, A.R. Chughtai, D.M. Smith, Determination of optical constants of polymer films using a fourier transform infrared reflection method; polyethylene terephthalate (PET), Appl. Spectrosc. 41 (1987) 154–157.
[12] G.M. Wallner, R.W. Lang, H. Schobermayr, H. Hegedys, R. Hausner, Development and application demonstration of a novel polymer film based transparent insulation wall heating system, Solar Energy Mater. Solar Cells 84 (2004) 441–457.

Paper 3: Development of Methods to Determine the Infrared-Optical Properties of Polymer Films

Oreski, G., Tscharnuter, D., Wallner, G.M.

Macromolecular Symposia 265 (2008), 124.

 DOI: 10.1002/masy.200850513

Development of Methods to Determine the Infrared-Optical Properties of Polymer Films

Gernot Oreski,[*1] *Daniel Tscharnuter,*[1] *Gernot M. Wallner*[2]

Summary: In this paper, two methods for the determination of infrared optical properties of thick polymer films, based on FTIR spectroscopy, were implemented and used. Complex index of refraction data were generated for various ethylene copolymer films. Transmittance and reflectance spectra were measured in the mid infrared range using a gold-coated 100 mm-diameter integrating sphere. For the investigated films n and k values ranging from 1.3 to 1.6 and from 10^{-4} to 0.25 were determined, respectively. Regarding n, a good agreement was obtained for both methods, the transmittance/reflectance procedure (T/R method) used for transparent and semi-transparent regions, and Single Substractive Kramers-Kronig (SSKK) algorithm applied for non-transparent regions. The highest k values were determined for the CH_2 stretching vibration. The k values are dependent on comonomer content and film thickness. The combination of both methods allows for an accurate determination of n and k in the entire IR region relevant for solar application.

Keywords: complex index of refraction; ethylene copolymer films; FTIR spectroscopy; Kramers-Kronig; solar applications

Introduction

Polymeric materials are already in use for many different solar energy related components. Concerning solar thermal systems plastics play a decisive role as transparent cover and/or convection suppressing material. For such applications the infrared (IR) optical properties of plastics are of prime importance. Contrary to silica glass, which is almost completely opaque to the IR spectrum, the transparency of plastics to the IR spectrum is ranging from highly transparent to almost completely opaque depending on the molecular structure of the polymer. While for solar thermal systems with a black absorber an infrared radiation absorbing cover material is favorable, for solar thermal systems with a selective absorber a non-absorbing cover material is advantageous. For solar thermal applications, an accurate prediction of infrared optical properties as a function of film thickness and temperature is crucial.[1–3] While for low IR absorbing materials (e.g. polymers) often simple methods assuming a constant real part of the refractive index are used, for high IR absorbing materials (e.g. glass, ceramics) comprehensive methods allowing for the determination of both, the real and imaginary part of refractive index (n,k), are a prerequisite.[3,4]

To determine n and k in the infrared range, several methods are described in the literature.[3–14] Currently, mainly spectroscopic ellipsometry (SE) is used for the evaluation of n and k over a wide range of wavelengths.[5–10] By systematic combination of SE with Fourier transform spectroscopy (FT) and development of accurate calibration procedures, the range of application was extended from UV-visible to the infrared.[5] The ellipsometric data are

[1] Polymer Competence Center Leoben GmbH, Roseggerstraße 12, A-8700 Leoben, Austria
Fax: +43 3842 429 626;
E-mail: oreski@pccl.at
[2] Institute of Materials Science and Testing of Plastics, University of Leoben, Franz-Josef-Straße 18, A-8700 Leoben, Austria

usually recorded over the whole spectral range at various angles of incidence. An optical model, which assumes geometry and microstructure, is then applied to calculate the complex index of refraction.[6] A significant drawback of the SE procedure is the necessity to investigate thin films, which are coated on a substrate (e.g. silicon wafers[7] or gold-coated glass slides[8]), or prepared as freestanding films of 12–15 μm thickness.[9] However, commercial polymer films, currently used for greenhouse or transparent insulation applications, are thicker with values ranging from 50 to several hundred microns. Roodenko et al. described the difficulties, which can occur by investigating the infrared optical properties of thick films by FTIR-SE, and the effect on ellipsometric parameters.[10]

In the past, spectroscopic methods were used for determination of the refractive index.[4,11–14] These methods, often requiring special sample preparation techniques, were limited to spectral regions with certain optical properties (transparent, semi-transparent or non-transparent) or based on assumptions such as a constant real part of refractive index. In a recent study, an advanced spectroscopic method, the transmission fringe depth method (RTFD),[11] has been developed for the determination of n and k. However, this method, which is based on the measurement of directional and hemispherical transmittance and reflectance spectra, is applicable only to thin films where interference effects can be observed.

The overall objective of this paper is to implement and apply spectroscopic methods to determine the infrared optical properties of thick polymer films for solar energy applications in all regions of the spectral range (transparent, semi-transparent and non-transparent regions). While for the transparent and semitransparent regions a simple method based on hemispherical transmittance and reflectance spectra was applied, for the non-transparent regions of the IR spectra a more sophisticated algorithm based on the Kramers-Kronig (KK) relation requiring was implemented and used.[3,15]

Experimental Part

Polar ethylene copolymer film types with comonomer contents between 1.7 and 30 wt-% and three different comonomer types (acids, acrylates and acetates) were investigated (Table 1). As to the acid comonomers acrylic acid (AA) and methacrylic acid (MAA) were chosen. Regarding acrylate comonomers butylacrylate (BA), ethylacrylate (EA) and methylacrylate (MA) are currently in use for ethylene (E) copolymer materials. Furthermore, widely used ethylene vinylacetate copolymers (EVA) as well as a terpolymer material with two different comonomers (acrylic acid and butylacrylate (AA/BA) were investigated. In comparison, a non-polar linear low-density polyethylene (LLDPE) was investigated.

The material resins were supplied by Arkema (EBA), Basell (EAA/BA), BP (EMAA), Dow (EAA, LLDPE), DuPont

Table 1.
Investigated ethylene (E) copolymers (material type, comonomer unit, comonomer content and film thickness).

Material type	Comonomer	Content, wt%	Film thickness
EAA	acrylic acid	9.7	125 μm
EMAA	methacrylic acid	1.7, 8.7	110 μm, 90 μm
EBA	butylacrylate	7	125 μm
EEA	ethylacrylate	12	115 μm
EMA	methylacrylate	9	100 μm
EVA	vinylacetate	9, 18	70 μm, 125 μm
EAA/BA	acrylic acid	AA 4	125 μm
	butylacrylate	BA 7	
LLDPE			42 μm, 105 μm

(EMAA, EEA, EMA, EVA). Films with various thicknesses ranging from 40 to 150 μm were cast on a Rosendahl RO400 single screw extruder (Pischelsdorf, Austria) with a chill roll unit of SML Maschinengesellschaft mbH (Lenzing, Austria).

The transmittance (T) and reflectance (R) spectra over the mid-IR range from 4000 to 580 cm^{-1} (2.5 to 17.2 μm) were recorded using a Perkin Elmer Spectrum GX (Perkin Elmer; Überlingen, Germany) with an external 100 mm diameter, gold-coated integrating sphere.

Mathematical Modelling

To calculate the complex index of refraction (n-ik), at least two input data are necessary to derive the two unknown quantities n and k. For transparent and semitransparent regions of the spectral range of the investigated sample, the infrared optical properties can be calculated by measurements of spectral transmittance (T) and reflectance (R) of a single sample.[3] Therefore this method is called T/R method. It is assumed that samples are plane-parallel and sample properties are measured normal to the sample surface. With multiple reflections taken into accounts, T and R can be expressed by surface reflectance ρ and the internal transmittance τ[16]:

$$R = \rho\left[1 + \left(\frac{(1-\rho)^2\tau^2}{1-\rho^2\tau^2}\right)\right] \tag{1}$$

$$T = \tau\frac{(1-\rho)^2}{1-\rho^2\tau^2} \tag{2}$$

First, to determine the complex refractive index, the surface reflectance ρ and the internal transmittance τ values are calculated from R and T:

$$\rho = \frac{1}{2(2-R)}\left[C - \sqrt{C^2 - 4R(2-R)}\right] \tag{3}$$

with

$$C = 1 + 2R + T^2 - R^2 \tag{4}$$

$$\tau = \left(\frac{R}{\rho} - 1\right)\frac{1}{T} \tag{5}$$

Second step is the determination of k. The absorption coefficient a can be calculated from τ and the sample thickness l, k is then derived from a and the wavelength λ:

$$a = -\frac{\ln\tau}{l} \tag{6}$$

$$k = \frac{a\lambda}{4\pi} \tag{7}$$

Finally, the real part of the complex index of refraction is given by:

$$n = \frac{1+\rho}{1-\rho} + \sqrt{\frac{4\rho}{(1-\rho)^2} - k^2} \tag{8}$$

The T/R method is sensitive to n and k as long as T is larger than zero.

If the sample material is non-transparent and the experimental determination of two independent optical properties i.e. the reflectance and transmittance is not possible, the complex refractive index may be calculated from a single quantity such as the reflectance by a Kramers-Kronig integral. If the reflectance has been measured, the phase of the complex reflection coefficient is given by

$$\varphi(\nu) = -\frac{\nu}{\pi}P\int_0^\infty \frac{\ln(R(x))}{(x^2-\nu^2)}dx \tag{9}$$

Because in practice the measurement can only be carried out over a finite range of wave numbers, extrapolation procedures have been developed for the inaccessible wave numbers. However, the result of the integration tends to depend on the kind of extrapolation.[15] To reduce the ambiguity associated with this dependence, Ahrenkiel[15] introduced the Singly Subtractive Kramers-Kronig method (SSKK). The idea is to use the phase known at one wave number, which is obtained by reflectance and transmittance measurements, to improve the convergence of the Kramers- Kronig integral and therefore make it less dependent on the extrapolation. By using the known phase φ_0 at a wave number ν_0 in the

Kramers-Kronig integral, Ahrenkiel derived the subtractive Kramers-Kronig integral

$$\varphi(\nu) = \frac{\nu}{\nu_0}\varphi(\nu_0) + \frac{\nu(\nu_0^2 - \nu^2)}{\pi} P \int_0^\infty \frac{\ln(R(x))}{(x^2 - \nu_0^2)(x^2 - \nu^2)} dx \quad (10)$$

By using cubic splines to represent ln(R(x)) the integrand is a proper rational function on each interval defined by the spline nodes and therefore the integral can be simplified by partial fraction decomposition,

$$\frac{ax^3 + bx^2 + cx + d}{(x^2 - \nu_0^2)(x^2 - \nu^2)} = \frac{A}{x - \nu} + \frac{B}{x + \nu} + \frac{C}{x - \nu_0} + \frac{D}{x + \nu_0} \quad (11)$$

where A, B, C and D depend on ν, ν_0 and the spline parameters a, b, c and d. For each of the four terms the standard integral as well as the Cauchy Principal Value integral, which needs to be taken when either ν or ν_0 are in the interval, can be solved in terms of logarithms.

However, the SSKK method is sensitive to n in the entire spectral region, but insensitive to k in the transparent and semitransparent region.[3]

Results and Discussion

For greenhouse or transparent insulation wall applications it is crucial to absorb the infrared radiation as well as possible in order to keep the heat radiation low. Thus, high IR absorption is required in the range between 200 and 1500 cm $^{-1}$, in which a blackbody at 20 °C emits mostly. Figure 1 displays the transmittance and reflectance spectra over the medium IR range for selected ethylene copolymer films with film thicknesses ranging from 40 to 125 μm.

Significant absorptions in the investigated polar polyethylene copolymers can be attributed to CH_2 and CH_3 groups (between 3000 and 2800, at about 1470, 1380 and 720 cm $^{-1}$), to C=O double bonds (between 1750 and 1700 cm $^{-1}$) to C–O single bonds (between 1300 and 1000 cm $^{-1}$) and to hydroxyl (O–H) groups in acid copolymers (at about 950 cm $^{-1}$). Below 1000 cm $^{-1}$ mainly molecular vibrations of the polymer chain contribute to the absorption. However, the molecular vibrations are rather weak for the investigated polymers. Close to the maximum of the emissive power function of a blackbody at 20 °C, the narrow absorption peak at 720 cm $^{-1}$ of the CH_2 group can be found for all investigated polymers. CH_2 groups are rather weak dipoles with low absorbance in the relevant IR wavelength range. In contrast, C–O and O–H single bonds are stronger dipoles with a higher specific absorbance in the relevant range. However, in polar ethylene copolymers CH_2 groups are dominating.

The reflectance values of all investigated polymer films are rather constant over the mid-IR range, only little variations can be seen in the areas of high absorbance. The reflectance values are well below 10%.

Figure 2 shows the integrated transmittance (T), reflectance (R) and absorbance values (A), which were determined by averaging the spectral values, weighted by a blackbody emissive power function, P(ν,T) at a temperature of 20 °C, at each wave number.[11–14] The reflection values of the investigated polymer films show little difference and are ranging from 0.042 to 0.048, except for the 18% EVA film (125 μm), with a significant lower value of 0.031, and for the EAA 9.7% film (125 μm) with a significant higher value of 0.056. As expected, the absorption of the LLDPE films was lowest, with transmission values of 0.82 (42 μm film) and 0.74 (105 μm film). For EMAA 1.7% also low absorption was observed, which can be attributed to its low comonomer content. The ethylene acrylate copolymers (EBA; EMA; EEA) exhibit medium transparency in the IR region with absorption values ranging from 0.33 to 0.38, despite the different film thicknesses and

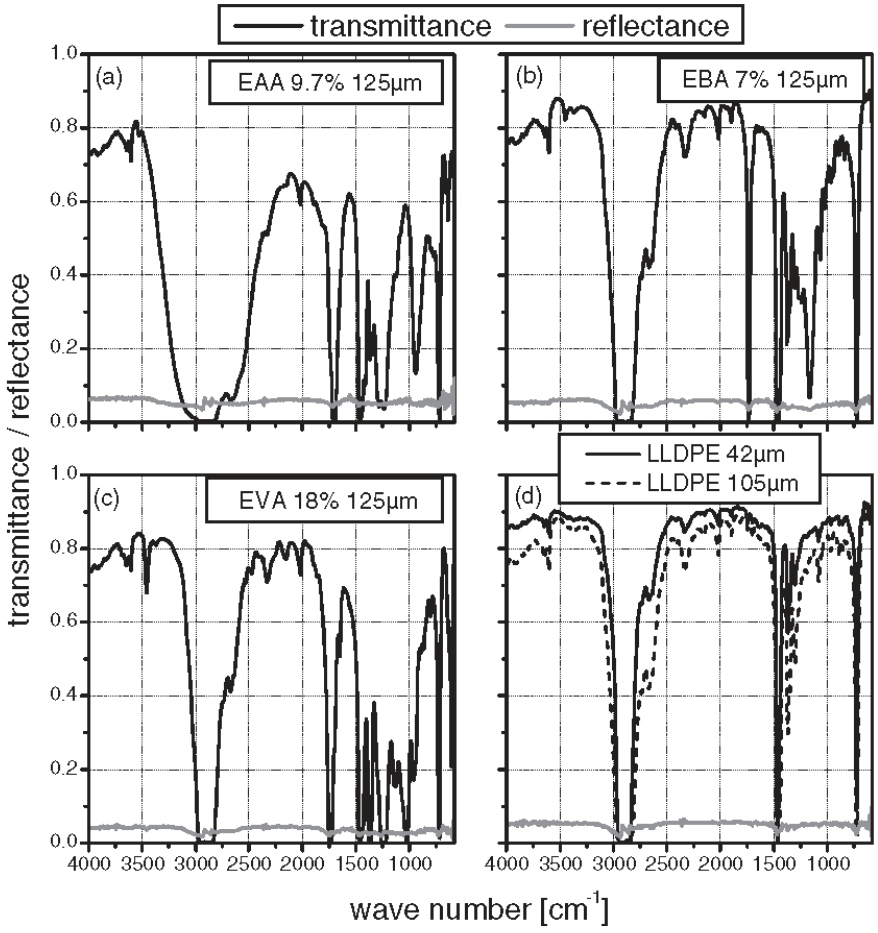

Figure 1.
Transmittance and reflectance spectra of (a) EAA 9.7% (125 µm film), (b) EBA 7% (125 µm film), (c) EVA 18% (125 µm film) and (d) LLDPE (42 and 105 µm film).

conomomer contents. In comparison, for the ethylene acid copolymers higher absorption values of about 0.41 for EMAA 8.7% (90 µm), 0.52 for EAA-BA 11% (125 µm) and EAA 9.7% (125 µm) were found. Due to the high amount of vinyl acetate groups EVA 18%, for these films the highest absorption values of about 0.6 were determined. As already reported in previous studies,[13,14] ethylene copolymers containing acid groups exhibit the highest infrared absorption values, provided that film thickness and comonomer content are identical. This can be attributed to material dependent differences in the IR spectra, especially in the region between 1300 and 900 cm^{-1}. Copolymers containing an acid group (EMAA, EAA, EAA-BA) show a medium peak at about 950 cm^{-1} (Figure 1a) caused by the carboxylic group of the polymer. This intense peak is located very next to the emittance maximum of a black body at 20 °C.[13,14]

Usually T, R and absorbance A are independent of film thickness in the transparent region of the spectral range. Banner et al.[17] defined the transparent region by an absorption coefficient $a < 10^0$ cm^{-1}. In the non-transparent region ($a > 10^3$ cm^{-1}), the internal transmittance becomes zero and reflectance and absorbance are almost surface properties. In the semitransparent region (absorption coefficient between 10^0 and 10^3 cm^{-1}) transmittance, reflectance and absorbance are strongly thickness dependent. In case of

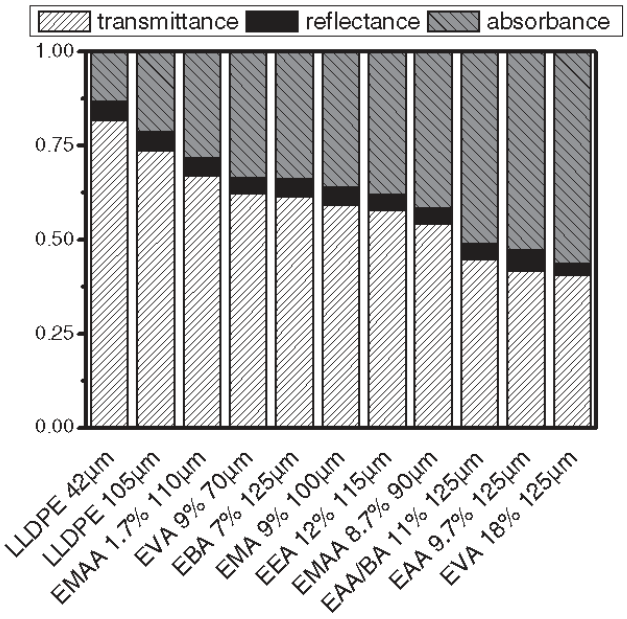

Figure 2.
Transmittance, reflectance and absorbance values, weighted with the emissive power function of a blackbody at 20 °C, for the investigated polymer films.

LLDPE (Figure 1(d)) it could be observed, that transmittance values show a higher dependence on film thickness than reflectance values, which are nearly identical.

In general, scattering in the infrared wavelength range of the material is neglected.[16] This assumption was confirmed by comparing hemispherical transmittance spectra measured with an integrating sphere to spectra measured directionally. The results for 125 µm thick EVA (18%) and EAA (9.7%) films are shown in Figure 3. Only small differences solely in areas of high transmittance can be seen.

In Figure 4 the validity regions of the T/R and the SSKK method is shown with reference to a transmittance spectrum of a 125 µm EAA 9.7% film. The threshold to distinguish the non-transparent from the semitransparent region was defined at a transmittance value of 0.01. Regarding the real part of the refractive index, the SSKK algorithm is sensitive over the whole spectral range and therefore the fastest method to determine n accurately. But, since the investigated ethylene copolymers are highly transparent in the IR range, also the T/R method is applicable nearly over the whole spectral range. Only small areas of total absorption have to be excluded. The determination of the imaginary part of the refractive index is more complicated. A combination of both methods (Figure 4)

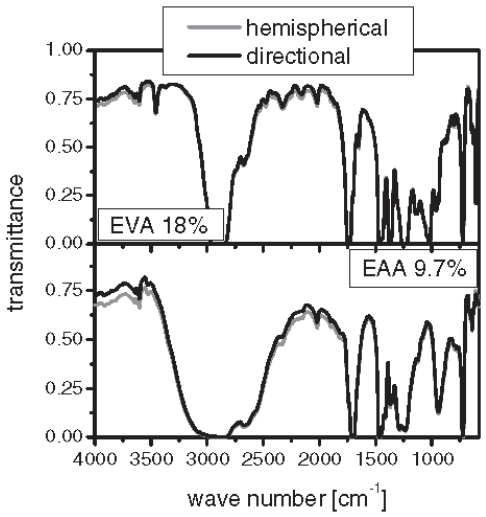

Figure 3.
Comparison of hemispherical (recorded with an integrating sphere) and directional transmittance spectra of 125 µm EVA 18% (top) and EAA 9.7% film (bottom).

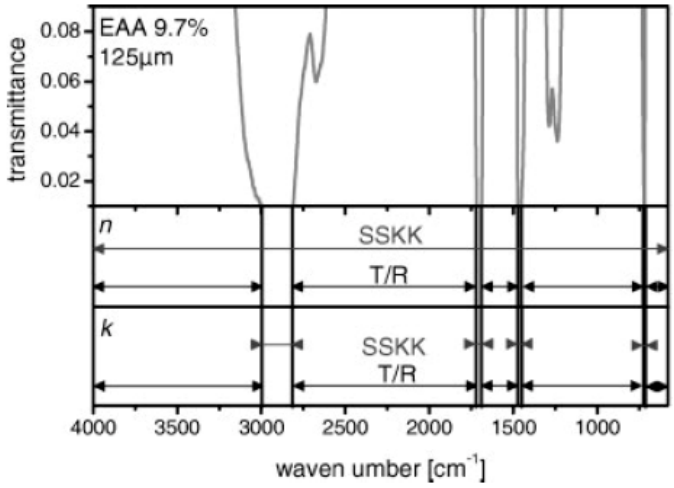

Figure 4.
Validity of the T/R and the SSKK method shown with reference to the transmittance spectra of 125 µm EAA 9.7% film.

has to be applied to calculate k over the whole spectral range.

The real part of the refractive index, determined by the SSKK algorithm, is shown in Figure 5 as a function of wave number for selected ethylene copolymer films. Whereas the highest values for *n* ranging from 1.5 and 1.6, were found for EAA 9.7%, EVA 18% exhibited the lowest values for *n* ranging from 1.3 and 1.4. The *n* values of the other ethylene copolymer films are lying between 1.4 and 1.5. The order of the n values is in agreement with the measured reflectance values.

For LLDPE it is observable, that slight differences in reflectance cause significant differences in *n* (Figure 6). On average, the 42 µm thick film showed a value of about 0.02 lower than the 105 µm thick film.

Figure 7 shows the real part of refractive index, calculated by the T/R and the SSKK

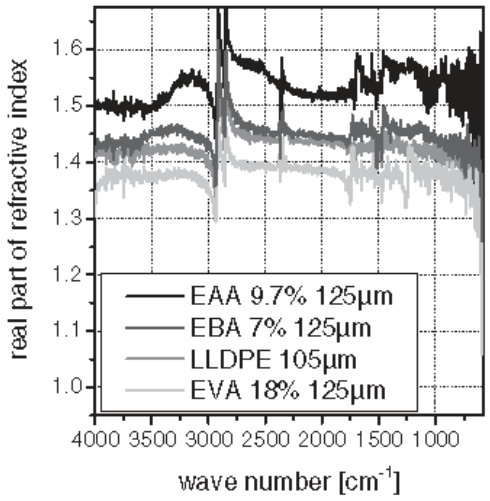

Figure 5.
Real part of refractive index calculated by the SSKK algorithm for selected ethylene copolymer films, as a function of wave number.

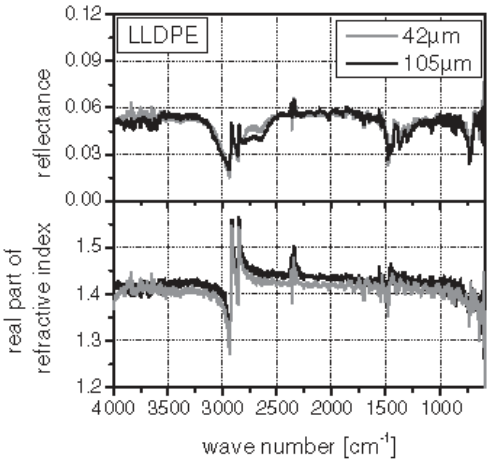

Figure 6.
Reflectance spectra and real part of refractive index, calculated by the SSKK algorithm for 42 and 105 µm thick LLDPE films as a function of wave number.

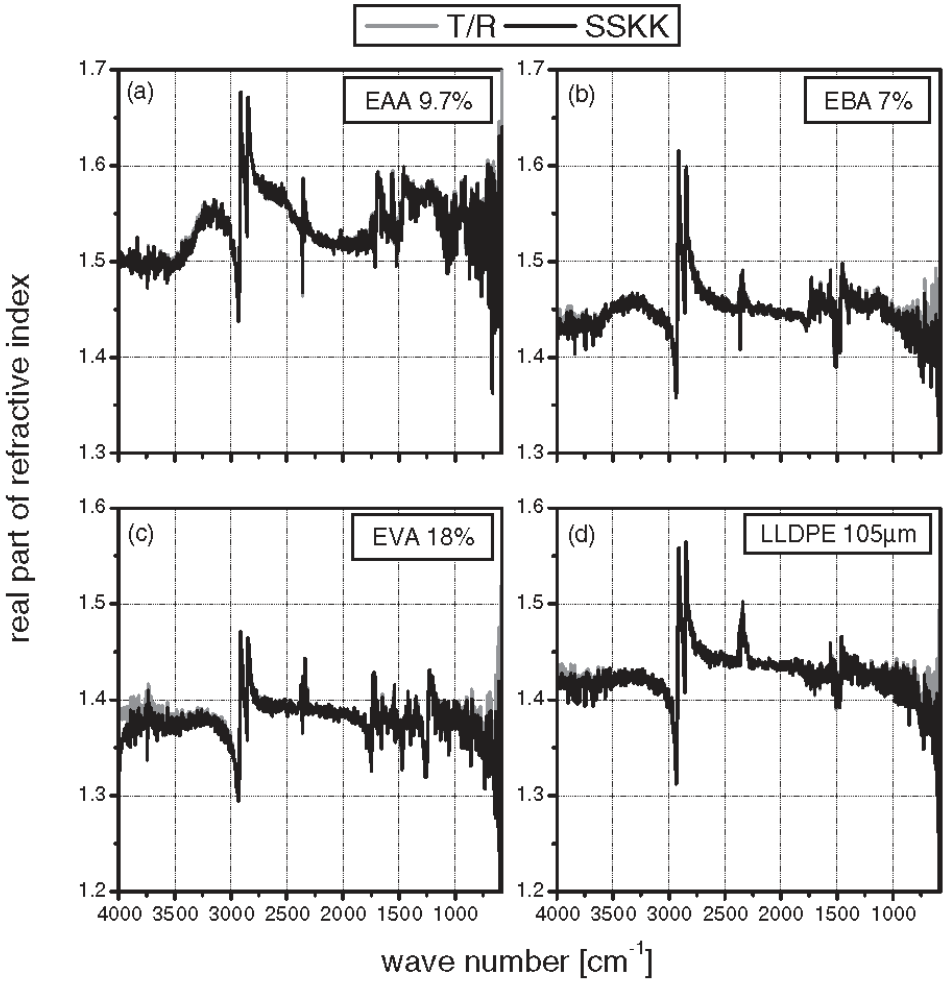

Figure 7.
Comparison of the T/R and the SSKK method for calculation of the real part of refractive index, shown for (a) EAA 9.7% (125 µm film), (b) EBA 7% (125 µm film), (c) EVA 18% (125 µm film) and (d) LLDPE (105 µm film).

method, as a function of wave number. In case of the T/R method, the non-valid values in non-transparent regions were excluded. In general, both methods are in good agreement regarding n. Slight differences can be seen only between 4000 and 3700 cm^{-1} and at wave numbers below 800 cm^{-1}.

Comparing both methods, the SSKK algorithm is more appropriate to calculate the real part of the refractive index, as it yields values for n without any limitations over the whole range of interest.

For the calculation of the imaginary part of the refractive index both methods have to be applied to obtain results over the whole spectral range. In Figure 8 the k values from 4000 to 580 cm^{-1} are shown for selected films. In the transparent region, the k is about 10^{-4}, increasing to 10^{-2} in the semitransparent region. In areas of total absorption, k values reach about 0.25 for the strongest absorption peak, (i.e. CH_2 stretching vibration between 3000 and 2800 cm^{-1}). Medium absorption bands (e.g. $\nu C{=}O$, $\nu C{-}O$, δCH_2, ρCH_2) exhibit k values up to 0.1. The area of change-over between the k values calculated by the T/R method and the values determined by the SSKK algorithm is not fully covered, especially at the absorption peaks below 1800 cm^{-1}. In some cases (e.g. ρCH_2 at

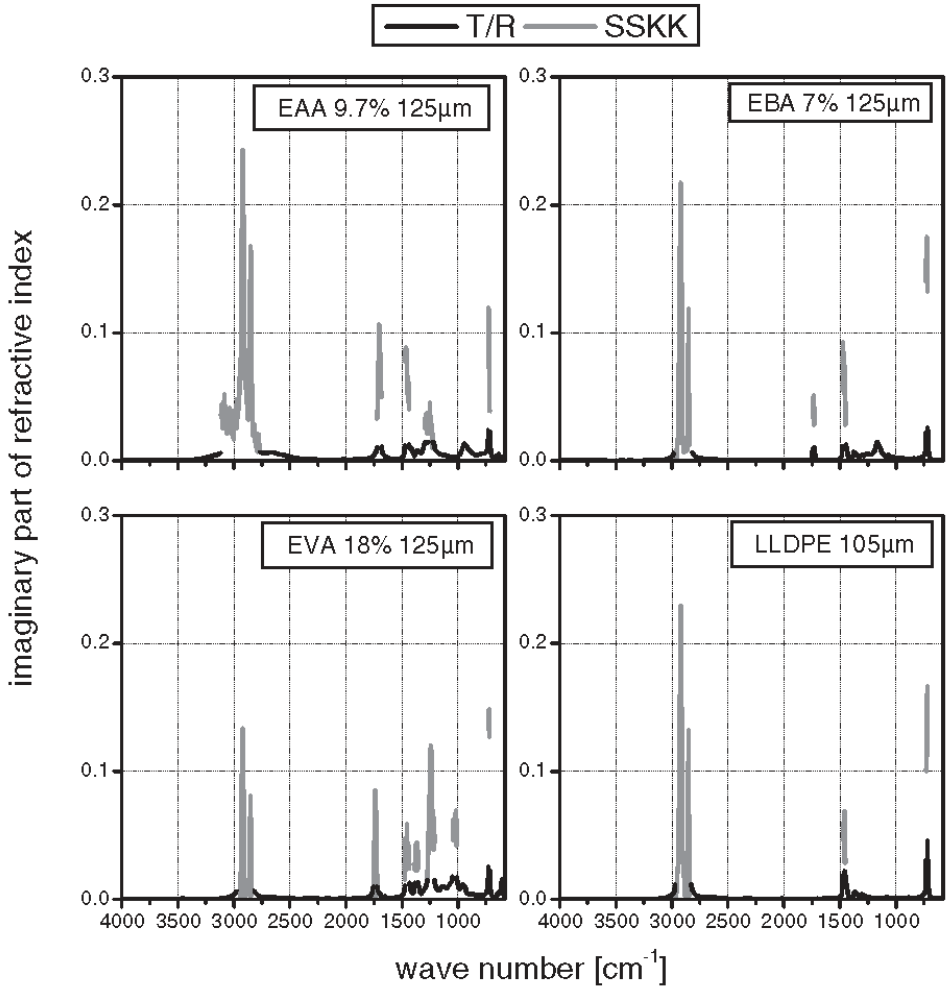

Figure 8.
Imaginary part of refractive index as a function of wave number, shown for (a) EAA 9.7% (125 µm film), (b) EBA 7% (125 µm film), (c) EVA 18% (125 µm film) and (d) LLDPE (105 µm film).

about 720 cm ^{1}) the values of k switch over one order of magnitude in one step. For a better definition of the change-over between both methods, higher resolution spectra should be measured.

Acknowledgements: This research work was performed at the Polymer Competence Center Leoben (PCCL) within the research project II-S.5 in cooperation with the Institute of Materials Science and Testing of Plastics at the University of Leoben. The PCCL is founded by the Austrian Government and the State Governments of Styria and Upper Austria within the K_{plus} program of the Austrian Ministry of Traffic, Innovation and Technology. The authors wish to express their gratitude to Arkema, Basell, DOW and DuPont for providing the materials.

[1] P. T. Tsilingiris, *Energy Conversion and Management* **2003**, *44*, 2839.
[2] G. Papadakis, D. Briassoulis, G. Scarascia Mugnozza, G. Vox, P. Feuilloley, J. A. Stoffers, *J. agri. Engng Res.* **2000**, *77*, 7.
[3] H. Mehling, *"Determination of infrared optical properties and phononic thermal conductivity of non-scattering inorganic and nonmetallic materials"*, PhD thesis, Universität Würzburg 1998.
[4] G. M. Wallner, W. Platzer, R. W. Lang, *Solar Energy* **2005**, *79*, 593.
[5] B. Drévillon, *Thin Solid Films* **1998**, *313–314*, 625.

[6] J. A. Wollam, C. Bungay, J. Hilfiker, T. Tiwald, *Nucl. Instrum. Methods Phys. Res., Sect. B* **2003**, *208*, 35.
[7] D. Tsankow, K. Hinrichs,, A. Röseler,, E. H. Korte, *phys. stat. Sol. (a)* **2001**, *188*, 1319.
[8] K. Hinrichs, M. Gensch, N. Nikonenko, J. Pionteck, K. J. Eichhorn, *Macromol. Symp.* **2005**, *230*, 26.
[9] M. Gioti, A. Laskarakis, S. Logothetidis, *Thin Solid Films* **2004**, *455–456*, 283.
[10] K. Roodenko, M. Gensch, H. M. Heise, U. Schade, N. Esser, K. Hinrichs, *Infrared Physics & Technology* **2006**, *49*, 39.
[11] Y. P. Zhang, X. S. Ge, *Solar Energy Materials and Solar Cells* **1995**, *37*, 379.
[12] G. Wallner, *"Kunststoffe für die transparente Wärmedämmung – Polymerphysikalische Einflüsse und Modellierung"*, PhD thesis, Montanuniversität Leoben 2000.
[13] G. Oreski, G. M. Wallner, *Solar Energy Materials & Solar Cells* **2006**, *90*, 1208.
[14] G. Oreski, G. M. Wallner, *Chemical Monthly* **2006**, *137*, 899.
[15] R. K. Ahrenkiel, *J. Opt. Soc. Am.* **1971**, *61*, 1651.
[16] R. Siegel, J. R. Howell, *"Thermal Radiation Heat Transfer"*, Hemisphere, Washington 1980.
[17] D. Banner, S. Klarsfeld, C. Langlais, *HighTemp – High Press* **1989**, *21*, 347.

3 Aging and Degradation Behavior of Polar Ethylene Copolymer Films

Knowledge and understanding of the degradation behavior of ethylene copolymer films is crucial for the application dependent lifetime. It is important to know how chemical and physical aging of the polymer films influence and change the overall performance.

Up to now the main focus has been given to investigate the thermal degradation behavior of polar ethylene copolymers with regards to changes in material chemistry (Allen et al., 2000; Allen et al., 2001; Jäger et al., 2002; McNeill and Barbour, 1987; McNeill and Mohammed, 1995; McNeill et al., 1998; Rodríguez-Vázquez et al., 2006; Sultan and Sörvik, 1991). Except for EVA, for polar ethylene copolymer films no studies on photo-degradation could be found. For EVA films investigations on a specimen level were conducted, and the impact of weathering in overall performance and reliability in application was discussed (Czanderna and Pern, 1996; Klemchuck et al., 1997; Kempe et al., 2007; Briassoulis et al., 1997; Dilara and Briassoulis, 1998). Regarding relevant characterization methods to describe the aging behavior and to predict reliability, usually ultimate mechanical properties derived from unnotched samples are determined neglecting the effect of film thickness on their significance (Briassoulis et al., 1997; Dilara and Briassoulis, 1998). Only in a few studies, not focusing on polar ethylene copolymer materials, also mechanical properties derived from notched specimen were considered as an indicator for aging (Fayolle et al., 2000; Fayolle et al., 2002; Wallner et al., 2004).

Hence, the main objective of this chapter is a detailed characterization and description of the aging behavior of ethylene copolymer films, with focus on the overall performance and reliability of the materials in application. Paper 4 focuses on the description of the aging behavior of commercially available EVA greenhouse films due to accelerated weathering, whereas the focus of Paper 5 was given to a screening testing of unstabilized ethylene copolymer films.

Commercially available stabilized multi-layer EVA films and several unstabilized ethylene copolymer films were weathered artificially. To characterize the films, on

the one hand, analytical test methods such as thermoanalysis, FTIR- and UV/VIS/NIR spectroscopy are applied to check physical and chemical changes. On the other hand, a comprehensive mechanical characterization was done. Finally, the ultimate mechanical properties are correlated to weathering induced morphological and chemical changes. The significance of analytical and mechanical methods to describe the aging behavior with respect to durability and reliability of polymeric films after weathering is checked. Special focus is given on the one hand to the separation of chemical and physical aging, and on the other hand, to the distinction of local (initial) and global aging. Furthermore, the intrinsic weathering stability of polar ethylene copolymers is investigated and the effect of degradation on the prime properties determined.

In Paper 4 of this Dissertation, the comparison of ATR and FTIR spectra with mechanical properties suggests that degradation of the investigated polymer films is strongly confined to the surface. Deformation at break values attained from tensile tests of notched specimens proved to be a sensitive indicator for global aging. By comparison, strain at break values gained from unnotched specimens were more sensitive to initial aging and local defects. A correlation between formation of degradation products within the bulk, indicated by FTIR spectroscopy, and ultimate mechanical properties was obtained. Tensile tests appeared to be the most versatile method in describing aging.

Paper 5 shows, that melting temperatures and degree of crystallinity were depending on comonomer content. Regarding mechanical properties, the ethylene copolymer films exhibited a highly ductile behavior and high flexibility. Though the comonomer content is comparable to the other copolymers, the acid copolymers showed higher tensile strength values than the acrylate and acetate copolymers. Due to formation of chromophoric degradation products, yellowing was observed. The investigated films revealed high embrittlement due to weathering. Secondary crystallization with a dramatic increase in degree of crystallinity was observed by DSC measurements.

Paper 4: Aging Characterization of Commercial Ethylene Copolymer Greenhouse Films by Analytical and Mechanical Methods

Oreski, G., Wallner, G.M.

submitted to Biosystems Engineering (August 2008)

Aging Characterization of Commercial Ethylene Copolymer Greenhouse Films by Analytical and Mechanical Methods*

Oreski G. [1], Wallner G.M. [2], Lang R.W. [2]

[1]Polymer Competence Center Leoben GmbH, Roseggerstraße 12, A-8700 Leoben, A

[2]Institute of Materials Science and Testing of Plastics, University of Leoben, Franz Josef Straße 18, A-8700 Leoben, A

Corresponding Author, email: oreski@pccl.at, fax: +43 3842 429 626

Abstract

This paper focuses on the description of the aging behavior of ethylene(vinylacetate) (EVA) greenhouse films due to accelerated weathering. Two commercially available multi-layer films were chosen as model materials. The degradation behavior was analyzed by infrared spectroscopy (IR) in transmittance and attenuated total reflectance (ATR)-mode, by UV/VIS/NIR-spectroscopy, differential scanning calorimetry (DSC) and by comprehensive mechanical characterization. Using IR spectroscopy hydroxyl, vinylidene and acid groups were identified as main degradation products. By IR and UV/VIS/NIR-spectroscopy the consumption of stabilizers was detected. Post crystallization was detected by DSC measurements. The analytical results of the weathered films were correlated to ultimate mechanical properties determined by investigating unnotched and notched specimens. The results suggest that degradation of the investigated polymer films is strongly confined to the surface. While both films were of different layer structure, in contrast to the 30 µm thick film, the aging processes on the surface of the 200 µm thick films are not reflected by mechanical properties. Nevertheless, tensile tests appeared to be the most versatile method for describing aging phenomena. Both chemical aging and physical aging as well as local (initial) and global aging effects are reflected by mechanical properties.

*Paper submitted to Biosystems Engineering (August 2008).

1. Introduction

Ethylene homo- and copolymer films are common greenhouse cover materials with some specific advantages compared to glass (e.g., easy to handle, good optical and mechanical properties, low weight and low-cost production). Nearly all greenhouse films on the market today are co-extruded films, which consist of several polyethylene (PE) and ethylene(vinylacetate) (EVA) layers. Additional EVA layers with 4-10m% vinylacetate comonomer increase the flexibility, the mechanical strength and the resistance to ultra-violet (UV) radiation (Dilara and Briassoulis, 2000). Furthermore, the spectral selectivity, which refers to high transparency in the solar range and absorbance in the infrared range, is enhanced by introducing EVA (Oreski and Wallner, 2006). When being used in outdoor applications, greenhouse films should provide a good resistance against environmental influences (e.g. solar radiation, temperature, wind and snow loads, hail, agrochemicals) and a certain level in mechanical properties needs to be maintained. The aging behavior and degradation mechanisms of EVA and especially of EVA greenhouse films are well described in the literature (Dilara and Briassoulis, 2000; Sultan and Sörvik, 1991; Allen et al., 2000; Allen et al., 2001; Rodríguez-Vázquez et al., 2006). However, in many studies the focus is given to the chemical material changes, without discussing the overall performance and reliability in application. Regarding relevant characterization methods to describe the aging behavior and to predict reliability, often ultimate mechanical properties derived from unnotched samples are determined neglecting the effect of film thickness on their significance (Briassoulis et al., 1997; Dilara and Briassoulis, 1998). Also, no difference between local (initial) aging and global aging, and in case of films, no difference in surface and volume aging has been made. In few studies, not focusing on polar ethylene copolymer greenhouse films, mechanical properties derived from notched specimens were considered as an indicator for global aging (Wallner et al., 2004).

Hence, the main objective of this paper is to check the significance of analytical and mechanical methods to describe the aging behavior. Special focus is given on the one hand to the separation of chemical and physical aging, and on the other hand, to the distinction of local (initial) and global aging. For that purpose

commercial EVA greenhouse films of unknown composition with two different thicknesses (30 and 200 µm) were chosen as model films and were weathered artificially. To characterize the films, on the one hand, analytical test methods such as thermoanalysis, FTIR- and UV/VIS/NIR spectroscopy were applied to check physical and chemical changes. On the other hand, a comprehensive mechanical characterization was done. Finally, the ultimate mechanical properties were correlated to weathering induced morphological and chemical changes.

2. Experimental

Two different Commercial greenhouse films with a thickness of 30µm and 200 µm were chosen as model material (Table 1). Unfortunately, the data sheets of both films provide no information as to the multi-layer build up and the precise nature of materials used for each layer.

Table 1: Investigated EVA films

Manufacturer	Abbreviation	Product name	Film thickness
Eiffel S.p.A (Parma, I)	Eif30	Film EVA	32 µm
	Eif200	Multisolar 33	200 µm

Artificial weathering of rectangular tensile test specimens with a width of 15 mm was done using a Xenon Arc artificial weathering chamber (Atlas Material Testing Technology LLC, Chicago, USA). The specimens were exposed to 60 W/m² UV-irradiance (300 to 400 nm) at a chamber temperature of 40 °C and a relative humidity of 65% for 250, 500, 1000, 2000 and 3000 hours.

The aging behavior was characterized by infrared spectroscopy (FTIR) and by UV/VIS/NIR spectroscopy, by differential scanning calorimetry (DSC) and tensile testing. FTIR analysis was done in transmittance and in attenuated total reflectance (ATR), using a Spectrum GX FTIR spectrometer (Perkin Elmer Analytical Sciences, Überlingen, D) with a Pike Miracle Micro-ATR device (Pike Technologies, Madison, USA). The transmittance spectra were recorded over the IR range from 4000 to 400 cm^{-1}, the ATR spectra from 4000 to 650 cm^{-1}. For better comparison, all ATR spectra were normalized. The wave number dependent

penetration depth was corrected using the Perkin Elmer Software integrated ATR correction.

The UV/VIS/NIR measurements were carried out using a Lambda 950 UV/VIS/NIR spectrometer with integrating sphere to measure hemispherical transmittance and reflectance spectra (Perkin Elmer Analytical Sciences, Überlingen, D). Spectra were recorded from 250 to 2500 nm.

Thermal analysis was performed using a Mettler DSC 821e instrument (Mettler Toledo GmbH, Schwerzenbach, CH). Thermograms were recorded under static air from ambient temperature to 300 °C at a heating rate of 10 K/min. A circular sample disc was cut with a punch, put in a 40 μl pan and closed with a perforated lid. Melting point and melting enthalpy were evaluated according to ISO 11257-2 and ISO 11257-3. Tensile tests on unnotched and double-edge notched samples were carried out with a screw driven universal test machine of the type Instron 4505 (Instron International Ltd., High Wycombe, UK) at 23 °C according to EN ISO 527-3. Specimens were cut prior to exposure using a device with fixed razor blades and rotating sample. The overall length and the measuring length of the samples were limited to 110 and 75 mm, respectively. After exposure the double-edge notches (length: 3.5 mm, remaining ligament length: 8 mm) were cut with a razor blade. The test speed was 50 mm/min. From a total of at least four specimens, for each test series average numbers for strain-at-break (σ_B) and strain-at-break (ε_B, unnotched samples) as well as maximum force (F_{max}) and deformation-at-break (s_B, notched samples) were deduced.

3. Results and Discussion

The initial step of EVA degradation is the formation of acetic acid and the formation of double bonds in the main chain. Further degradation products reported in the literature are lactones, formed by intramolecular back-biting by the acetate group and the evolution of methane, and the production of ketones and acetaldehyde (Sultan and Sörvik, 1991; Allen et al., 2000; Allen et al., 2001; Rodríguez-Vázquez et al., 2006). Furthermore, α,β-unsaturated carbonyl groups, hydroperoxides and anhydrides are formed during oxidation process (Allen et al., 2000).

Figure 1 shows the ATR absorbance spectra of unaged and weathered EVA greenhouse films with a thickness of 30 µm (Eif30) and 200 µm (Eif200). Unaged spectra show the typical peaks of EVA at 2916, 2848, 1463, 1370 and 730 cm^{-1} caused by the vibrations of the CH_2 and CH_3 groups and at 1740, 1238 and 1020 cm^{-1} related to carbon oxygen double and single bonds, respectively.

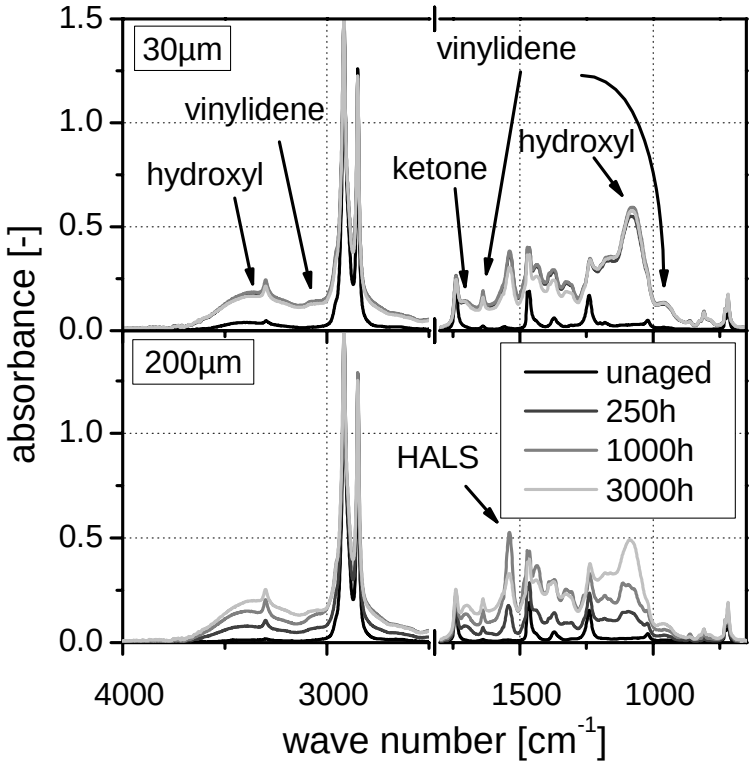

Fig. 1: ATR absorbance spectra of unaged and weathered EVA greenhouse films. Top: Eif30 (30 µm); bottom: Eif200 (200 µm).

Several additional peaks can be identified in the spectra of the weathered greenhouse films. The broad bands between 3700 and 3100 cm^{-1} and between 1200 and 1050 cm^{-1} can be assigned to hydroxyl groups of alcohols, peroxides and hydroperoxides. In the region between 1800 and 1650 cm^{-1} several peaks developed, which can be attributed to the formation of lactones (1780 cm^{-1}), aliphatic esters (1740 cm^{-1}) and saturated and unsaturated acid groups (1680-1710 cm^{-1}). The weak peaks at 1180 (carbonyl stretch vibration of ketone) and 1159 cm^{-1} (C-O-C stretch vibration of aliphatic ester) confirm this assignment (Allen et al., 2000).

Peaks appearing at 1641 cm^{-1} (C=C stretch), 960 cm^{-1} (trans vinylidene groups, out-of-plane bending) and the shoulder at 3010 cm^{-1} (=CH Stretch) are related to the formation of double bonds. Whereas for the 200 µm thick film the peaks related to degradation products develop continuously, indicating the progress of photo-degradation from the surface to the bulk, the spectrum of the 30 µm film does not reveal significant differences in the intensities of the absorption peaks related to degradation products after 250 h of weathering time. The constant absorption intensities of the degradation products after 250 h of artificial weathering suggest a rapid consumption of the stabilizers.

Additional bands appeared at 1540, 861 and 809 cm^{-1}. The peak at 1540 cm^{-1} can be assigned to the triazine group of a hindered amine light stabilizer (HALS). For the 30 µm thick film a steep increase of the band intensity is observable within the first 250 h of weathering. After reaching a maximum at 500 h, a slow decrease of the absorption intensity was found. For 200 µm film a rather constant increase of the intensity was detected until 1000 h of weathering. After the maximum reached at 1000 h, a more pronounced decrease in absorption intensity occurs compared to the 30 µm film. The peaks at 861 cm^{-1} and at 809 cm^{-1} are duo to the aromatic ring of hindered phenols (antioxidants) and hydroxybenzophenones (UV-absorber). For both peaks a similar behavior due to weathering compared to HALS was observed.

Figure 2 depicts the FTIR absorbance spectra of 30 and 200 µm thick films. For 30 µm thick films only slight changes due to weathering were observed. Broad bands between 3700 and 3100 cm^{-1} and between 1200 and 1050 cm^{-1} indicate the formation of hydroxyl groups. Carbon double bonds are seen in the peak appearing at 1641 cm^{-1}. However, compared to ATR spectra no peaks due to stabilizers were detected. For 200 µm film an even lesser increase in the area between Broad bands between 3700 and 3100 cm^{-1} and 1200 and 1050 cm^{-1} was observed. Only the peak at 1540 cm^{-1}, which can be assigned to HALS, showed a significant decrease after 2000 h of weathering. Both absorbance spectra from FTIR and ATR spectroscopy indicate the diffusion of HALS additives to the surface and the subsequent consumption and loss. Peaks due to aromatic rings of antioxidants and UV absorber were not detectable. As the main focus of this paper

is on mechanical properties as they are affected by aging, no further investigations on stabilizer migration and consumption were done.

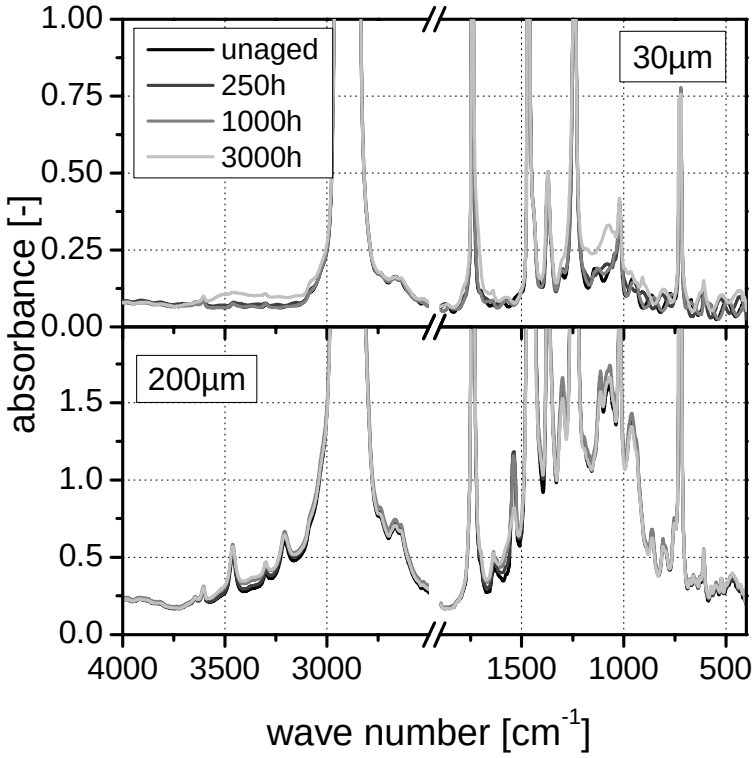

Fig. 2: FTIR absorbance spectra of unaged and weathered EVA greenhouse films. Top: Eif30 (30 µm); bottom: Eif200 (200 µm).

Figure 3 shows the UV/VIS/NIR spectrum of unaged and weathered greenhouse films with a thickness of 30 µm (Eif30) and 200 µm (Eif200). While the peak at 285 nm can be assigned to the aromatic ring of antioxidants and the UV-absorber, the peak at 325 nm is related to the keto-enol tautomerism of the hydroxybenzophenone group in the UV Absorber. For the 200 µm thick film, a rather constant decrease in the UV absorbance at 285 and 325 nm was observable, indicating a still effective UV protection after 3000 h. In contrast, the 30 µm thick films showed very low absorption in the UV region indicating only small amounts of UV-absorber. After 250 h of weathering the UV-absorber is depleted and no distinctive peak is observable. The increase of absorption from 250 to 500 nm after 3000 h of aging can be attributed to chromophoric species, which are formed during weathering (Allen et al., 2000; Allen et al., 2001; Rodríguez-Vázquez et al., 2006).

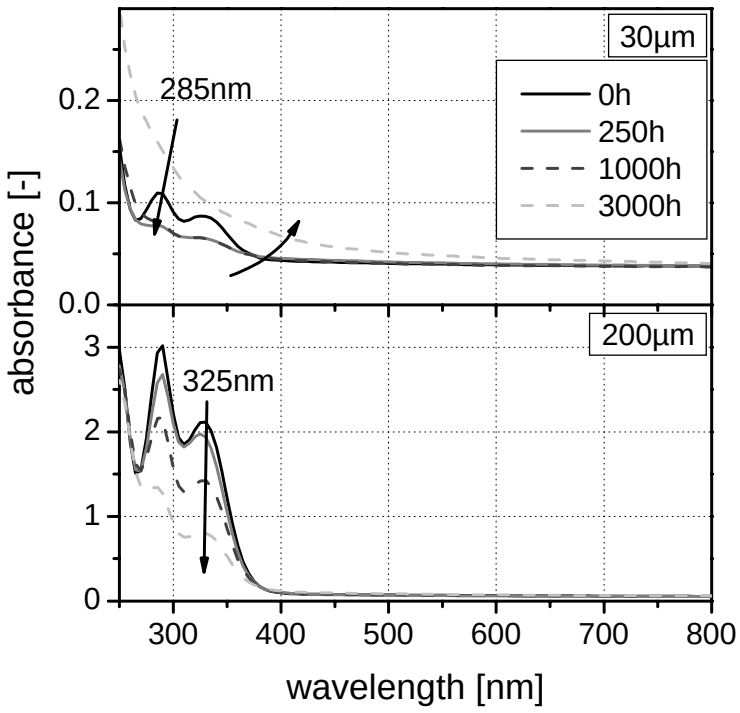

Fig. 3: UV/VIS of weathered EVA greenhouse films. Top: Eif30 (30 µm); Bottom: Eif200 (200 µm)

The results of the DSC measurements are shown in Fig. 4 and displayed in Table 2. Due to the multi-layer build-up, all polymer films exhibit several melting peaks between 95 and 125 °C. The different melting temperatures correspond with different VA contents of the single layers. For the 30 µm thick films the melting peak of about 119 °C can be assigned to low density polyethylene (PE-LD). Since the ATR spectra of all investigated films showed no difference between top and bottom side, a three-layer build-up with equal top and bottom sides is suggested. Furthermore, a weak endothermic peak at about 45 °C was observed for all films, which can be attributed to a secondary, less organized crystal phase (Brogly et al., 1997). The oxidation temperature T_{ox} reaches values of 225 °C for the 200µm thick films and 207 °C for 30 µm thick films.

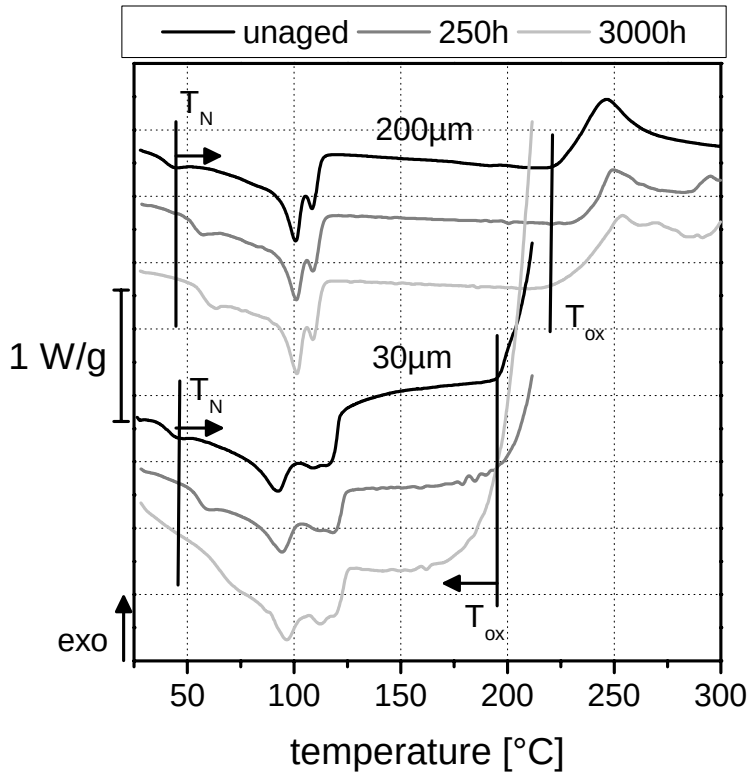

Fig. 4: DSC thermograms of unaged and weathered 30 µm (Eif30) and 200 µm (Eif200) thick greenhouse films.

Table 2: Endothermic peak and oxidation temperatures of the investigated greenhouse films. Main melting peaks are marked with an *.

film	**endothermic peaks**			**oxidation**
	T_N [°C]	T_{M1} [°C]	T_{M2} [°C]	T_{OX} [°C]
Eif30	45.9±2.1	94.4±0.8	119.0±0.0*	206.9±0.9
Eif200	45.0±1.9	101.0±0.8*	107.5±1.8	225.3±4.4

The melting peaks remained constant after weathering. In case of the 200 µm thick film, the initial T_{ox} value of 225 °C remained nearly constant up to 3000 h of xenon weathering. In contrast, for the 30 µm film a slight decrease of the oxidation temperature from 207°C to 196 °C was observed. As shown in Fig. 4, for the first 250 h of xenon aging a significant increase of the secondary crystallization peak temperature can be observed, which levels off at temperature values of about

60 °C for the 200 µm thick film. The 30 µm thick film showed an increase in peak temperature between 2000 and 3000 h to about 70 °C. Brogly et al. (1997) attributed the secondary melting peak in EVA to a less organized crystal phase. Loo et al. (2005) assigned a weak endothermic peak of ethylene acrylic acid copolymer to secondary crystals, which are formed in the area between the primary crystal during slow cooling or storage at ambient temperatures (Loo et al., 2005). For linear low density polyethylene (PE-LLD, copolymerised with octene), Androsch showed that the melting process starts immediately above the glass transition (-33 °C) and is finished at 82 °C (Androsch, 1999). Furthermore, a shift of the peak temperature after storage at ambient temperature was reported and it was suggested that structural rearrangements are possible even at room temperature (Loo et al., 2005; Androsch, 1999). Polyethylene copolymers in general show a quite similar morphology, as they are random copolymers consisting of linear ethylene sequences and regions with short chain branches introduced by the comonomers (e.g. vinylacetate, octane). Therefore, the increase in the peak temperature can be assigned to the perfection and growth of secondary crystals at the elevated temperatures during xenon weathering. Interestingly, 30 and 200 µm thick films exhibit the same trend in change of the secondary crystallization peak. For both film thicknesses physical aging occurs within the first 250 h of weathering.

Relevant mechanical properties of the unaged films derived from tensile tests on unnotched and notched specimen are summarized in Table 3. The unaged films exhibit a ductile behaviour and high flexibility with no pronounced yield point. For 30 µm thick films an elastic modulus of 118 MPa, a stress-at-break value of 25 MPa and a strain-at-break value of 480% was obtained. For 200 µm thick film an elastic modulus value of 129 MPa, a stress at break value of 16 MPa and a strain at break value of 756% was measured. The fracture tests on notched specimens also revealed ductile behavior and stable crack propagation for all investigated films. For 200 µm thick film a maximum force value of 14 N and a deformation-at-break value 13 mm was measured. In contrast, the 30 µm film showed a significant lower maximum force value of 3 N and a slightly higher deformation-at-break value of 18 mm. Moreover, the 200 µm thick film reached the point of maximum force at lower deformation than the 30 µm film.

Table 3: Results of tensile test on unnotched and notched specimen: elastic modulus (E), stress-at-break (σ_b), strain-at-break (ε_b), maximum force (F_{max}) and deformation-at-break (s_b).

materials	unnotched specimens			notched specimens	
	E [MPa]	**σ_b** [MPa]	**ε_b** [%]	**F_{max}** [N]	**s_b** [mm]
Eif30	118 ± 8	24.9 ± 0.1	480 ± 18	3.2 ± 0.2	17.9 ± 0.5
Eif200	129 ± 0	15.6 ± 0.0	756 ± 10	14.3 ± 0.4	13.1 ± 0.9

The influence of weathering on the mechanical properties on the 30 and 200 µm thick films is shown in Figs. 5 and 6. While the stress-strain curves of 30 µm thick films showed a significant decrease of stress-at-break and strain-at-break, the ultimate mechanical properties of 200 µm thick exhibited only a slight decrease (Fig. 5). Regarding elastic modulus, both films showed a significant increase due to weathering. For the 200 µm thick films the elastic modulus of 130 MPa increased in the first 1000 h of aging and then leveled off to a value around 200 MPa. For 30 µm thick films, a strong increase from 120 to 230 MPa could be observed in the first 250 h. After 500 h, a value of 160 MPa was measured, which increased linearly to 220 MPa after 2000 h. Due to strong embrittlement of Eif30, the mechanical properties after 3000 h of weathering could not be measured. The increase of elastic modulus due to weathering can be attributed to physical aging. This correlates well with the DSC measurements, where significant post-crystallization was found for both films. For both film thicknesses, the greenhouse films showed significant variations of the stress-strain curves in the different stages of aging.

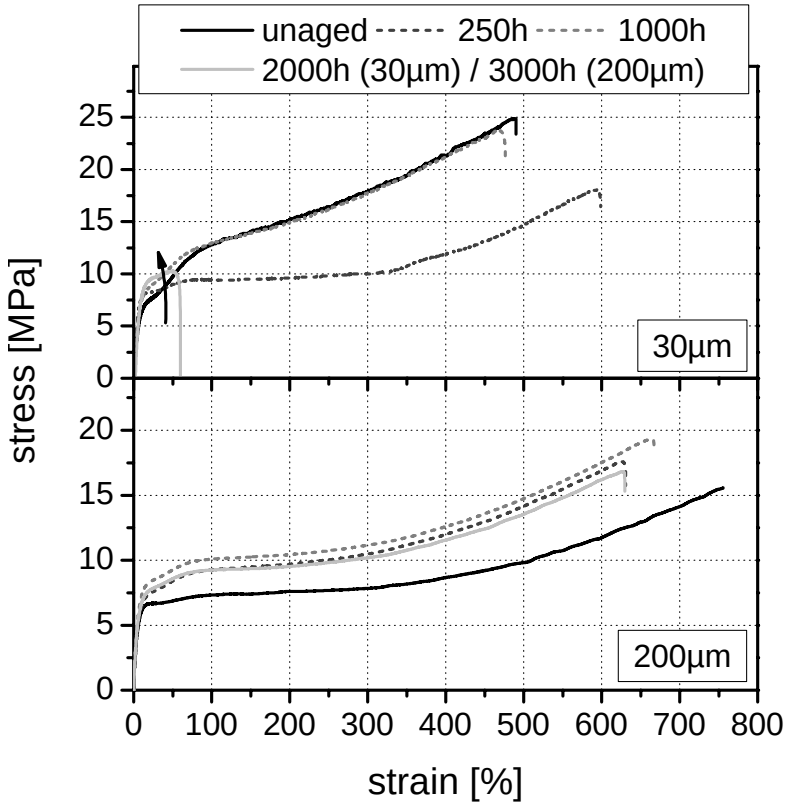

Fig. 5: Stress-strain curves of unnotched specimens of unaged and aged 30 µm and 200 µm thick EVA greenhouse films.

For notched specimens, a decrease in deformation-at-break, a shift of maximum force to lower displacements, a steeper initial slope of the load-displacement curves and an inconsistent behavior in the changes of the maximum force after weathering is observable (s. Figure 6). The increase in the initial slope of load displacement curves after weathering can be attributed to the post-crystallization showed by DSC measurements. The maximum force of 30 µm thick film showed a little decrease from 3.2 to 2.6 N after 3000 h weathering. Eif200 showed an increasing maximum force up to 500h followed by a slight decrease. The changes in strain at break and deformation at break values relative to the initial value of the unaged films after weathering are displayed in Fig. 7. For 30 µm thick films a strong decrease of the strain at break value was observed. In contrast, 200 µm thick films showed only a small decrease of strain at break values after 3000 h of weathering. The decrease in ultimate mechanical values can be attributed to chemical aging, i.e. mainly to chain scission and thus to changes in molecular

mass. Whereas the strain at break values of the unnotched specimen varied significantly in their reproducibility for all weathering stages, a more consistent behavior was found for deformation at break values from the notched tensile tests. The 200 µm film showed only a slight decrease in deformation at break values, whereas for the 30 µm thick film a more significant decrease in deformation at break values was observed.

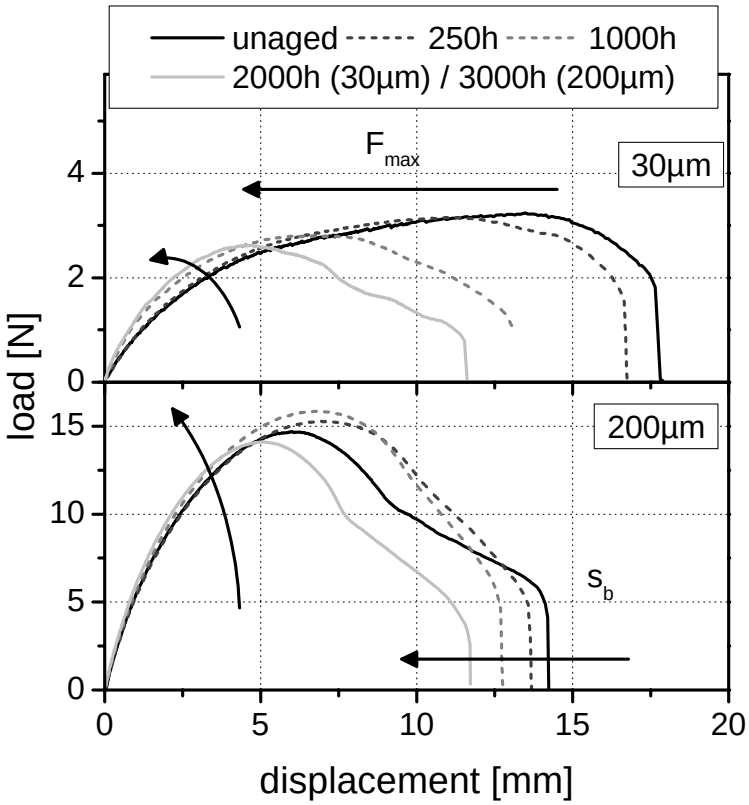

Fig. 6: Load-displacement curves of unnotched specimens of unaged and aged 30 µm and 200 µm thick EVA greenhouse films.

Dilara and Briassoulis (2000) established that the useful lifetime of a greenhouse film is reached when its initial ultimate mechanical properties derived from unnotched specimen are reduced by 50%. For the 30 µm thick Eif30 film, by monitoring strain at break values the useful lifetime is reached after 1000 h. In contrast, deformation at break values showed a constant decrease but after 2000 h the value is far above the 50% of the initial value. For the 200 µm thick film both strain at break and deformation at break values remained significantly above 50% of its initial value.

The results of the tensile tests on unnotched and notched specimen revealed bigger variances in the stress-strain curves of the unnotched samples than in the load-displacement curves of the notched samples. One reason for these strong variations could be the multi-layer build up of the investigated films. The films consist of at least two layers with different molecular composition and thus different mechanical properties. Small-scale variations in layer and film thickness could cause a significant change in the mechanical properties of the multi-layer films. Furthermore, it is well known for semi-crystalline polymers, that oxidation occurs only in amorphous regions and leads to material embrittlement.

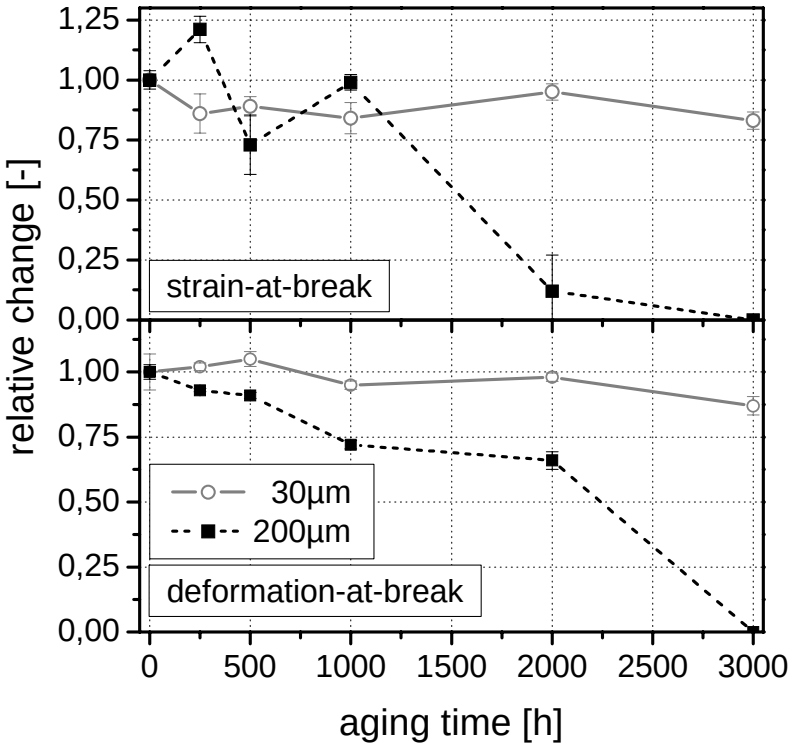

Fig. 7: Relative change of strain-at-break and deformation-at-break after weathering for the investigated EVA greenhouse films.

Fayolle et al. stated that tensile testing is not an adequate experimental tool to study ageing of initially ductile polymer films, because failure occurs always at defects, whose nature and geometry play an important rule in fracture (Fayolle et al., 2000; Fayolle et al., 2002). The essential work of fracture (EWF) approach appeared to be an appropriate tool to describe oxidation induced embrittlement in ductile films. But as EWF analysis is time and specimen consuming, tensile tests

on notched samples with one ligament length should provide the same advantages as EWF, like geometry independence and negligence of local defects or oxidized spots (Fayolle et al., 2002). The dependence of common tensile testing on local defects is the reason for the high scattering of the strain-at-break values after weathering. Therefore, the ultimate strain value gained from simple tensile test seems to be more sensitive for initial (local) aging, whereas deformation-at-break values are a sensitive indicator for global aging (Wallner et al., 2004).

In Figs. 8 and 9 the changes in absorption peak intensities of degradation products relative to its initial value are compared for both 30 and 200 µm thick films to the relative changes of mechanical properties. The hydroxyl peak at 3395 cm^{-1} was chosen as it was the only visible peak in both FTIR and ATR absorbance spectra.

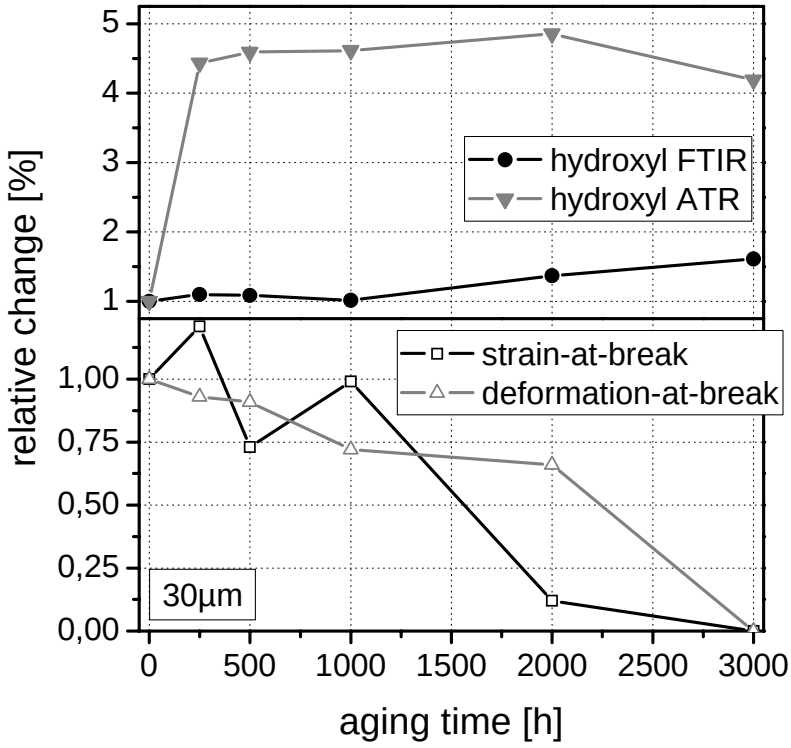

Fig. 8: Comparison of relative changes in absorption peak intensities of degradation products, measured by FTIR and ATR spectroscopy, and corresponding change in mechanical properties for unnotched (strain at break) and notched (deformation at break) 30 µm film samples (Eif30). Top: hydroxyl peak at 3395 cm^{-1}; bottom: mechanical properties strain-at-break and deformation-at-break.

As shown by ATR, for the 30 µm thick film (Fig. 8) the formation of degradation products took place within the first 250 h and then remained rather constant. This indicates a very fast initial degradation at the surface. This assumption is confirmed by FTIR spectroscopy. In the first 1000 h of weathering no significant changes in the area between 3700 and 3100 cm^{-1} were detected. After 3000 h a weak peak due to hydroxyl groups was observable. By comparison, surface sensitive ATR measurements showed a significant higher change in peak intensity. In accordance with the drop in ultimate mechanical properties after 2000 h, a significant increase of the FTIR hydroxyl absorbance was detected.

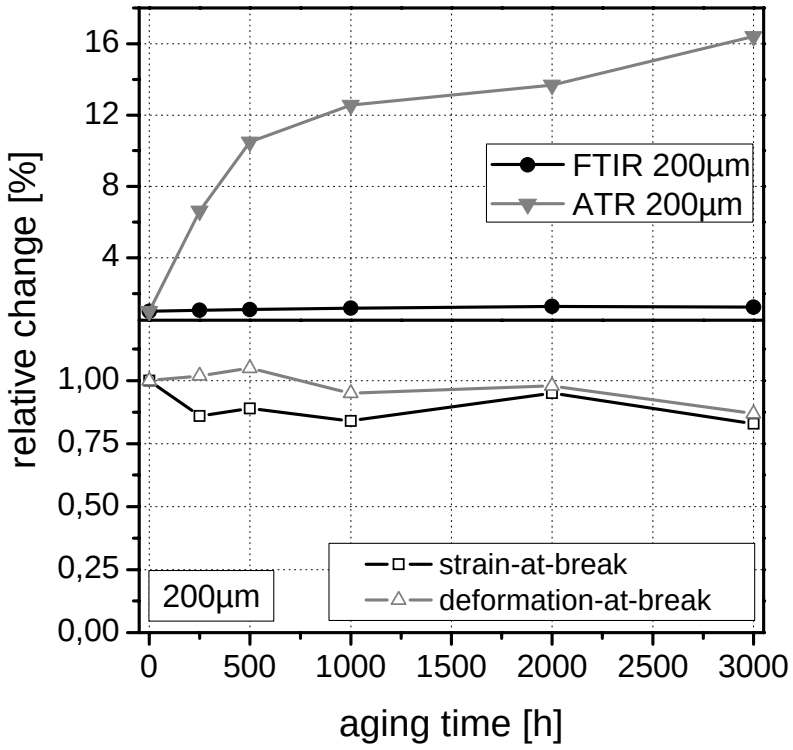

Fig. 9: Comparison of relative changes in absorption peak intensities of degradation products, measured by FTIR and ATR spectroscopy, and corresponding change in mechanical properties for unnotched (strain at break) and notched (deformation at break) 200 µm film samples (Eif200). Top: hydroxyl peak at 3395 cm^{-1}; bottom: mechanical properties strain-at-break and deformation-at-break.

Regarding ATR spectra, the 200 µm thick film showed an ongoing degradation process, depicted by the continuing increase in oxidation products (s. Fig. 9) and

the decrease in UV absorber content (s. Fig. 3). By comparison, FTIR spectra showed no significant changes or formation of degradation products due to weathering over the whole thickness. This is in agreement with the ultimate mechanical properties, which remained nearly constant after weathering. Interestingly, aging on the surface as reflected by ATR did not cause embrittlement of the film. One reason for the higher stability of 200 µm films is the higher film thickness followed by the far better ability to stabilize thicker films. This was shown before by UV/VIS/NIR spectroscopy (s. Fig. 3), were the UV absorber content after 3000 h of weathering is still significantly higher than for the unaged 30 µm thick film. The comparison of surface sensitive ATR spectra with FTIR spectra with mechanical properties suggests that for both films degradation takes place in surface near regions.

Both IR and UV/VIS/NIR spectroscopy refer to changes in chemical structure. Any changes in polymer morphology could not be detected with spectroscopy. Furthermore, both methods measure transmission spectra over the whole film thickness and therefore are sensitive to global aging of the total bulk material. Although ATR is a surface sensitive technique, no conclusions on local aging in the sense of local spots of aging onset could be made. Except for oxidation temperature, changes in DSC thermograms can be assigned to physical aging over the whole volume. Tensile tests appeared to be the most versatile method in describing aging. Whereas post-yield effects like changes in the ultimate mechanical properties (ε_b, s_b) are a very sensitive indicator for chemical aging, pre-yield and yield effects can are predominantly associated with physical aging. Furthermore, tensile tests on unnotched samples better reflect local, initial aging effects, while tests on notched samples allow a better description of global effects.

4. Summary and Conclusions

The aging behavior of two commercially available multi-layer EVA greenhouse films due to accelerated weathering was described. Using ATR spectroscopy hydroxyl-, vinylidene- and acid-groups were identified as main degradation products of the investigated EVA films. Whereas for 30 µm thick film degradation products developed within the first 250 h, for 200 µm thick films an ongoing degradation process was observed. FTIR spectra showed only little changes due

to weathering. The consumption of UV absorber was detected by UV/VIS/NIR spectroscopy. Secondary crystals and their growth during weathering were revealed by DSC measurements. While at the film surface degradation products develop within the first 250 h of weathering, the ultimate mechanical properties of investigated 30 µm thick films remain nearly constant up to 1000 h. Thicker films provide good resistance against artificial weathering with mechanical properties remaining nearly constant for up to 3000 h. The comparison of ATR and FTIR spectra with mechanical properties suggests that degradation of the investigated polymer films is strongly confined to the surface. Nevertheless, the deformation-at-break values proved to be a sensitive indicator for global aging, whereas strain-at-break value is sensitive to initial aging. A correlation between formation of degradation products within the bulk, indicated by FTIR spectroscopy, and ultimate mechanical properties was obtained. Tensile tests appeared to be the most versatile method in describing aging.

5. References

Allen, N.S., Edge, M., Rodriguez, M., Liauw, C.M., Fontan, E. (2000). Polym. Deg. Stab. **88**, 363.

Allen, N.S., Edge, M., Rodriguez, M., Liauw, C.M., Fontan, E. (2001). Polym. Deg. Stab. **71**, 1.

Androsch, R. (1999). Polymer **40**, 2805.

Briassoulis, D., Waaijenberg, D., Gratraud, J., von Elsner, B. (1997). J. Agric. Eng. Res. **67**, 171.

Brogly, M., Nardin, M., Schultz, J. (1997) J. Appl. Polym. Sci. **64**, 1903.

Dilara, P.A., Briassoulis, D. (1998). Polym. Test. **17**, 549.

Dilara, P.A., Briassoulis, D. (2000). J. Agric. Eng. Res. **76**, 309.

Fayolle, B., Audouin, L., Verdu J. (2000). Polym. Deg. Stab. **70**, 333.

Fayolle, B., Audouin, L., Verdu, J. (2002). Polym. Deg. Stab. **75**, 123.

Loo, Y.L., Wakabayashi, K., Huang, E., Register, R.A., Hsiao, B.S. (2005). Polymer **46**, 5118.

Oreski, G., Wallner, G.M. (2006). Sol. Energ. Mat. Sol. C. **90**, 1208.

Rodríguez-Vázquez, M., Liauw, C.M., Allen, N.S., Edge, M., Fontan, E. (2006). Polym. Deg. Stab. **91**, 154.

Sultan, B. Å., Sörvik, (1991). *E.* J. Appl. Polym. Sci., **43**, 1737.

Sultan, B. Å., Sörvik, (1991). *E.* J. Appl. Polym. Sci., **43**, 1747.

Sultan, B. Å., Sörvik, (1991). *E.* J. Appl. Polym. Sci., **43**, 1761.

Wallner, G.M., Weigl, C., Leitgeb, R., Lang, R.W. (2004) Polym. Deg. Stab. **85**,1065.

Paper 5: Evaluation of the Aging Behavior of Ethylene Copolymer Films for Solar Applications under Accelerated Weathering Conditions

Oreski, G., Wallner, G.M.

submitted to Solar Energy (August 2008)

Evaluation of the Aging Behavior of Ethylene Copolymer Films for Solar Applications under Accelerated Weathering Conditions*

Oreski G. [1], Wallner G.M. [2]

[1]Polymer Competence Center Leoben GmbH, Roseggerstraße 12, A-8700 Leoben, A

[2]Institute of Materials Science and Testing of Plastics, University of Leoben, Franz Josef Straße 18, A-8700 Leoben, A

Corresponding Author, email: oreski@pccl.at, fax: +43 3842 429 626

Abstract

Ethylene copolymers based on acrylic acids and acrylates are an interesting alternative to ethylene(vinylacetate) (EVA) for photovoltaic (PV) encapsulation. These materials provide similar or better mechanical and optical properties and a slightly better aging behavior, but without the formation of corrosive acetic acid during aging, which is particularly of importance in PV applications. The focus of the research work was to evaluate and screen the aging behavior of ethylene copolymers containing different types of comonomers for solar applications. To investigate the intrinsic weathering behavior of the materials, unstabilized films with comonomer contents around 10% were exposed to temperature, humidity and solar radiation. Special attention was given to the optical and mechanical properties. All investigated films showed high transparency in the solar range with hemispheric transmittance values above 91%. Regarding mechanical properties, the ethylene copolymer films exhibited a highly ductile behavior and high flexibility. Similar degradation behavior could be observed for all investigated films. Due to formation of chromophoric degradation products, yellowing could be observed and hemispheric transmittance values dropped slightly to values between 88.5 and 90.5%. The unstabilized films showed significant embrittlement due to weathering. After 750h of weathering both strain-at-break and stress-at-break values of all ethylene copolymer films dropped significantly below 50% of the initial values.

*Paper submitted to Solar Energy (August 2008).

1. Introduction

Ethylene copolymer films based on vinylacetates and acrylic acids are already used for different solar applications with some specific advantages like easy handling, good optical and mechanical properties, low weight and low-cost production. One important application is the encapsulation of solar cells in photovoltaic (PV) modules, where the material has to fulfill several basic functions. These include to provide structural support and physical isolation of the solar cells, to maintain electrical isolation and to be highly transparent in a selected spectral region, according to the cell technology used (Czanderna and Pern, 1996). To deal with different thermal expansions of the materials used in a module (glass, solar cell, interconnects) and to avoid over-stressing and cracking, the material has to be a low modulus, elastomeric material. Furthermore, for PV modules a lifetime of 20 to 30 years with a maximum total loss in module performance of 20% over a 20 year period needs to be guaranteed (Czanderna and Pern, 1996).

The dominant encapsulation material for PV-modules currently is ethylene(vinylacetate) copolymer (EVA). The aging behavior and degradation mechanism of EVA and especially of EVA as PV encapsulation material are well described in the literature (Czanderna and Pern, 1996; Sultan and Sörvik, 1991; Klemchuk et al. 1997; Allen et al., 2000; Allen et al., 2001; Rodríguez-Vázquez et al., 2006; Kempe et al., 2007). The initial step of EVA degradation is the formation of acetic acid and double bonds in the main chain. Further degradation products reported in the literature are lactones, formed by intramolecular back-biting by the acetate group and the evolution of methane, and the production of ketones and acetaldehyde (Sultan and Sörvik, 1991; Klemchuk et al. 1997; Allen et al., 2000; Allen et al., 2001; Rodríguez-Vázquez et al., 2006; Kempe et al., 2007). Furthermore, α,β-unsaturated carbonyl groups, hydroperoxides and anhydrides are formed during the oxidation process (Allen et al., 2000). With increasing vinyl acetate content the degradation rate is enhanced (Sultan and Sörvik, 1991). The major drawback of EVA is the formation of acetic acid during oxidation. Acetic acid can lead to corrosion of the metal parts in a PV module and to loss in adhesion and subsequent delamination in the multi-layer encapsulation (Czanderna and Pern,; 1996; Klemchuk et al., 1997; Kempe et al., 2007). Furthermore the formed

acetic acid accelerates the oxidation process (Sultan and Sörvik, 1991; Kempe et al., 2007).

Films made of ionized ethylene(acrylic acid) copolymers (ionomers) are relatively new on the market (Roekens and Beyer, 2007), providing similar properties to EVA with the advantage of a physical cross linking process. In addition, no acetic acid is formed during weathering (McNeill and Barbour, 1987; McNeill and Alston, 1998). The degradation of ethylene acrylic acid copolymers is determined by chain scission and transfer reactions. In general, ethylene(acrylic acid) copolymers show quite a high thermal stability. Depolymerization was not observed. The onset of degradation is by side group scission in the acid group with carbon monoxide as its main volatile degradation product (McNeill and Barbour, 1987; McNeill and Alston, 1998). Furthermore, ethylene, propylene, dimethyl ketene and shorter chain fragments with terminal vinyl groups are formed due to backbone chain scission. At highest degradation temperatures also anhydride structures were found to be possible (McNeill and Alston, 1998).

Besides EVA and ethylene(acrylic acid) copolymers, further polar ethylene copolymers with acrylate side groups such as ethylene(methylacrylate) (EMA), ethylene(ethylacrylate) (EEA) and ethylene(butylacrylate) (EBA) have been developed (Sultan and Sörvik, 1991; McNeill and Mohammed, 1995; Jäger et al., 2002). These polymers are already used for cable and wire applications (McNeill and Mohammed, 1995), where the introduction of polar carbonyl side groups improves the adhesion properties compared to non-polar ethylene homopolymers. The mechanical and optical properties are comparable to EVA. Degradation studies on EVA, EBA, EEA and EMA showed that acrylate side groups of EBA, EEA and EMA showed higher thermal stability than the VA side group of EVA. For all these polymers a decrease and broadening of the carbonyl stretching peak around 1740cm^{-1} was found. EVA showed the fastest decrease. Ethylene and butylene are the main volatile degradation products of EEA and EBA, which are formed due to ester pyrolysis. Furthermore, the formation of carboxylic acids and anhydrides along the polymer chain is reported (Sultan and Sörvik, 1991; Jäger et al., 2002). Ester pyrolysis was not observed for EMA, as it is unable to form an olefinic compound, but the formation of carboxylic acid was found (Jäger et al.,

2002). Generally, the introduction of acrylate groups supports chain cleavage, and polymers which undergo a ester pyrolysis show a higher tendency for chain cleavage (EEA > EBA > EMA), which results in the formation of vinyl and vinylidene groups.

Up to now the focus has been given to investigate the degradation behavior of polar ethylene copolymers, with regard to changes in material chemistry. In contrast, the overall performance and reliability of the material in application has not been investigated. Hence, the intention of this study is to screen various polar ethylene copolymers as to their aging behavior under solar engineering relevant conditions. To check the intrinsic weathering stability, unstabilized polymer grades were chosen, and the effect of aging on the prime properties wass investigated. It should be emphasized, however, that it is not intended nor is it possible to predict the lifetime performance based on the data exhibited.

2. Experimental

Typical comonomer contents for PV encapsulation materials are 33 m% for EVA (Czanderna and Pern, 1996) and 10 to 15 m% for the Ionomer (according data sheetswww.dupont.com). Due to limited availability and for better comparison, unstabilized ethylene copolymer types based on acrylic acid, acrylate and vinyl acetate with comonomer contents of about 10 m% were chosen. The investigated polymer films are displayed in Table 1. As to the acid comonomers, acrylic acid (AA) and methacrylic acid (MAA) were chosen. Regarding acrylate comonomers butylacrylate (BA), ethylacrylate (EA) and methylacrylate (MA) are currently in use for ethylene (E) copolymer materials. Furthermore, widely used ethylene(vinylacetate) copolymers (EVA) as well as a terpolymer material with two different comonomers (acrylic acid and butylacrylate (AA/BA) were investigated. The material resins were supplied by Arkema (Colombes, F) (EBA), Basell (Hoofddorp, NL) (EAA/BA), Dow (Midland, USA) (EAA) and DuPont (Wilmington, USA) (EMAA, EEA, EMA, EVA). Except for processing aids the materials did not contain any stabilizers and additives.

Films with thicknesses ranging from 70 to 125 µm were cast at the Institute of Polymer Processing, University of Leoben, using a Rosendahl RO400 single

screw extruder (Rosendahl Maschinen GmbH, Pischelsdorf, A) with a chill roll unit of SML Maschinengesellschaft mbH (Lenzing, A).

Table 1: Investigated ethylene copolymer films (material designation, comonomer, comonomer content and film thickness).

material designation	comonomer	comonomer content	film thickness
		[m%]	[µm]
EAA	acrylic acid	9.7	100
EMAA	methacrylic acid	8.7	110
EAA/BA	acrylic acid, butyl acrylate	7/4	110
EMA	methyl acrylate	9	105
EEA	ethyl acrylate	12	100
EBA	butyl acrylate	6-8	110
EVA	vinyl acetate	9	120

Artificial weathering was done using a Xenon Arc artificial weathering chamber (Atlas Material Testing Technology LLC, Chicago, USA). The specimens were exposed to 60 W/m² UV-irradiance (300 to 400 nm) at a black standard temperature of 65 °C and a relative humidity of 50% for 250, 500, 750, 1000 and 1500 hours. The aging behavior was characterized by infrared spectroscopy (FTIR), by UV/VIS/NIR spectroscopy, by differential scanning calorimetry (DSC) and by tensile testing.

FTIR analysis was done in transmittance and in the attenuated total reflectance (ATR) mode, using a Spectrum GX FTIR spectrometer (Perkin Elmer Analytical Sciences, Überlingen, D) with a Pike Miracle Micro-ATR device (Pike Technologies, Madison, USA). The transmittance spectra were recorded over the IR range from 4000 to 450 cm^{-1}, the ATR spectra from 4000 to 650 cm^{-1}. For better comparison, all ATR spectra were normalized. The wave number dependent penetration depth was corrected using the Perkin Elmer Software integrated ATR correction.

The UV/VIS/NIR measurements were carried out using a Lambda 950 UV/VIS/NIR spectrometer with an integrating sphere to measure hemispherical and diffuse transmittance and reflectance spectra (Perkin Elmer Analytical Sciences, Überlingen, D). Spectra were recorded from 250 to 2500 nm.

Thermal analysis was performed using a Mettler DSC 821e instrument (Mettler Toledo GmbH, Schwerzenbach, CH). Thermograms were recorded under static air from -60°C to 300 °C at a heating rate of 10 K/min. To identify irreversible effects, samples were heated from –60 to 150 °C, cooled to -60 °C and again heated to 300 °C. A circular sample disc was cut with a punch, put in a 40 μl pan and closed with a perforated lid. Melting point and melting enthalpy were evaluated according to ISO 11257-2 and ISO 11257-3. The degree of crystallinity was determined as the ratio between the melting enthalpy of the sample and the melting enthalpy of the 100% crystalline polymer. The enthalpy values for 100% crystalline polymer grades were taken from ATHAS Data Bank (ATHAS Data Bank, http:web.utk.edu/~athas/databank/ Ed. M. Pyda, 1994). As the side groups of ethylene copolymers (i.e. vinylacetate, acrylic acid, and acrylate), do not enter the crystalline regions, the enthalpy of polyethylene (293 J/g) was taken to calculate the degree of crystallinity (Brogly et al., 1997).

Tensile tests were carried out with a screw driven universal test machine of the type Instron 4505 (Instron International Ltd., High Wycombe, UK) at 23 °C according to EN ISO 527-3. Rectangular specimens of 100 mm in length and 15 mm in width were cut prior to exposure using a device with fixed razor blades and rotating sample. The test speed was 50 mm/min. From a total of at least five specimens for each test series, average numbers for elastic modulus (E), stress-at-break (σ_B) and strain-at-break (ε_B) were deduced.

3. Results and Discussion

In the following the results will be described and discussed considering both changes in chemical structure and conformation and its impact on performance relevant properties. It should be mentioned, that the accelerated weathering conditions investigated do not represent real service conditions in PV encapsulation. Concerning the UV light intensity, the angle of incidence and the

temperature, the conditions selected are significantly more intensive than those in real application of PV devices. In practice, PV encapsulation materials are installed behind a partly UV absorbing glass pane. Thus, the results shown cannot directly be used for life time predictions of polymeric materials for PV encapsulation. Furthermore, encapsulation materials are equipped with antioxidants, light stabilizers and UV absorbers to enhance service life time. In contrast, the chosen materials did not contain any stabilizers, as the main focus was to investigate the inherent weathering stability of the various material grades.

Figures 1 and 2 show representative ATR and FTIR absorbance spectra of EAA and EMA films. Several changes and new peaks due to weathering could be observed in the FTIR spectra (Fig. 1). The broad bands between 3700 and 3100 cm^{-1} and between 1200 and 1050 cm^{-1} can be assigned to hydroxyl groups of alcohols, acids, peroxides and hydroperoxides.

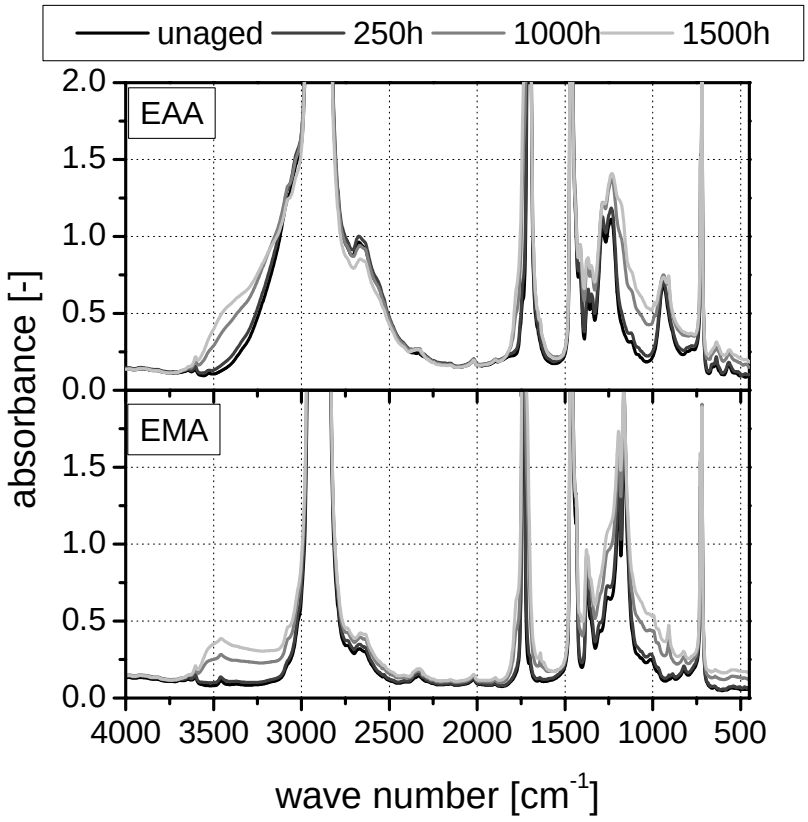

Fig. 1: FTIR absorbance spectra of EAA and EMA.

As described in the literature (Sultan and Sörvik, 1991), the FTIR absorbance spectra showed a broadening of the carbonyl stretching peak. A decrease in the

carbonyl peak absorption could not be observed in the FTIR spectra, as the CH_2 and C=O groups showed intense absorption and could not be resolved spectrally. ATR spectra confirmed the findings in literature and revealed a decrease of the carbonyl peak intensity (Fig. 2) in the first 500 h of weathering, followed by a broadening of the peak. New shoulders and peaks can be attributed to the formation of lactones and anhydrides (1800-1770 cm^{-1}), aliphatic esters (1735 cm^{-1}) and saturated and unsaturated acid and ketone groups (1715-1680 cm^{-1}). The additional peaks between 1300 and 1000 cm^{-1} due to C-O-C stretch vibration confirm this assignment (Allen et al., 2000). Chain cleavage and the formation of vinyl end groups could be confirmed by the peaks at 1641, 991 and 909 cm^{-1}, which can be attributed to stretching and wagging vibrations of the C=C double bond.

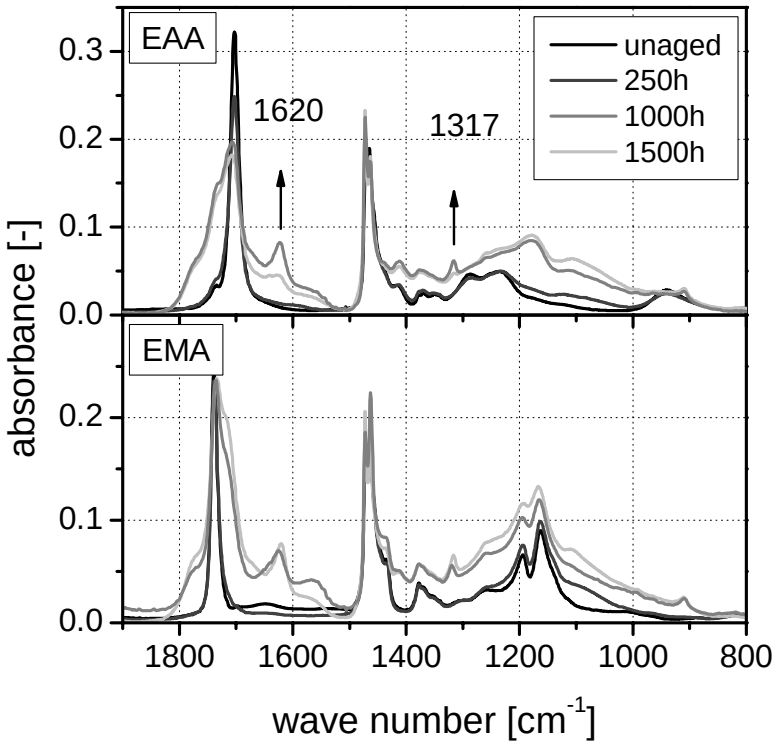

Fig. 2: ATR absorbance spectra of EAA and EMA.

After 750 h of weathering, the ATR spectra of all investigated films exhibited additional peaks at 1620 and 1317 cm^{-1}. These peaks can be assigned to asymmetric and symmetric carbonyl stretching vibrations of oxalate ions (Deng et al., 2006, Monte, 2003). Monte reported oxalate film formation caused by fungus

(Monte, 2003). Presumably the oxalate originated from the reverse osmosis water treatment device for the xenon tester. As these peaks were not found in FTIR spectra, the formation of a very thin oxalate layer on the surface is assumed.

In order to compare degradation caused by photo-oxidation, the Ford Motor Company introduced a photo-degradation index (Gerlock et al., 2003). It measures the accumulation of degradation products by increase in OH region absorbance areas of FTIR spectra, which are caused by formation of hydroperoxide, carboxylic acid and alcohol groups. Therefore the region from 2200 to 3800 cm^{-1} was integrated and the area due to CH_2 absorbance between 2700 and 3050 cm^{-1} was subtracted to obtain the OH absorbance area. At different exposure times t, the photo-degradation index (PD index) is then given by

$$PD(t) = \left(\frac{Area(OH)}{Area(CH_2)} \right)_{Exposed} - \left(\frac{Area(OH)}{Area(CH_2)} \right)_{Unexposed} \quad (1)$$

Figure 3 shows the photo-degradation index of the investigated polymer films. All materials exhibited a similar behavior with a more or less linear increase in degradation index after 250 h of weathering. The acid copolymers EAA and EMAA showed the highest degradation rate in the first 250 h, which is decreasing slightly after 250 h. By comparison, the degradation rate after 250 h increased for the acrylate and vinyl acetate copolymers (EMA, EEA, EBA, EVA). After 1500 h of weathering, EAA-BA terpolymer revealed the lowest accumulation of degradation products, followed by the acid copolymers EAA and EMAA. For EVA the highest PD index was obtained. The acrylate polymers EMA and EEA showed a lesser PD index than EVA, but more degradation than the acid copolymers after 1500 h of xenon weathering. For EBA no samples after 1500 h were available due to the strong embrittlement.

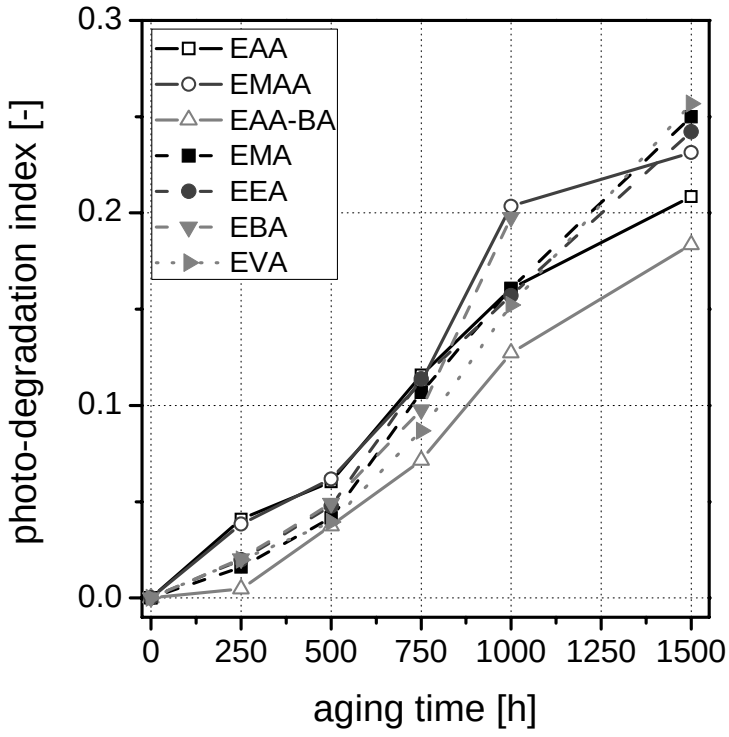

Fig. 3: Photo-degradation index as a function of aging time for all investigated polymer films.

The investigated ethylene copolymer films are highly transparent in the solar range of radiation, with hemispheric transmittance values above 91% and hemispheric reflectance values of about 8%. The diffuse transmittance values range from 8 to 38%, the diffuse reflectance values from 2.5 to 7%. Significant absorptions can be seen above 1000 nm due to IR overtones and below 300 nm due to the carbonyl group of the comonomer groups. Figure 4 depicts the hemispheric transmittance spectra of unaged and aged EAA and EMA film in the range from 250 to 800 nm, where changes due to photo-degradation are expected. A significant increase in the absorption between 250 and 450 nm due to formation of chromophoric degradation products, mainly C=O and C=C double bonds, could be detected after weathering. Therefore significant yellowing was observed for all investigated films. The hemispheric transmittance of the investigated ethylene copolymer films after 1500 h of weathering decreased slightly to values between 88.8 and 90.5%. In case of EMAA, the value dropped to 75% after 1000 h and 86% after 1500 h. Compared to the other materials, where the reflectance remained rather constant

after weathering, the reflectance values increased from about 8% in the unaged state to 13% after 1000 h and to 11% after 1500 h of weathering. The latter finding can be explained by the oxalate layer which was detected by the ATR spectroscopy. EMAA showed the most pronounced IR absorption peaks due to the oxalate groups. In contrast to the other materials, the oxalate layer was visible on the EMAA film after 1000 and 1500 h of weathering, which gave the film a hazy appearance. The decrease from 13 to 11% from 1000 to 1500 h is perhaps an artifact of the limited space in the weathering device. As the samples for 1000 and 1500 h were exposed consecutively, assumedly slight variations in the reverse osmosis water treatment device caused these differences.

Except for EMAA, which exhibited a significant increase in diffuse transmittance and reflectance value at 1000 and 1500 h due to the oxalate layer, the diffuse transmittance values remained constant or decreased slightly, whereas the diffuse reflectance values showed a slight increase for the investigated polymer films.

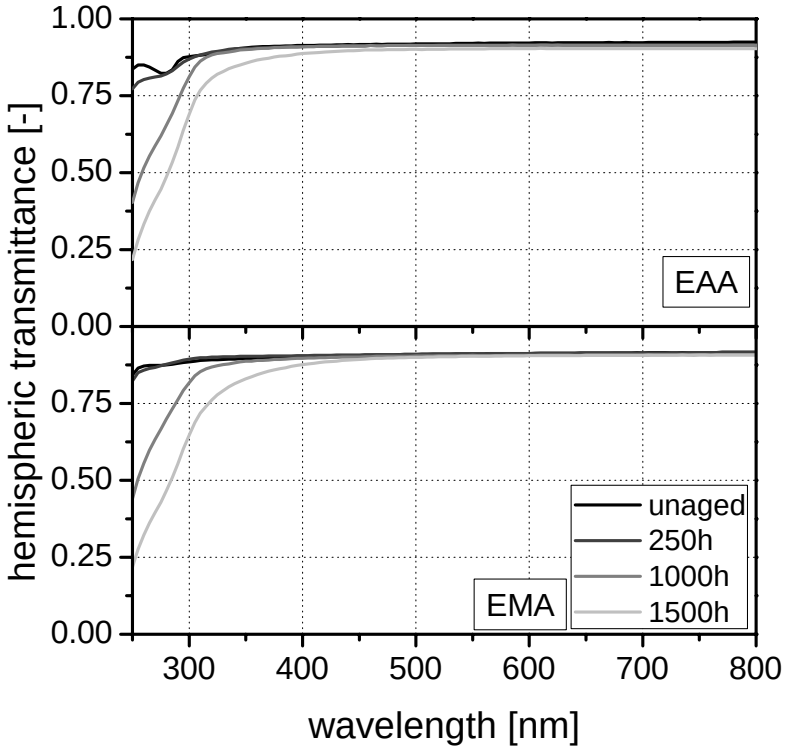

Fig. 4: Hemispheric transmittance spectra of unaged and aged EAA and EMA film.

Hemispherical transmittance values decreased only slightly due to weathering. Changes in the measured spectra occurred mainly below 300 nm. Regarding optical properties, an initial transmittance >90% and a loss of less than 5% after 20 years of module lifetime are required (Czanderna and Pern, 1996). Except for EMAA, none of the ethylene copolymer films showed a loss in transmittance of more than 5%. While it is difficult to transfer the results of this investigation to the true service life of PV modules, they may, however, indicate a ranking of the materials in terms of their aging behavior. It should also be kept in mind, that PV encapsulation materials are protected by a partly UV absorbing glass sheet. Moreover, the materials are usually equipped with UV-absorbers, light stabilizers and antioxidants.

The integration of the UV/VIS absorbance spectra between 250 and 800 nm seems a more appropriate parameter for degradation, as it is a measure of formation of chromophoric degradation products, mainly C=O and C=C double bonds. To consider the intrinsic absorptions in the UV region due to the carbonyl group, the integrated area of the unexposed samples was subtracted from the area of the exposed samples at the given time t. The hemispheric reflectance is considered to be constant, therefore for EMAA no values could be obtained as the reflectance changes due to the oxalate layer.

$$A_{UV/VIS}(t) = \int_{250}^{800} A_{exposed}(t,\lambda)d\lambda - \int_{250}^{800} A_{unxposed}(t_0,\lambda)d\lambda \qquad (2)$$

Figure 5 compares the changes in hemispherical transmittance and UV/VIS absorbance due to weathering. Up to 1000 h of weathering only small differences were obtained for the investigated films. EAA-BA showed the lowest accumulation of degradation products. General trends, which are reported in literature (Sultan and Sörvik, 1991; Jäger et al., 2002), could not be ascertained. In contrast to the findings in the literature, up to 1000 h for EVA films the accumulation of degradation products is similar to the acrylate copolymers (Sultan and Sörvik, 1991). But after 1500h of weathering EVA showed the highest PD index as well as the highest UV/VIS absorbance. Nevertheless, the change in hemispherical

transmittance was comparable to EAA and EMA. Interestingly, EAA-BA exhibited the smallest increase in UV-absorbance, but the highest decrease in hemispherical transmittance and therefore significant yellowing.

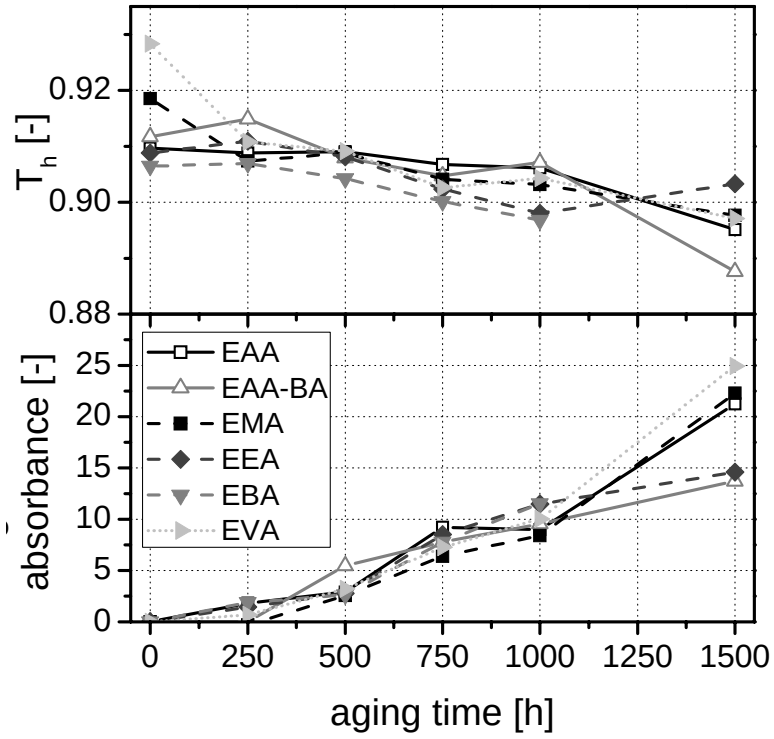

Fig. 5: Comparison of change in UV/VIS absorbance with hemispherical transmittance values after weathering.

In general, the acid copolymers showed more yellowing than acrylate and vinyl acetate copolymers. The highest hemispherical transmittance values after 1500 h with minimal yellowing was found for EEA.

Relevant thermal properties of the unaged films are summarized in Table 2. All investigated films showed a broad area of melting, starting immediately above the glass transition around -30 °C to about 110 °C (Androsch, 1999) with melting temperatures ranging from 85 to 103 °C. The degree of crystallinity varies from 26 to 39%, depending on the comonomer content. Furthermore, a secondary crystallization peak around 45 °C could be observed for all polymer films. The secondary peaks can be attributed to a less organized crystal phase, which is formed in the area between the primary crystal during slow cooling or storage at

ambient temperatures (Brogly et al., 1997, Loo et al., 2005). After the first 250 h of xenon aging, a significant increase of the secondary crystallization peak temperature from 45 to 65 °C can be observed, which levels off to temperature values between 73 and 76 °C after 1500 h. In addition, the degree of crystallinity increased significantly due to weathering. In case of EAA and EVA an increase in degree of crystallinity of more than 50% was observed. Due to the broad melting region from -30 to 110 °C, physical aging by means of secondary crystallization is an ongoing process. The increase in the peak temperature and degree of crystallinity can be assigned to perfection and growth of secondary crystals at the elevated temperatures during xenon weathering (Androsch, 1999, Loo et al., 2005).

Table 2: Thermal (melting temperature, degree of crystallinity) and mechanical properties (elastic modulus, stress at break, strain at break) of the investigated ethylene copolymer films.

	melting temperature	**degree of crystallinity**	**elastic modulus**	**stress-at-break**	**strain-at-break**
	[°C]	[%]	[MPa]	[MPa]	[%]
EAA	100.1 ± 0.0	29.9 ± 0.4	105 ± 4	34.4 ± 2.3	695 ± 40
EMAA	99.3 ± 0.3	32.3 ± 0.7	130 ± 21	37.8 ± 4.0	369 ± 57
EAA-BA	97.0 ± 0.2	30.7 ± 0.8	67 ± 4	21.7 ± 1.6	826 ± 33
EMA	101.3 ± 0.5	33.7 ± 2.5	64 ± 8	19.2 ± 2.4	665 ± 110
EEA	99.3 ± 0.7	32.6 ± 0.7	53 ± 5	23.1 ± 2.0	671 ± 71
EBA	103.2 ± 0.5	38.9 ± 2.4	86 ± 3	18.5 ± 1.7	647 ± 79
EVA	97.4 ± 1.0	35.8 ± 0.2	68 ± 8	16.9 ± 0.8	704 ± 42

Representative stress strain curves of unaged and aged EAA and EMA films are shown in Fig. 6 and relevant mechanical properties of the unaged materials are also listed in Table 2. The investigated unaged films exhibit a highly ductile behavior and high flexibility with no pronounced yield point. All polymers show strain-at-break values between 650 and 850%, except for EMAA with a strain-at-break of about 370%. Regarding elastic modulus, the acid copolymers EAA and EMAA exhibited values above 100 MPa, whereas the elastic modulus values of the acrylate and acetate copolymers were found to range from 45 to 85 MPa. A

similar trend was obtained for the stress-at-break results. While the acid copolymers exhibited values around 35 MPa, stress at break of the acrylate and acetate copolymers is about 20 MPa. Though the comonomer content is comparable to the other copolymers, the acid copolymers showed higher tensile strength than the acrylate and acetate copolymers.

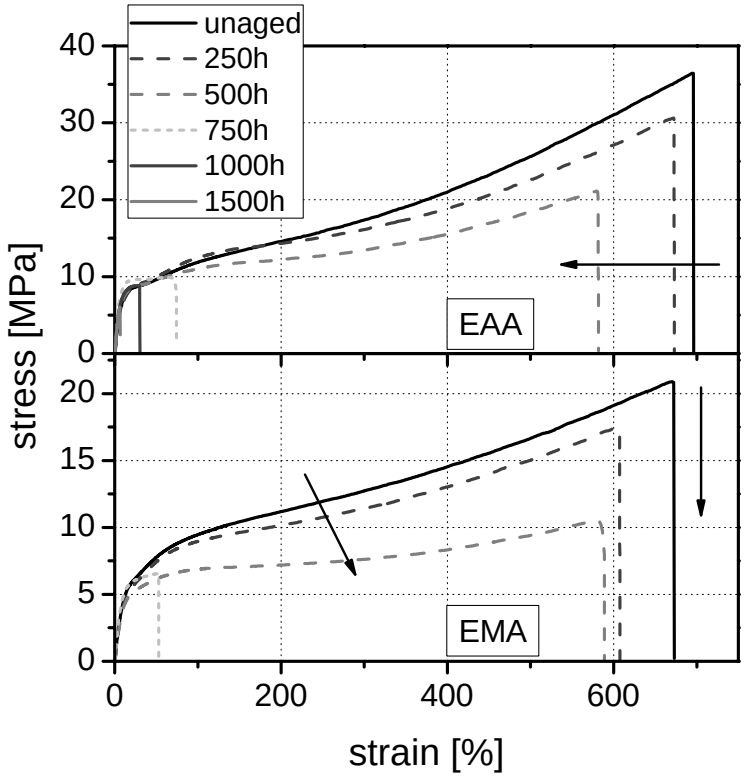

Fig. 6: Stress-strain curves of unaged and aged EAA and EMA films.

The influence of weathering on strain-at-break and stress-at-break values of EAA and EMA is shown in Fig. 7. Significant embrittlement due to weathering could be observed for all films. Except for EMAA only small changes in strain-at-break could be observed in the first 250 h of weathering. But after 750h all polymer films lost their mechanical stability and flexibility, showing dramatically decreased strain-at-break values below 10% of the initial values. After 1000 h only the acid copolymers (EAA, EMAA, EAA-BA) and EBA showed sufficient mechanical stability to record stress strain curves, after 1500 h of weathering only EAA and EMAA. All other polymer films broke during exposure or mounting in the tensile test machine. Stress-at-break values showed a less pronounced decrease. After

750 h of weathering stress-at-break values dropped to 20 to 45% of its initial values.

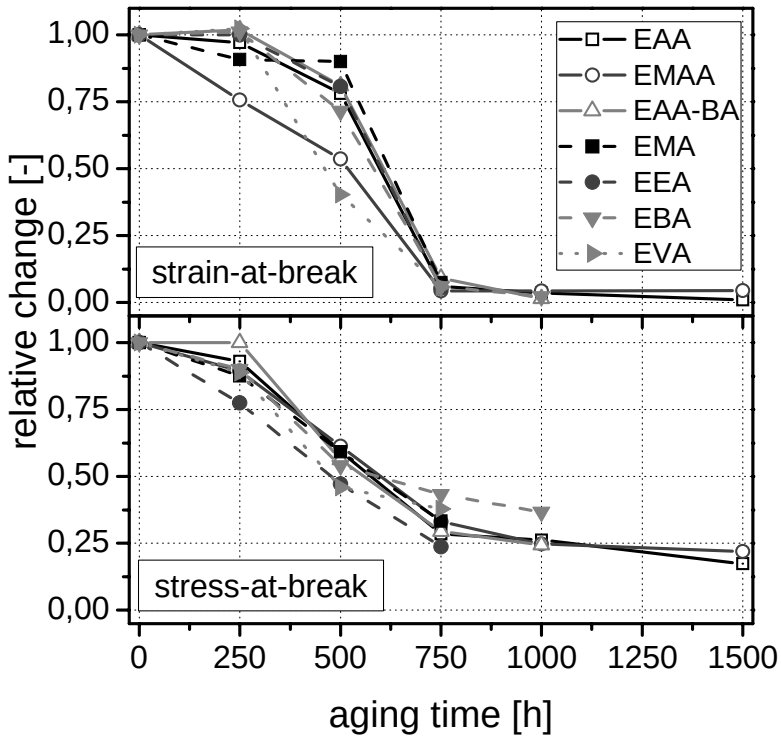

Fig. 7: Relative change of initial strain-at-break and stress-at-break values due to weathering.

The different characterization methods revealed the changes which occur in the material during xenon weathering. Figure 8 compares the changes in photo-degradation index and in UV/VIS absorbance with relative changes in strain-at-break values after weathering. These methods are sensitive to chemical aging. As discussed before, photo-degradation index and UV/VIS absorbance, which are a measure of accumulation of oxidation products, showed a more or less linear increase in degradation products after 250 h. But unlike strain-at-break or stress-at-break values from tensile tests, these parameters do not indicate material failure.

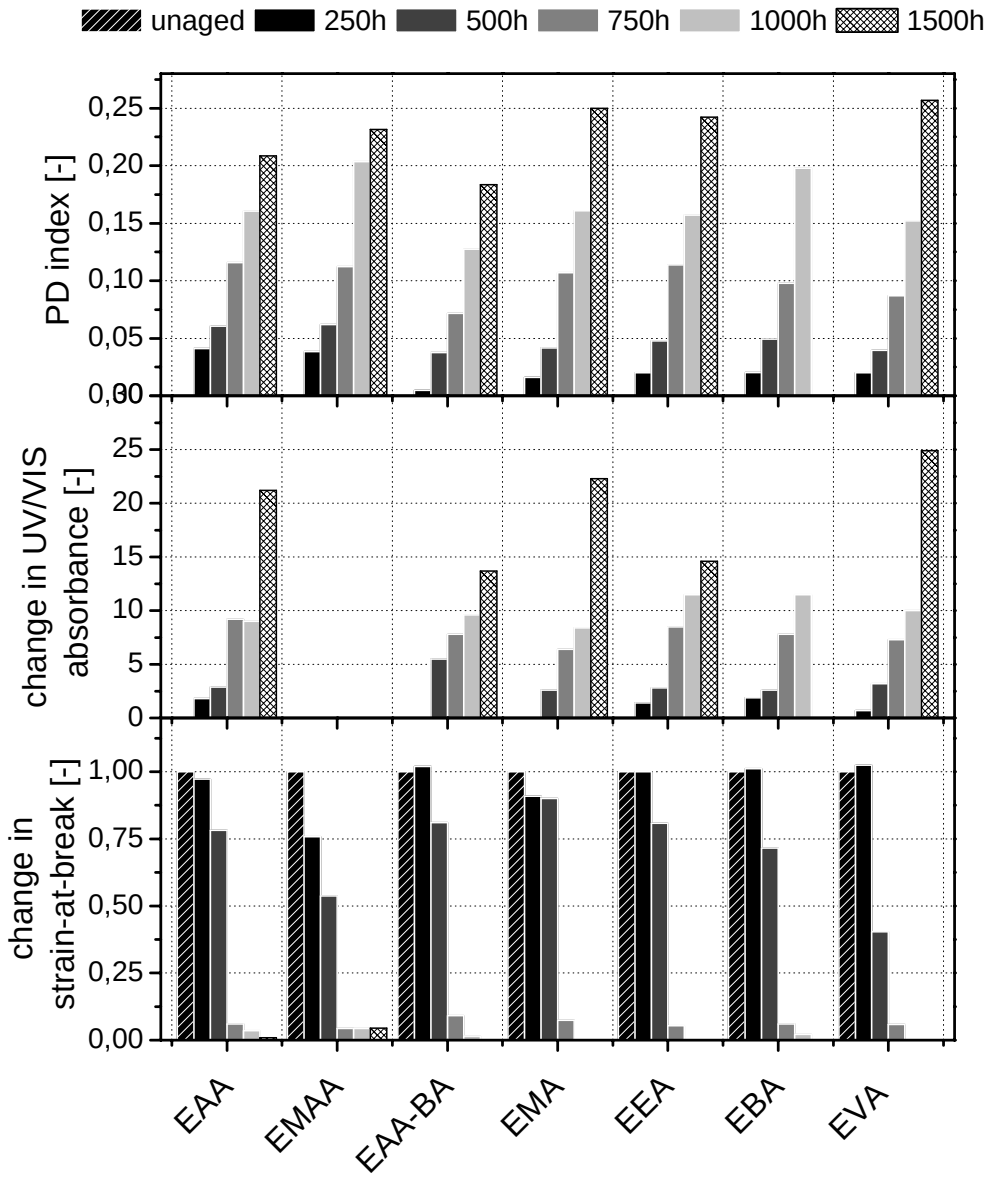

Fig. 8: Comparison of photo-degradation index and change in UV/VIS absorbance with relative change in strain-at-break values after weathering.

According to one proposal in the literature, regarding mechanical properties the useful lifetime of a film is reached when its initial ultimate mechanical properties are reduced by 50% (Dilara and Briassoulis, 2000). After 750 h of weathering both strain-at-break and stress-at-break values of the investigated ethylene copolymer films dropped significantly below 50%. For some films the 50% level was reached already after 500 h (EMAA, EVA). Although EAA and EMAA showed nearly the

same increase in PD index after 250 and 500 h, EMAA exhibited a more pronounced decrease in strain-at-break. EVA showed the least stability after 500 h. As reported in literature (Jäger et al., 2002), after 500 h of weathering EMA revealed a higher stability than EEA and EBA. Only the acid copolymers EAA and EMAA exhibited sufficient mechanical stability to conduct tensile tests after 1000 and 1500 h.

4. Summary and Conclusions

Ethylene copolymers based on acrylates and acrylic acids are an interesting alternative to EVA. These materials provide similar or better mechanical and optical properties before and after weathering as well as an aging behavior without the formation of acetic acid.

The investigated ethylene copolymer films showed high transparency in the solar range, with hemispheric transmittance values above 91%. Melting temperatures (ranging from 85 to 103 °C) and degree of crystallinity (from 26 to 39%) are depending on comonomer content. Regarding mechanical properties, the ethylene copolymer films exhibited a highly ductile behavior and high flexibility. Though the comonomer content is comparable to the other copolymers, the acid copolymers showed higher tensile strength than the acrylate and acetate copolymers.

Similar degradation behavior could be observed for all investigated films. Photo-degradation index and UV/VIS absorbance indicated a more or less linear accumulation of degradation products up to 250 h of xenon weathering. Due to formation of chromophoric degradation products, yellowing could be observed, and hemispheric transmittance values dropped slightly to values between 88.5 and 90.5%. EAA-BA showed the smallest accumulation of degradation products, but the biggest decrease in hemispherical transmittance.

The investigated films showed tendency towards high embrittlement due to weathering. Secondary crystallization with a dramatic increase in degree of crystallinity was observed by DSC measurements. After 750 h of weathering, both strain-at-break and stress-at-break values of all ethylene copolymer films dropped significantly below 50% of the initial values. Only the acid copolymers EAA and

EMAA exhibited sufficient mechanical stability to conduct tensile tests after 1000 and 1500 h of weathering exposure.

5. References

Allen, N.S., Edge, M., Rodriguez, M., Liauw, C.M., Fontan, E. (2000). Polym. Deg. Stab. **88**, 363.

Allen, N.S., Edge, M., Rodriguez, M., Liauw, C.M., Fontan, E. (2001). Polym. Deg. Stab. **71**, 1.

Androsch, R. (1999). Polymer **40**, 2805.

ATHAS Data Bank, http:web.utk.edu/~athas/databank/ Ed. M. Pyda (1994).

Brogly, M., Nardin, M., Schultz, J. (1997). J. Appl. Polym. Sci. **64**, 1903.

Czanderna, A.W., Pern, F.J. (1996). Sol. Energ. Mat. Sol. C. **43**, 101.

Deng, S.P., Zheng, H., Ouyang, J.M. (2006) Mat. Sci. Eng. C. **26**, 683.

Dilara, P.A., Briassoulis, D. (2000). J. Agric. Eng. Res. **76**, 309.

Gerlock, J.L., Smith, C.A., Cooper, V.A., Dusbiber, T.G., Weber, W.H. (2003). Polym. Deg. Stab. **97**, 225.

Jäger, K.M., Dammert, R.C., Sultan, B.A. (2002). J. Appl. Polym. Sci. **84**, 1465.

Kempe, M.D., Jorgensen, G., Terwilliger, K.M., McMahon, T., Kennedy, C.E., Borek, T.T. (2007). Sol. Energ. Mat. Sol. C. **91**, 315.

Klemchuk, P., Ezrin, M., Lavigne, G., Hollex, W., Gallica, J., Agro, S. (1997). Polym. Deg. Stab. **55**, 347.

Loo, Y.L., Wakabayashi, K., Huang, E., Register, R.A., Hsiao, B.S. (2005). Polymer **46**, 5118.

McNeill, I.C., Barbour, M. (1987). J. Anal. Appl. Pyrol. **11**, 163.

McNeill, I.C., Mohammed, M.H. (1995). Polym. Deg. Stab. **48**, 175.

McNeill, I.C., Alston, A. (1998). Angew. Makromol. Chem. **261/26**2, 157.

Monte, R. (2003). J. cult. Herit. **4**, 255.

Rodríguez-Vázquez, M., Liauw, C.M., Allen, N.S., Edge, M., Fontan, E. (2006). Polym. Deg. Stab. **91**, 154.

Roekens, H., Beyer, A. (2007). Kunststoffe **5/2007**, 92.

Sultan, B. Å., Sörvik, (1991). *E.* J. Appl. Polym. Sci., **43**, 1737.

Sultan, B. Å., Sörvik, (1991). *E.* J. Appl. Polym. Sci., **43**, 1747.

Sultan, B. Å., Sörvik, (1991). *E.* J. Appl. Polym. Sci., **43**, 1761.

4 Summary and Future Work

In this Dissertation, a good understanding of the optical properties of transparent ethylene copolymer films from the ultraviolet (UV) to the infrared range (IR) of light is provided. Second, a detailed characterization and description of the degradation behavior of ethylene copolymer films after accelerated aging was done. Moreover, based on the findings of this dissertation, several issues and aspects remain to be done in the future.

In Paper 1 (Chapter 2.1), the absorption and scattering behavior of ethylene copolymer films was determined in the solar range of radiation. Two different methods based on 4 and 5-fluxes were implemented and used. No differences in optical properties due to comonomer type and comonomer content could be observed. Both models revealed a significant forward scattering behavior of the films. The 4-flux model fitted hemispheric and diffuse transmittance far better than the 5-flux model. Diffuse reflectance values were strongly underestimated by both models. Due to the strong forward scattering behavior of all investigated films the diffuse reflectance is nearly exclusively confined to the surface. Hence, future work should focus on the establishment of correlations between the surface morphology and the solar optical properties of polar ethylene copolymer films. Furthermore, scattering mechanisms on the surface have to be implemented in more appropriate n-flux models.

Papers 2 and 3 (Chapter 2.2) dealt with infrared optical properties of ethylene copolymer films. In Paper 2, integral infrared optical properties were calculated based on published theories and formulas assuming a constant index of refraction from the visible range as input parameter. A linear correlation between the concentration of the highly effective carbon–oxygen group within the macromolecular structure and the infrared optical thickness was found for 50 µm thick films. This correlation fitted well in an established correlation for better infrared radiation absorbing polymeric materials consisting of carbon, hydrogen and oxygen atoms. In Paper 3 advanced methods to determine the spectral infrared optical properties of high absorbing, thick polymer films in all regions of

the spectral range (transparent, semi-transparent and non-transparent regions) were implemented and applied. Complex index of refraction data (n, k) were generated for various ethylene copolymer films. The k values were dependent on comonomer content and film thickness. The implemented methods have been used in the dissertation for polymers consisting of carbon, hydrogen and oxygen atoms (COH-polymers). Due to the fact that for solar applications also other polymer types with more IR absorbing functional groups are used, future work should focus on the determination of spectral infrared optical properties for the whole variety of polymeric materials.

The main focus of Papers 4 and 5 (Chaper 3) was a detailed characterization and description of the aging behavior of ethylene copolymer films, with focus on the overall performance and reliability of the materials in application.

In Paper 4, the significance of analytical and mechanical methods to describe the aging behavior was checked on commercially available, stabilized multi-layer EVA films. While at the film surface degradation products developed within the first 250 h of weathering, the ultimate mechanical properties of investigated 30 µm thick films remained nearly constant up to 1000 h. Thicker films provided good resistance against artificial weathering with mechanical properties remaining nearly constant for up to 3000 h. The comparison of ATR and FTIR spectra with mechanical properties suggests that degradation of the investigated polymer films is strongly confined to the surface. Nevertheless, the deformation-at-break values of notched specimens proved to be a sensitive indicator for global aging, whereas strain-at-break values of unnotched specimens are sensitive to initial aging and local defects. A correlation between formation of degradation products within the bulk, indicated by FTIR spectroscopy, and ultimate mechanical properties was obtained. Tensile tests appeared to be the most versatile method in describing aging.

The focus of Paper 5 was to evaluate and screen the aging behavior of ethylene copolymers containing different types of comonomers for solar applications. To investigate the intrinsic weathering behavior of the materials, unstabilized films with comonomer contents around 10 m% were exposed to temperature, humidity and solar radiation. Similar degradation behavior was obtained for the investigated

films. However, in contrast to commercially used EVA no acetic acid was formed as degradation product. Due to formation of chromophoric degradation products, yellowing could be observed. After 750 h of weathering, both strain-at-break and stress-at-break values of all ethylene copolymer films dropped significantly below 50% of the initial values. The next step in the description of the aging and degradation behavior would be an investigation of stabilized ethylene copolymer under application relevant conditions. Furthermore, the investigations should be extended to the component level and the impact of polymer degradation on overall performance should be assessed.

5 References

Allen, N.S., Edge, M., Rodriguez, M., Liauw, C.M., Fontan, E. (2000). Polym. Deg. Stab. **88**, 363.

Allen, N.S., Edge, M., Rodriguez, M., Liauw, C.M., Fontan, E. (2001). Polym. Deg. Stab. **71**, 1.

Ahrenkiel, R.K. (1971). J. Opt. Soc. Am. **61**, 1651.

Bheda J.H., Spruiell, J.E. (1986). Polym. Eng. Sci. **26**, 736.

Burger, T. (1998). „Radiative Transfer in Disperse Media - New Procedures in Spectroscopic Infrared Analysis", Dissertation, Universität Würzburg, D.

Chandrasekhar, S. (1960). "Radiative Transfer", Dover Publications Inc, Mineola.

Czanderna, A.W., Pern, F.J. (1996). Sol. Energ. Mat. Sol. C. **43**, 101.

Dilara, P.A., Briassoulis, D. (1998). Polym. Test. **17**, 549.

Dilara, P.A., Briassoulis, D. (2000). J. Agric. Eng. Res. **76**, 309.

Fayolle, B., Audouin, L., Verdu J. (2000). Polym. Deg. Stab. **70**, 333.

Fayolle, B., Audouin, L., Verdu, J. (2002). Polym. Deg. Stab. **75**, 123.

Goetzberger, A., Wittwer, V. (1993) "Sonnenenergie – Thermische Nutzung", B.G. Teubner, Stuttgart.

Günzler, H., Heise, H.M. (1996) „IR-Spektroskopie", 3. Aufl., VCH, Weinheim.

Jäger, K.M., Dammert, R.C., Sultan, B.A. (2002). J. Appl. Polym. Sci. **84**, 1465.

Kempe, M.D., Jorgensen, G., Terwilliger, K.M., McMahon, T., Kennedy, C.E., Borek, T.T. (2007). Sol. Energ. Mat. Sol. C. **91**, 315.

Kittas, C., Baille, A. (1998). J. Agric. Eng. Res. **71**, 193.

Klemchuk, P., Ezrin, M., Lavigne, G., Hollex, W., Gallica, J., Agro, S. (1997). Polym. Deg. Stab. **55**, 347.

Krauter, S., Hanitsch, R. (1996). Sol. Energ. Mat. Sol. C. **41/42**, 557.

Kubelka, P., Munk, F. (1931). Z. techn. Phys. **12** , 593.

Maheu, B., Letoulouzan, J.N., Gouesbet, G. (1984). Appl. Optics **23**, 3353.

Manara, J., Caps, R., Fricke, J. (2005). Int. J. Thermophys. **26**, 531.

McNeill, I.C., Barbour, M. (1987). J. Anal. Appl. Pyrol. **11**, 163.

McNeill, I.C., Mohammed, M.H. (1995). Polym. Deg. Stab. **48**, 175.

McNeill, I.C., Alston, A. (1998). Angew. Makromol. Chem. **261/26**2, 157.

Mehling, H. (1998). "Determination of infrared optical properties and phononic thermal conductivity of nonscattering inorganic and nonmetallic materials" Dissertation, Universität Würzburg, D.

Oreski, G., Wallner, G.M. (2005). Sol. Energy **79**, 612.

Rodríguez-Vázquez, M., Liauw, C.M., Allen, N.S., Edge, M., Fontan, E. (2006). Polym. Deg. Stab. **91**, 154.

Roekens, H., Beyer, A. (2007). Kunststoffe **5/2007**, 92.

Papadakis, G., Briassoulis, D., Scarascia Mugnozza, G., Vox, G., Feuilloley, P., Stoffers, J.A. (2000)J. Agric. Eng. Res. **77**, 7.

Pern, F.J. (1996). Sol. Energ. Mat. Sol. C. **41/42**, 587.

Platzer, W.J. (1988). „Solare Transmission und Wärmetransportmechanismen bei transparenten Wärmdämmaterialien“, Dissertation, Albert Ludwigs Universität, Freiburg, D.

Pollet, I.V., Pietersa, J.G., Deltourb, J., Verschoorea, R. (2005). Sol. Energ. Mat. Sol. C. **86**, 177.

Rubin, M. (1982). Sol. Energ. Mat. **6**, 375.

Sultan, B. Å., Sörvik, (1991). *E.* J. Appl. Polym. Sci., **43**, 1737.

Sultan, B. Å., Sörvik, (1991). *E.* J. Appl. Polym. Sci., **43**, 1747.

Sultan, B. Å., Sörvik, (1991). *E.* J. Appl. Polym. Sci., **43**, 1761.

Teichert, C., Haas, A., Wallner, G.M., Lang, R.W. (2002). Macromol. Symp. **181**, 457.

Vargas, W.E., Niklasson, G.A. (1997). J. Opt. Soc. Am. A **14**, 2243.

Vargas, W.E., Lushiku, E.M., Niklasson, G.A., Nilsson, T.M.J. (1998). Sol. Energ. Mat. Sol. C. **52**, 343.

Wallner, G.M., Lang, R.W., Platzer, W., Teichert, C. (2002). Macromol. Symp. **181**, 399.

Wallner, G.M., Weigl, C., Leitgeb, R., Lang, R.W. (2004) Polym. Deg. Stab. **85**,1065.

Wallner, G.M., Platzer, W., Lang, R.W. (2005). Sol. Energy **79**, 583.

Wallner, G.M., Platzer, W., Lang, R.W. (2005). Sol. Energy **79**, 593.

White, J.L., Matsakura, Y., Kang, H.J., Yamane, H. (1987). Int. Polym. Proc. **1**, 83.